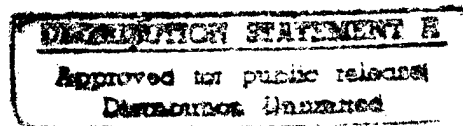


TRANSDUCER-BAFFLE INTERACTION

A Thesis
Presented to
the Academic Faculty

by

Laurie Deane Marshall



In Partial Fulfillment
of the Requirements for the Degree
Master of Science in Mechanical Engineering

Georgia Institute of Technology
September 1995

19970508 037

E-25-694

REPORT DOCUMENTATION PAGE

Form Approved
OMB No. 0704-0188

Public reporting burden for the collection of information is estimated to average 1 hour per response, including the time for reviewing instructions, searching existing data sources, gathering and maintaining the data needed, and completing and reviewing the collection of information. Send comments regarding this burden estimate or any other aspect of the collection of information, including suggestions for reducing the burden to Washington Headquarters Services, Directorate for Information Operations and Reports, 1215 Jefferson Davis Highway, Suite 1204, Arlington, VA 22202-4302, and to the Office of Management and Budget, Paperwork Reduction Project (0704-0188), Washington, DC 20503

1. AGENCY USE ONLY (Leave Blank)		2. REPORT DATE June 21, 1996	3. REPORT TYPE AND DATES COVERED 01 OCT 91 - 30 SEPT 94	
4. TITLE AND SUBTITLE Transducer-Baffle Interactions			5. FUNDING NUMBERS N00014-91-J-4173	
6. AUTHOR(S) Jacek Jarzynski and Laurie Deane Marshall				
7. PERFORMING ORGANIZATION NAME(S) AND ADDRESS(ES) Dr. Jacek Jarzynski School of Mechanical Engineering Georgia Institute of Technology Atlanta, GA 30332-0405			8. PERFORMING ORGANIZATION REPORT NUMBER E25-694	
9. SPONSORING / MONITORING AGENCY NAME(S) AND ADDRESS(ES) Office of Naval Research 800 North Quincy Street Arlington, VA 22217-5660			10. SPONSORING / MONITORING AGENCY REPORT NUMBER	
11. SUPPLEMENTARY NOTES COR: COR: Geoffrey Main				
12a. DISTRIBUTION / AVAILABILITY STATEMENT Unlimited			12b. DISTRIBUTION CODE	
13. ABSTRACT (Maximum 200 words) A finite element (FE) code was used to model the radiation of sound from a piezoelectric ceramic (PZT) projector located near an elastic baffle (a cylindrical shell). The use of a finite element code allows, for the first time, to simultaneously model the elastic response of the baffle, the piezoelectric response of the projector, and their interaction. The present study was limited to two projector-baffled configurations - a plane strain configuration and an axisymmetric finite shell configuration. Both of these configurations could be modeled with the two dimensional (2D) version of the SARA finite element code using a reasonable number of finite elements. (3) Three different sizes of piezoelectric projector were modeled, with 4.5°, 9.0°, and 18° angular extent. For the 4.5° and 9.0° projectors the TVR in the forward direction is not significantly affected by the presence of the baffle. (4) The 18° projector was the only source which showed significant deviations from ideal source performance. In particular, the TVR for this projector in the vicinity of the baffle is significantly different from the TVR under free field conditions. The 18° projector is the only source modeled whose dimensions (width) are comparable to the flexural (shortest) wavelength in the baffle, and in the PZT projector.				
14. SUBJECT TERMS Underwater acoustics, transducers, sonar systems			15. NUMBER OF PAGES 126	
			16. PRICE CODE	
17. SECURITY CLASSIFICATION OF REPORT Unclassified	18. SECURITY CLASSIFICATION OF THIS PAGE Unclassified	19. SECURITY CLASSIFICATION OF ABSTRACT Unclassified	20. LIMITATION OF ABSTRACT Unlimited	

**Summary of the Transducer-Baffle Interaction Study
(ONR Contract No. N00014-91-J-4173)**

The main features and results of the study are as follows:

- A finite element (FE) code was used to model the radiation of sound from a piezoelectric ceramic (PZT) projector located near an elastic baffle (a cylindrical shell). The use of a finite element code allows, for the first time, to simultaneously model the elastic response of the baffle, the piezoelectric response of the projector, and their interaction.

- The present study was limited to two projector-baffle configurations - a plane strain configuration and an axisymmetric finite shell configuration. Both of these configurations could be modeled with the two dimensional (2D) version of the SARA finite element code using a reasonable number of finite elements. The SARA 2D code was available, and had already been extensively tested, when the present study was begun.
A convenient feature of the SARA code is the calculation of the far-field pressure. This pressure is determined by numerically evaluating the Helmholtz integral over all vibrating surfaces. In the present study this allows one to separately determine the far-field pressure due to the sound scattered from the baffle and the pressure due to direct propagation of sound from the source.

- The radial dimensions of the cylindrical shell baffles were chosen to be similar to the dimensions of shells used in experimental underwater acoustics studies at Georgia Tech. However, the shell thickness in the numerical simulations was chosen to be relatively large (inner radius/outer radius = 0.9) to avoid very thin finite elements. Thinner shells can be modeled in the future, but this will require a larger number of finite elements and larger computer facilities. All calculations were made at two frequencies - one frequency ($ka=2$) below the ring resonance of the shell, and the second frequency ($ka=5$) above the ring resonance. The projector was located close to the baffle, separated from the baffle by a thin (less than one tenth of the acoustic wavelength) layer of water.

- The FE calculations and the analysis of the data were arranged under the following main topics:
 - (1) The normal velocity and the acoustic pressure at the surface of the baffle and the use of this data to determine what elastic waves are excited in the baffle by the adjacent projector.
 - (2) The far-field pressure directivity patterns for the projector-baffle system and comparison with the directivity patterns for the same projector under free-field conditions.
 - (3) The transmitting voltage response (TVR) of the projector in the vicinity of the baffle and comparison with the corresponding TVR of the projector under free-field conditions.

(4) Comparison of the ideal source to the finite piezoelectric source. Previous studies approximated the projectors as acoustically transparent, ideal point or line sources. It is of interest to determine under what conditions (frequency range, source dimensions) is the above approximation valid.

- The main results for each of the above topics are as follows:

(1) Analysis of the normal velocity pattern at the surface of the baffle shows that the projector excites mainly flexural waves in the baffle. There is some evidence of weak excitation of the fast, extensional wave at $ka=5$.

(2) The main differences between the far-field pressure from the projector near the baffle and the projector in the free field are probably due to interference between the direct sound from the projector and the sound reflected from the baffle.

(3) Three different sizes of piezoelectric projector were modeled, with 4.5° , 9.0° , and 18° angular extent. For the 4.5° and 9.0° projectors the TVR in the forward direction is not significantly affected by the presence of the baffle. This indicates that the source strength of the projector is not significantly changed by the presence of the baffle. The main differences between baffle and free-field conditions along other directions are probably due to interference between the direct and reflected sound signals.

(4) The 18° projector was the only source which showed significant deviations from ideal source performance. In particular, the TVR for this projector in the vicinity of the baffle is significantly different from the TVR under free field conditions. The 18° projector is the only source modeled whose dimensions (width) are comparable to the flexural (shortest) wavelength in the baffle, and in the PZT projector. Therefore, the present calculations suggest that the projector near a baffle can be modeled as an ideal, acoustically transparent source as long as its dimensions are less than about one quarter of the shortest elastic wavelength in the system (baffle or projector). The above conclusion is tentative and further studies are needed over a range of values of the relevant parameters. In particular, the above conclusion applies for projectors at the single, fixed distance from the baffle which was used in this study. The distance of the projector from the baffle is an important parameter which should be investigated.

TRANSDUCER-BAFFLE INTERACTION

**A Thesis
Presented to
the Academic Faculty**

by

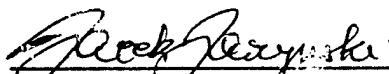
Laurie Deane Marshall

**In Partial Fulfillment
of the Requirements for the Degree
Master of Science in Mechanical Engineering**

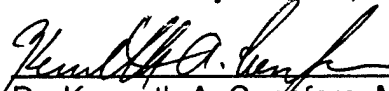
**Georgia Institute of Technology
September 1995**

TRANSDUCER-BAFFLE INTERACTIONS

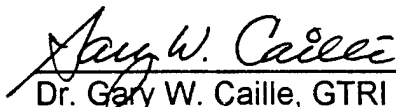
Approved:



Dr. Jacek Jarzynski, ME, Chair



Dr. Kenneth A. Cuffare, ME



Dr. Gary W. Caille, GTRI

Date Approved June 19, 1985

ACKNOWLEDGMENTS

I would like to thank my advisor Dr. Jacek Jarzynski for the knowledge that I gained from studying under him. I would also like to thank Dr. Calie and Dr. Cunefare for serving on my thesis committee. Much thanks is extended to the Mechanical Engineering faculty and student body for the enriching learning experience that I undertook while enrolled at Georgia Tech, it is an experience I will always remember. I would also like to thank the graduate office for their efficiency and sincere concern of the graduate students.

Much thanks is extended to the Navy for the grant they gave to Georgia Tech, for it was this grant that helped me further my education. I thank all of my co-workers at the Naval Research Lab in Orlando, Florida for their experience and expertise were very beneficial to my research. Special thanks is extended towards Dr. Michele McCollum, who is not only a co-worker of mine but a very dear friend.

Of utmost importance to me I would like to thank my husband Jay Marshall, it was his encouragement and understanding that enabled me to obtain my Master's degree. Last but by no means least, I would like to thank the most important people in my life, my immediate family for all the support they gave me.

TABLE of CONTENTS

ACKNOWLEDGMENTS	iii
LIST OF TABLES	vi
LIST OF FIGURES	viii
NOMENCLATURE	xv
SUMMARY	xvii

CHAPTER	PAGE
I. INTRODUCTION	1
A. Introduction	1
B. Background	3
C. Finite Elements	6
D. Configuration	7
E. Summary	10
II. LITERATURE REVIEW	16
A. Methodology	19
B. Summary	21
III. MODELS	22
A. Introduction	22

CHAPTER	PAGE
B. Theory	22
C. Analytical Model	27
D. Finite Element Model	28
E. Elements	29
F. Material Properties	32
G. Source Drive	34
H. Verification of Finite Element Model	37
I. Data	39
IV. RESULTS and DISCUSSION	48
A. Introduction	48
B. Plane Strain Model	48
C. Axisymmetric Model	60
D. Data	65
V. CONCLUSIONS	113
APPENDIX I	115
APPENDIX II	118
BIBLIOGRAPHY	124

LIST OF TABLES

TABLE		PAGE
3.1	Number of elements/wavelength used in the finite element models	31
3.2	The material properties of Navy Type I used in the finite element model.	33
3.3	The material properties of steel and water used in the finite element model.	34
3.4	The required voltage for each source at both frequencies to produce the same volume velocity as the ideal line source.	37
4.1	Calculated wavelengths	49
4.2	Transmitting voltage response of a 4.5 ° piezoelectric source under free-field conditions, while in the vicinity of the structure, and of the source-baffle system, at $ka=2$.	55
4.3	Transmitting voltage response of a 9.0 ° piezoelectric source under free-field conditions, while in the vicinity of the structure, and of the source-baffle system, at $ka=2$.	55
4.4	Transmitting voltage response of a 18.0 ° piezoelectric source under free-field conditions, while in the vicinity of the structure, and of the source-baffle system, at $ka=2$.	56
4.5	Transmitting voltage response of a 4.5 ° piezoelectric source under free-field conditions, while in the vicinity of the structure, and of the source-baffle system, at $ka=5$.	56
4.6	Transmitting voltage response of a 9.0 ° piezoelectric source under free-field conditions, while in the vicinity of the structure, and of the source-baffle system, at $ka=5$.	57

TABLE	PAGE
4.7 Transmitting voltage response of a 18.0° piezoelectric source under free-field conditions, while in the vicinity of the structure, and of the source-baffle system, at $ka=5$.	57
4.8 Sources' arc length.	59
4.9 Wavelengths in the cylindrical baffle determined from the axisymmetric shell equations.	62

LIST OF FIGURES

FIGURE		PAGE
1.1a	Plane strain model of a piezoelectric line source located in the vicinity of a cylindrical structure.	11
1.1b	Plane strain model of an ideal line source located in the vicinity of a cylindrical structure.	12
1.2a	Axisymmetric model of a piezoelectric ring source located in the vicinity of a cylindrical structure with hemispherical end caps.	13
1.2b	Axisymmetric model of an ideal ring source located in the vicinity of a cylindrical structure with hemispherical end caps.	14
1.3	All of the components that will make up the scattered pressure field for the case of an incident cylindrical wave on an elastic cylindrical structure.	15
3.1	Directivity pattern of three piezoelectric sources under free-field conditions at $ka=2$, 4.5° piezoelectric source (solid line), 9.0° piezoelectric source (dotted line), and an 18.0° piezoelectric source (dashed line). Each ring is 10 dB.	39
3.2	Magnitude of the normal velocity on the outer surface of the cylinder versus theta at $ka=2$, for an ideal line source excitation. The solid line is the analytical solution and the dotted line is the finite element solution.	40
3.3	(a) real normal velocity on the outer surface of the cylinder (b) imaginary normal velocity on the outer surface of the cylinder, both are at $ka=2$ and are due to an ideal line source excitation. The solid line is the analytical solution and the dotted line is the finite element solution.	41
3.4	Magnitude of the normal velocity on the outer surface of the cylinder at $ka=5$, for an ideal line source excitation. The solid line is the analytical solution and the dotted line is the finite element solution.	42

FIGURE	PAGE
3.5 (a) real normal velocity on the outer surface of the cylinder (b) imaginary normal velocity on the outer surface of the cylinder, both are at $ka=5$ and for an ideal line source excitation. The solid line is the analytical solution and the dotted line is the finite element solution.	45
3.6 Magnitude of the total pressure on the outer surface of the cylinder verses theta $ka=2$, for an ideal line source excitation. The solid line is the analytical solution and the dotted line is the finite element solution.	44
3.7 (a) real total pressure on the outer surface of the cylinder (b) imaginary total pressure on the outer surface of the cylinder, both are at $ka=2$ for an ideal line source excitation. The solid line is the analytical solution and the dotted line is the finite element solution.	45
3.8 Magnitude of the total pressure on the outer surface of the cylinder verses theta at $ka=5$, for an ideal line source. The solid line is the analytical solution and the dotted line is the finite element solution.	46
3.9 (a) real total pressure on the outer surface of the cylinder (b) imaginary total pressure on the outer surface of the cylinder, both are at $ka=5$ for an ideal line source excitation. The solid line is the analytical solution and the dotted line is the finite element solution.	47
4.1 Magnitude of the normal velocity on the outer surface of the cylinder verses theta at $ka=2$, for four different sources: an ideal line source (solid line), a 4.5° piezoelectric source (dotted line), a 9.0° piezoelectric source (dashed line), and an 18.0° piezoelectric source (dash-dot line).	65
4.2 (a) real normal velocity on the outer surface of the cylinder verses theta, (b) imaginary normal velocity on the outer surface of the cylinder verses theta; both are at $ka=2$, for four different sources: an ideal line source (solid line), a 4.5° piezoelectric source (dotted line), a 9.0° piezoelectric source (dashed line), and an 18.0° piezoelectric source (dash-dot line).	66
4.3 Magnitude of the normal velocity on the outer surface of the cylinder verses theta at $ka=5$, for four different sources: an ideal line source (solid line), a 4.5° piezoelectric source (dotted line), a 9.0° piezoelectric source (dashed line), and an 18.0° piezoelectric source (dash-dot line).	67

FIGURE	PAGE
4.4 (a) real normal velocity on the outer surface of the cylinder verses theta, (b) imaginary normal velocity on the outer surface of the cylinder verses theta; both are at $ka=5$, for four different sources: an ideal line source (solid line), a 4.5° piezoelectric source (dotted line), a 9.0° piezoelectric source (dashed line), and an 18.0° piezoelectric source (dash-dot line).	68
4.5 Magnitude of the total pressure on the outer surface of the cylinder verses theta at $ka=2$, for four different sources: an ideal line source (solid line), a 4.5° piezoelectric source (dotted line), a 9.0° piezoelectric source (dashed line), and an 18.0° piezoelectric source (dash-dot line).	69
4.6 (a) real total pressure on the outer surface of the cylinder verses theta, (b) imaginary total pressure on the outer surface of the cylinder verses theta; both are at $ka=2$, for four different sources: an ideal line source (solid line), a 4.5° piezoelectric source (dotted line), a 9.0° piezoelectric source (dashed line), and an 18.0° piezoelectric source (dash-dot line).	70
4.7 Magnitude of the total pressure on the outer surface of the cylinder verses theta at $ka=5$, for four different sources: an ideal line source (solid line), a 4.5° piezoelectric source (dotted line), a 9.0° piezoelectric source (dashed line), and an 18.0° piezoelectric source (dash-dot line).	71
4.8 (a) real total pressure on the outer surface of the cylinder verses theta, (b) imaginary total pressure on the outer surface of the cylinder verses theta; both are at $ka=5$, for four different sources: an ideal line source (solid line), a 4.5° piezoelectric source (dotted line), a 9.0° piezoelectric source (dashed line), and an 18.0° piezoelectric source (dash-dot line).	72
4.9 Wavenumber spectrum for the normal surface velocity. The spectrum was determined from the normal velocity versus theta on the outer surface of the cylinder which was initially excited by a 4.5° piezoelectric source. The results are at $ka=2$.	73
4.10 Wavenumber spectrum for the normal surface velocity. The spectrum was determined from the normal velocity versus theta on the outer surface of the cylinder which was initially excited by a 9.0° piezoelectric source. The results are at $ka=2$.	74

FIGURE	PAGE
4.11 Wavenumber spectrum for the normal surface velocity. The spectrum was determined from the normal velocity versus theta on the outer surface of the cylinder which was initially excited by a 18.0 ° piezoelectric source. The results are at ka=2.	75
4.12 Wavenumber spectrum for the normal surface velocity. The spectrum was determined from the normal velocity versus theta on the outer surface of the cylinder which was initially excited by a 4.5 ° piezoelectric source. The results are at ka=5.	76
4.13 Wavenumber spectrum for the normal surface velocity. The spectrum was determined from the normal velocity versus theta on the outer surface of the cylinder which was initially excited by a 9.0 ° piezoelectric source. The results are at ka=5.	77
4.14 Wavenumber spectrum for the normal surface velocity. The spectrum was determined from the normal velocity versus theta on the outer surface of the cylinder which was initially excited by a 18.0 ° piezoelectric source. The results are at ka=5.	78
4.15 Static shape of the plane strain cylinder with each element numbered.	79
4.16 Displaced shape of the cylinder (magnified 20 times) due to a 4.5 ° piezoelectric source excitation at ka=2.	80
4.17 Displaced shape of the cylinder (magnified 20 times) due to a 9.0 ° piezoelectric source excitation at ka=2.	81
4.18 Displaced shape of the cylinder (magnified 20 times) due to a 18.0 ° piezoelectric source excitation at ka=2.	82
4.19 Displaced shape of the cylinder (magnified 20 times) due to a 4.5 ° piezoelectric source excitation at ka=5.	83
4.20 Displaced shape of the cylinder (magnified 20 times) due to a 9.0 ° piezoelectric source excitation at ka=5.	84
4.21 Displaced shape of the cylinder (magnified 20 times) due to a 18.0 ° piezoelectric source excitation at ka=5.	85

FIGURE	PAGE
4.22 Far-field scattered pressure (dB) at $ka=2$, due to four different sources: an ideal line source (solid line), a 4.5° piezoelectric source (dotted line), a 9.0° piezoelectric source (dashed line), and an 18.0° piezoelectric source (dash-dot line). 10 dB/division	86
4.23 Far-field scattered pressure (dB) at $ka=5$, due to four different source excitations: an ideal line source (solid line), a 4.5° piezoelectric source (dotted line), a 9.0° piezoelectric source (dashed line), and an 18.0° piezoelectric source (dash-dot line). 10 dB/division	87
4.24 Far-field scattered pressure at $ka=2$ from an elastic cylindrical shell (solid line) and from a rigid cylindrical shell (dotted line) due to an ideal line source excitation.	88
4.25 Far-field scattered pressure at $ka=5$ from an elastic cylindrical shell (solid line) and from a rigid cylindrical shell (dotted line) due to an ideal line source excitation.	89
4.26 Far-field total pressure (dB) at $ka=2$, due to three different sources: a 4.5° piezoelectric source (solid line), a 9.0° piezoelectric source (dotted line), and an 18.0° piezoelectric source (dash-dot line). 10 dB/division	90
4.27 Far-field total pressure (dB) at $ka=5$, due to three different source excitations: a 4.5° piezoelectric source (solid line), a 9.0° piezoelectric source (dotted line), and an 18.0° piezoelectric source (dash-dot line). 10 dB/division	91
4.28 Magnitude and phase of the normal velocity on the outer surface of the cylindrical shell with hemispherical end caps at $ka=2$. The excitation is due to an ideal ring source located at position P1.	92
4.29 Magnitude and phase of the total pressure on the outer surface of the cylindrical shell with hemispherical end caps at $ka=2$. The excitation is due to an ideal ring source located at position P1.	93
4.30 Magnitude and phase of the normal velocity on the outer surface of the cylindrical shell with hemispherical end caps at $ka=2$. The excitation is due to an ideal ring source located at position P2.	94

FIGURE	PAGE
4.31 Magnitude and phase of the total pressure on the outer surface of the cylindrical shell with hemispherical end caps at $ka=2$. The excitation is due to an ideal ring source located at position P2.	95
4.32 Magnitude and phase of the normal velocity on the outer surface of the cylindrical shell with hemispherical end caps at $ka=2$. The excitation is due to an ideal ring source located at position P3.	96
4.33 Magnitude and phase of the total pressure on the outer surface of the cylindrical shell with hemispherical end caps at $ka=2$. The excitation is due to an ideal ring source located at position P3.	97
4.34 Magnitude and phase of the normal velocity on the outer surface of the cylindrical shell with hemispherical end caps at $ka=5$. The excitation is due to an ideal ring source located at position P1.	98
4.35 Magnitude and phase of the total pressure on the outer surface of the cylindrical shell with hemispherical end caps at $ka=5$. The excitation is due to an ideal ring source located at position P1.	99
4.36 Magnitude and phase of the normal velocity on the outer surface of the cylindrical shell with hemispherical end caps at $ka=5$. The excitation is due to an ideal ring source located at position P2.	100
4.37 Magnitude and phase of the total pressure on the outer surface of the cylindrical shell with hemispherical end caps at $ka=5$. The excitation is due to an ideal ring source located at position P2.	101
4.38 Magnitude and phase of the normal velocity on the outer surface of the cylindrical shell with hemispherical end caps at $ka=5$. The excitation is due to an ideal ring source located at position P3.	102
4.39 Magnitude and phase of the total pressure on the outer surface of the cylindrical shell with hemispherical end caps at $ka=5$. The excitation is due to an ideal ring source located at position P3.	103
4.40 Far-field scattered pressure from the cylindrical shell with hemispherical end caps at $ka=2$. The excitation is due to an ideal ring source located at position P1.	104

FIGURE	PAGE
4.41 Far-field scattered pressure from the cylindrical shell with hemispherical end caps at $ka=2$. The excitation is due to an ideal ring source located at position P2.	105
4.42 Far-field scattered pressure from the cylindrical shell with hemispherical end caps at $ka=2$. The excitation is due to an ideal ring source located at position P3.	106
4.43 Far-field scattered pressure from the cylindrical shell with hemispherical end caps at $ka=5$. The excitation is due to an ideal ring source located at position P1.	107
4.44 Far-field scattered pressure from the cylindrical shell with hemispherical end caps at $ka=5$. The excitation is due to an ideal ring source located at position P2.	108
4.45 Far-field scattered pressure from the cylindrical shell with hemispherical end caps at $ka=5$. The excitation is due to an ideal ring source located at position P3.	109
4.46 Total far-field pressure (solid line) and scattered far-field pressure (dotted line) at $ka=2$. The finite cylindrical structure with hemispherical end caps is excited by a finite piezoelectric source located at position P1. 10 dB/division	110
4.47 Total far-field total pressure (solid line) and scattered far-field pressure (dotted line) at $ka=5$. The finite cylindrical structure with hemispherical end caps is excited by a finite piezoelectric source located at position P1. 10 dB/division	111
4.48 Free-field directivity pattern of a finite piezoelectric ring source at $ka=2$ (solid line) and $ka=5$ (dashed line).	112

NOMENCLATURE

λ	lame coefficient
G	lame coefficient
ν	poisson's ratio
ξ	displacement
∇	del operator
\times	curl
$\frac{\partial^n}{\partial x^n}$	n th derivative with respect to x
ρ_0	density of cylinder
ϕ	scalor potential
\vec{A}	vector potential
c	sound speed in first fluid medium
c_L	longitudinal wave speed in cylinder
c_s	shear wave speed in cylinder
B	bulk modulus
P_s	scattered pressure
P_i	incident pressure
P_t	pressure transmitted into second fluid medium
r	distance to some field point referenced from center of cylinder
d	distance from center of cylinder to center of source
P_0	pressure amplitude
k	wave number in first fluid medium
k_s	shear wave number
k_L	longitudinal wave number
θ	theta
a	inner radius of cylinder
b	outer radius of cylinder

J_n	cylindrical bessel funtion
Y_n	cylindrical neumann funtion
$H_n^{(2)}$	hankle funtion of the second kind
$i = \sqrt{-1}$	imaginary
A_n, B_n	coefficients associated with scalar potential
D_n, E_n	coefficient associated with vector potential
M_n	coefficient associated with pressure expression for second fluid
C_n	coefficient associated with the scattered pressure
A_n, B_n	coefficients associated with scalar potential
D_n, E_n	coefficients associated with vector potential
M_n	coefficient associated with pressure expression for second fluid medium
C_n	coefficient associated with scattured pressure
$[rr]$	normal component of stress
$[r\theta]$	tangential component of shear stress
$[rz]$	tangential component of shear stress
A_z	z component of vector potential
t	time
$\xi_{i,r}$	radial component of displacement for incident wave
$\xi_{s,r}$	radial componenet of displacement for scattered wave
ξ_θ	theta component of displacement in cylinder
ξ_r	radial componenet of displacement in cylinder
ξ_z	z component of displacement in cylinder
ϵ_n	neumann factor
ω	angular frequency
E	youngs modulus
C_E	phase velocity of extensional wave in a thin plate
C_f	phase velocity of flexural wave in a thin plate
f_n	ring frequency

SUMMARY

The main features and results of the study are as follows:

- A finite element code (SARA) was used to model the radiation of sound from a piezoelectric ceramic projector located near an elastic baffle (a cylindrical shell). The use of a finite element code allows, for the first time, to simultaneously model the elastic response of the baffle, the piezoelectric response of the projector, and their interaction.
- The present study was limited to two projector-baffle configurations—a plane strain configuration and an axisymmetric finite shell configuration. Both of these configurations could be modeled with the two dimensional (2D) version of the SARA finite element code using a reasonable number of finite elements. The SARA 2D code was available, and had already been extensively tested and bench marked by the NAVY, when the present study was begun. A convenient feature of the SARA code is the calculation of the far-field pressure. This pressure is determined by numerically evaluating the Helmholtz integral over all vibrating surfaces. In the present study this allows one to separately determine the far-field pressure due to the sound scattered from the baffle and the pressure due to direct propagation of sound from the source.
- The radial dimensions of the cylindrical shell baffles were chosen to be similar to the dimensions of shells used in experimental underwater acoustics studies at Georgia Tech. However, the shell thickness in the numerical simulations were chosen to be relatively large (inner radius/outer radius=0.9) to avoid very thin finite elements. Thinner shells can be modeled in the future, but this will require a larger number of

finite elements and larger computer facilities. All calculations were made at two frequencies-one frequency ($ka=2$) below the ring resonance of the shell, and the second frequency ($ka=5$) above the ring resonance. The projector was located close to the baffle, separated from the baffle by a thin (less than one tenth of the acoustic wavelength) layer of water.

The finite element calculations and the analysis of the data were arranged under the following main topics:

- The normal velocity and the acoustic pressure at the surface of the baffle and the use of this data to determine what elastic waves are excited in the baffle by the adjacent projector.
- The far-field pressure directivity patterns for the projector-baffle system and comparison with the directivity patterns for the same projector under free-field condition.
- The transmitting voltage response (TVR) of the projector in the vicinity of the baffle and comparison with the corresponding TVR of the projector under free-field conditions. The TVR of the transducer-baffle system.
- Comparison of the ideal source to the finite piezoelectric source. Previous studies approximated the projectors as acoustically transparent, ideal point or line sources. It is of interest to determine under what conditions (frequency range, source dimensions) is the above approximation valid.

The main results for each of the above topics are as follows:

- Analysis of the normal velocity pattern at the surface of the baffle shows that the projector excites mainly flexural waves in the baffle. There is some evidence of weak excitation of the fast, extensional wave at $ka=5$.
- The main differences between the far-field pressure from the projector near the baffle and the projector in the free-field are probably due to interference between the direct sound from the projector and the sound reflected from the baffle.
- Three different sizes of piezoelectric projector were modeled, with 4.5° , 9.0° , and 18.0° angular extent. For the 4.5° and 9.0° projectors the TVR in the forward direction is not significantly affected by the presence of the baffle. This indicates that the source strength of the projector is not significantly changed by the presence of the baffle. The main differences between baffle and free-field conditions along other directions are probably due to interference between the direct and reflected sound signals.
- The 18.0° projector was the only source which showed significant deviations from ideal source performance. In particular, the TVR for this projector in the vicinity of the baffle is significantly different from the TVR under free-field conditions. The 18.0° projector is the only source modeled whose dimensions (width) are comparable to the flexural (shortest) wavelength in the baffle, and in the piezoelectric projector. Therefore, the present calculations suggest that the projector near a baffle can be modeled as an ideal, acoustically transparent source as long as its dimensions are less than about one quarter of the shortest elastic wavelength in the system (baffle or projector). The above conclusion applies for projectors at the single, fixed distance

from the baffle which was used in this study. The distance of the projector from the baffle is an important parameter which should be investigated.

CHAPTER I

INTRODUCTION

A. Introduction

Transducer-baffle interactions play a critical role in the design of transducers used in underwater applications, because receiving and transmitting transducers are often mounted on the hull of a ship, which acts as an elastic baffle. The baffle can change the fluid loading on the transducer which may greatly affect the operation of the transducer, e.g., altering its directivity. For the present research the behavior of a transducer in the vicinity of a fluid-loaded elastic baffle will be investigated, using finite element and analytical techniques. This research focuses primarily on two questions: (1) how does the baffle affect the transducer and (2) how does the transducer affect the baffle. A secondary focus will be to determine how best to model the transducer, i.e., under what conditions can it be treated as an ideal source.

The investigation of the baffle's effect on the transducer will be accomplished by studying the transducer's directivity pattern and transmitting voltage response (TVR) and comparing it to the free-field results. The investigation of the transducer's effect on the baffle will be accomplished by examining the normal velocity and total pressure on the surface of the baffle and the displaced shape of the baffle. In determining how to model the transducer, the results obtained using ideal sources will be compared to those obtained using finite (realistic) sources.

Previous studies of transducer-baffle interactions either approximated the transducer as an ideal line or point source, or approximated the baffle as a rigid boundary condition. The present work employs a baffle geometry that is realistic for underwater acoustic applications and is unique because it models the elastic response of the baffle, the piezoelectric processes in the transducer, and the transducer-baffle interaction through the surrounding water. In this study the above effects are modeled by using finite elements.

The finite element code used in this study is SARA [1], developed at Bolt, Beranek and Newman (BNN). There are two-dimensional (2D) and three-dimensional (3D) versions of this code, both of which include piezoelectric elements. The 3D version was developed only recently and experience with the use of this code is limited. Therefore, in planning the present study it was decided to start with simple transducer-baffle configurations which could be modeled with the 2D code. Also, one of the configurations chosen could be independently modeled with an analytical modal expansion. Comparisons between the modal expansion and finite element results were a very useful check during the initial development of the finite element program.

The two transducer-baffle configurations chosen for the present study are a plane strain configuration in which the baffle is an infinite cylindrical shell, and an axisymmetric configuration in which the baffle is a finite cylindrical shell with hemispherical end caps. For the plane strain model two different sources were used. One source is a piezoelectric transducer configured as a segment of an infinite cylinder parallel to the shell (Figure 1.1a) while the other is an ideal line source (Figure 1.1b). For the axisymmetric model there were also two sources. One is a finite ring transducer (Figure 1.2a) while the other is an ideal ring source (Figure 1.2b). All of the sources are driven continuously. Although in practice sources are generally pulsed, it is advantageous to have a continuous drive on the sources in the models because it allows one to look at the normal velocity and total

pressure profiles on the surface of the baffle as standing wave patterns. In each case the cylindrical shell has an outer to inner radius ratio=1.08. The total length to outer radius ratio of the axisymmetric configuration was selected to correlate with an experimental effort currently taking place at Georgia Institute of Technology, but the baffle thickness was increased for modeling simplicity.

B. Background

Sound that is radiated from transducers mounted on or near elastic baffles will be influenced by the baffle. The radiated energy which strikes the baffle will then be reflected, transmitted, or absorbed. The fate of the incident acoustic wave when it strikes the baffle depends on many parameters, one of which is the material of the baffle. A wave incident upon an elastic baffle may excite the structure. An elastic structure has many natural modes of vibration, and if the structure is excited at a natural mode, large displacements will occur for even a small excitation. If the elastic structure is excited at a frequency other than a natural mode, the structure will still vibrate but with much smaller displacements. Sound will be radiated into the surrounding medium from both the vibrating transducer and the vibrating structure. The pressure-field resulting solely from the vibration of the structure is referred to as scattered pressure, whereas that radiated and scattered by the combination of the vibration of the structure and the motion of the transducer is referred to as total pressure. There will be interaction between the transducer and the baffle that may affect the directivity pattern and the transmitting voltage response of the source. The amount of interaction between the source and the structure depends on many parameters, such as: the source size, the source's location in reference to the structure, the driving frequency of the source, the geometry of the structure, the material of the structure, and the size of the structure. In determining the

amount of interaction between the source and the structure all of the above parameters are initially defined; however, several different source sizes are investigated.

To investigate this problem, it is important to understand the concept of scattering because the sound radiated by the transducer will be scattered by the baffle. Scattering means multiple reflections in many directions. For an elastic body, there are four basic contributions to the scattered field: diffraction echo (creeping waves), specular reflection, elastic echo (reflection-transmission inside the scatterer), and scattering due to elastic waves in the shell. To have a good understanding of what is happening, we can use the example of a wave propagating in the medium and then striking a cylinder in a direction perpendicular to the circumference (Figure 1.3). Upon impact the wave splits into two waves, one traveling counterclockwise and the other traveling clockwise, both around the circumference of the cylinder in the external fluid. These circumferential waves travel at a slightly slower speed than the speed of sound in the external fluid and are called creeping waves. The creeping wave radiates into the external fluid as it travels around the shell, although this radiation is usually smaller than the specular echo. A specular reflected wave is a wave that propagates in a single direction. It is a direct reflection from the point of impact on the cylinder. An elastic echo is a reflection from the interior of the cylinder. An elastic echo only occurs if the incident wave penetrates the cylinder and then re-exits. The percentage of incident wave that penetrates the interior of the cylinder is determined by the impedance mismatch between the two mediums. For this study, there is a large impedance mismatch between the cylinder and the enclosed vacuum therefore, the contribution of the elastic echo is virtually insignificant. Finally, there will be elastic waves in the shell. For a thin shell two waves will exist: a fast, extensional wave, and a slow, flexural wave. When the speed of the elastic wave is greater than the speed of sound in

the surrounding medium (water), this wave will radiate back into the water as it travels around the shell.

Although the baffle will scatter sound when the transducer excites it, the sound waves may be evanescent, i.e., they may decay exponentially with distance, so that no energy reaches the far-field. The amount of far-field radiation produced by the baffle, due to the propagating waves in the baffle depends on the wave speeds. When the speed at which the wave travels is faster than the speed of sound in the surrounding fluid, the wave is said to be supersonic. Supersonic waves tend to be good radiators. When the speed at which the wave travels is slower than the speed in the surrounding fluid, the wave is said to be subsonic. Subsonic waves tend to be poor radiators.

Another parameter that is of equal importance as the wave speed, in determining the efficiency of a radiator, is the mode of vibration, i.e., the displaced shape of the structure. For a transducer to radiate efficiently, it has to be well coupled to the surrounding fluid. An example of a mode that is well coupled is a monopole, which is also referred to as a breathing mode. A monopole moves uniformly in phase and is a good radiator because it produces a net volume change.

The modes of vibration of the baffle depend on the types of waves that propagate in it. Because the baffle is an elastic material, it can support two waves, a longitudinal wave and a shear wave. A longitudinal wave (also called a dilatational wave) produces a particle displacement in the same direction as that in which the wave is traveling. A shear wave (also known as a transverse wave) produces a particle displacement that is perpendicular to the wave propagation direction. The longitudinal and shear waves will combine in the thin cylindrical structure to form two distinct modes of vibration, a flexural and an extensional mode. The thin cylindrical structure acts as a waveguide. Any waveguide mode in a thin plate is referred to as a Lamb mode. For a cylindrical shell the

phase velocity for the lamb modes is a function of the direction of propagation. For propagation around the circumference, the extensional and flexural phase velocities can be approximately determined from the equivalent expressions in a flat plate [2]. However, propagation along the axial direction is much more complicated. Only the symmetric Lamb (extensional) mode exists below the ring frequency of the cylindrical baffle. Above the ring frequency both Lamb modes exist, and the cylindrical shell may be approximated as an equivalent flat plate [3]. For a thin plate, the two lowest Lamb waves are the extensional wave (also known as a quasi-longitudinal wave) and the flexural wave. The extensional wave is a symmetric Lamb wave; it has a particle displacement that is in the plane of the plate and produces a stretching motion. The extensional wave is a fast propagating wave in steel. The speed at which this wave propagates is a function of the modulus of elasticity of the material. The flexural wave is the first antisymmetric Lamb wave; it has a particle displacement that is out of plane and produces a bending motion. The flexural wave is dispersive and propagates at a much slower speed than that of the quasi-longitudinal wave. The speed at which the flexural wave propagates in the plate is a function of frequency, Young's modulus and Poisson's ratio of the material; as well as the thickness of the plate.

C. Finite Elements

Finite elements will be used in this study to model the behavior of a transducer in the vicinity of a baffle. The two types of models used are a plane strain model and an axisymmetric model, both of which are two-dimensional. A plane strain model is one in which there is no variation of strain (displacement) along the length of the geometry, an example of this is a plate that is very long in one dimension. A plane strain model is

informative for examining the combined radial and circumferential motion. An axisymmetric model, on the other hand, has no variation of strain around the circumference. This model is informative for studying the combined radial and axial motion.

D. Configuration

To examine both the axial and circumferential vibration using two-dimensional models, two different configurations are required. The first configuration (Figure 1.1a and 1.1b) is a plane strain model in which the baffle is an infinite, homogeneous, isotropic, elastic, hollow steel cylinder enclosing a vacuum and surrounded by water. The cylinder has an inner radius $a=31.75$ cm and an outer radius $b=34.29$ cm, with an outer to inner radius ratio of 1.08. The diameter was selected to correlate with an experimental effort currently taking place at Georgia Institute of Technology. However, the baffle thickness was increased from $b/a=1.008$ to $b/a=1.08$ for modeling simplicity. The material losses will be neglected. The plane strain model is infinite in the z-direction; therefore all parameters are independent of the z coordinate. For the plane strain model, several different sound sources will be investigated, all of which are infinite in the z-direction. The first sound source is an ideal line source located 36.83 cm from the center of the cylinder. It is dimensionless and has a prescribed volume velocity. The volume velocity is specified as that required to give a root mean square (rms) pressure of 20 Pa at 1 m in the free-field for a 1000 Hz signal. The three other sources are made of a piezoelectric material and are driven with a voltage. Each of the piezoelectric sources is a cylindrical segment that is specified by the angle it subtends at the cylinder axis, with an inner radius of 36.83 cm and a wall thickness of 1.27 cm (these dimensions were arbitrarily chosen).

The three sources modeled are 4.5, 9.0, and 18.0 degrees in arc. From this choice of angles, it is hoped to determine a limiting arc dimension at which the source behaves ideally. All sources are symmetric about zero degrees. Each piezoelectric source is driven by the voltage required to produce the same volume velocity as the ideal line source in the free-field. The models will be exercised at two frequencies: 1376 Hz ($ka=2$, where k is the wave number and a is the radius of the cylinder), and 3439 Hz ($ka=5$).

Verification of the finite element model based on an ideal line source will be accomplished by comparing the magnitude of the normal velocity of the outer surface of the cylinder and the total pressure on the outer surface of the cylinder to results obtained from an analytical model. Upon establishing the validity of the finite element model, comparisons will be made between the results obtained with piezoelectric sources and the ideal line source, both in the near-field and in the far-field. In the near-field, the real and imaginary normal velocity and the total pressure on the outer surface of the cylinder will be compared for the different sources. In the far-field the scattered pressure and the total pressure will be compared for the different sources. In addition, the displaced shape of the baffle will be displayed. With the finite element models, the electromechanical transduction process is modeled directly. In addition, both compressional and shear waves are included in the elastic cylinder.

The second geometrical configuration (Figure 1.2a and 1.2b) that will be used in the study of transducer-baffle interaction is an axisymmetric model. In the axisymmetric model the baffle is a finite cylindrical shell with hemispherical end caps made of a homogeneous, isotropic, elastic material (steel). Like the previous configuration the finite baffle is submerged in water and encloses a vacuum and again all material losses will be neglected. The total length of this baffle is 195.58 cm, while each end cap has an outer radius of 34.29 cm. The axisymmetric baffle has a length to outer radius ratio of 5.7. The

ratio of the total length to the outer radius of the axisymmetric baffle was chosen to correlate with an experimental structure at Georgia Institute of Technology. As in the plane strain model the baffle thickness was increased to 2.54 cm. Although the structure thickness has been increased, it is still relatively thin because the baffle thickness is much less than the wavelength in steel. For this configuration two kinds of sound sources will be investigated. The first is an ideal (dimensionless) ring source. The ideal ring source has a unit volume velocity. The ideal ring source will be located 36.83 cm from the axis of symmetry of the cylinder, and at three different locations along the length of the baffle (marked P1, P2, and P3 in Figure 1.2b). All locations will be referenced to the center of the baffle. They are defined as follows: (P1) center of the length, (P2) just prior to the intersection of the cylinder and the end cap, 58.42 cm off the center, and (P3) the center of the end cap. The other source will be a finite piezoelectric ring source that is also located 36.83 cm from the axis of symmetry of the cylinder. The dimensions of the piezoelectric source are arbitrarily chosen to be: length=5.08 cm and thickness=2.54 cm. The source is driven with a unit voltage. The ideal ring source and the finite piezoelectric ring source do not produce the same volume velocity, however, direct comparisons can be made between the two sources because everything is linear and can be normalized. As before, the models will be exercised at two frequencies, 1376 and 3439 Hz. Comparisons of the finite piezoelectric source to that of the ideal ring source will be made both in the near-field and in the far-field. In the near-field the magnitude and phase of the normal velocity and the total pressure on the outer surface of the baffle will be compared for the two situations. In the far-field, for the two sound sources, the scattered pressure and the total pressure will be compared. To help understand the effects of the baffle on the transducer, it is important to look at the individual sources both in the vicinity of the baffle and also under free-field conditions.

E. Summary

By using finite element and analytical models this study will show the interaction that takes place between the sound source and the baffle. The baffle is a homogeneous, isotropic, elastic steel structure. Several piezoelectric sound source geometries will be used at two distinct frequencies. Two baffles will be investigated: an infinite cylindrical shell and a finite cylindrical shell with hemispherical end caps. In both cases a cylindrical geometry was chosen for the baffle, for it best simulates the hull of a ship or a submarine. Both the effects of the source on the baffle and the effects of the baffle on the sound source will be explained. For a better understanding of how the baffle affects the sound source, the study will show how the structure affects the transducer's directivity pattern and the transmitting voltage response of the transducer. Also, because the piezoelectric sound sources are driven with a fixed voltage and are not assumed to move in a specified manner, the source's performance in the free-field will be compared to the performance when the source is near the structure. For a better understanding of how the source affects the baffle, the scattered far-field pressure will be presented along with the displaced shapes of the baffle for the different sources.

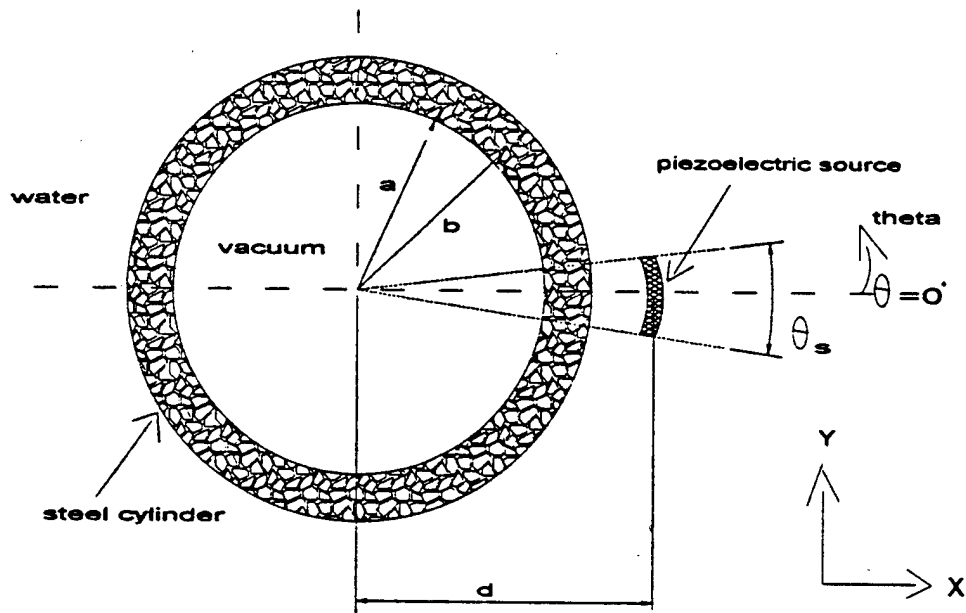


Figure 1.1a Plane strain model of a piezoelectric source in the vicinity of the cylindrical structure.

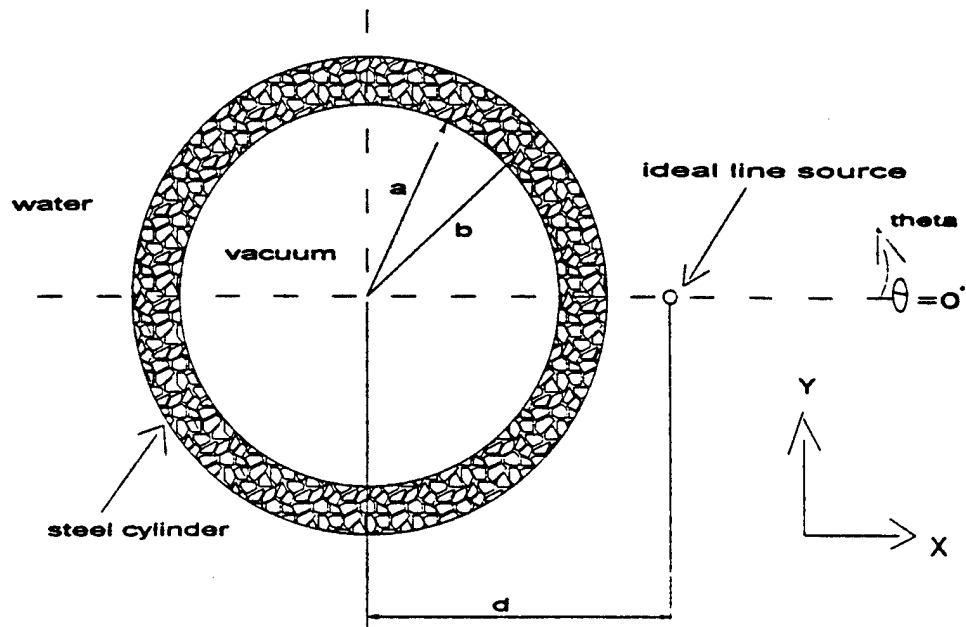


Figure 1.1b Plane strain model of an ideal line source in the vicinity of the cylindrical structure.

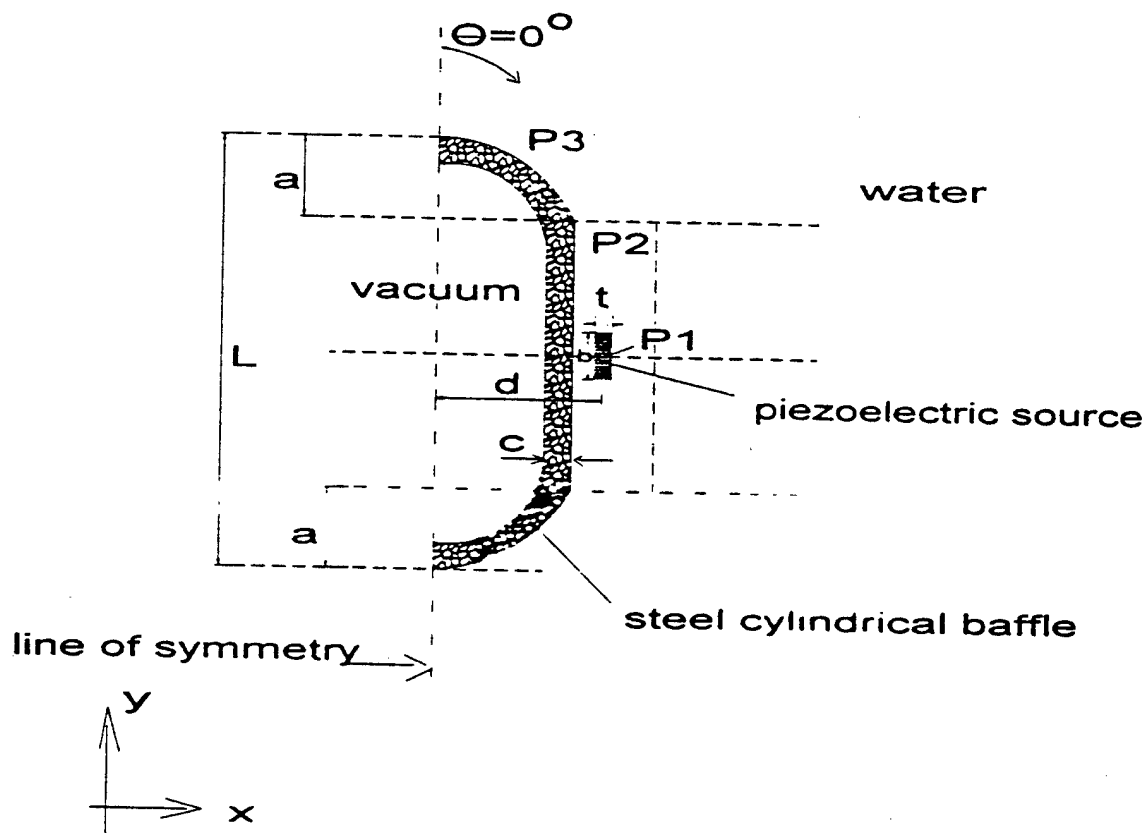


Figure 1.2a Axisymmetric model of piezoelectric source located in the vicinity of a cylindrical structure with hemispherical end caps.

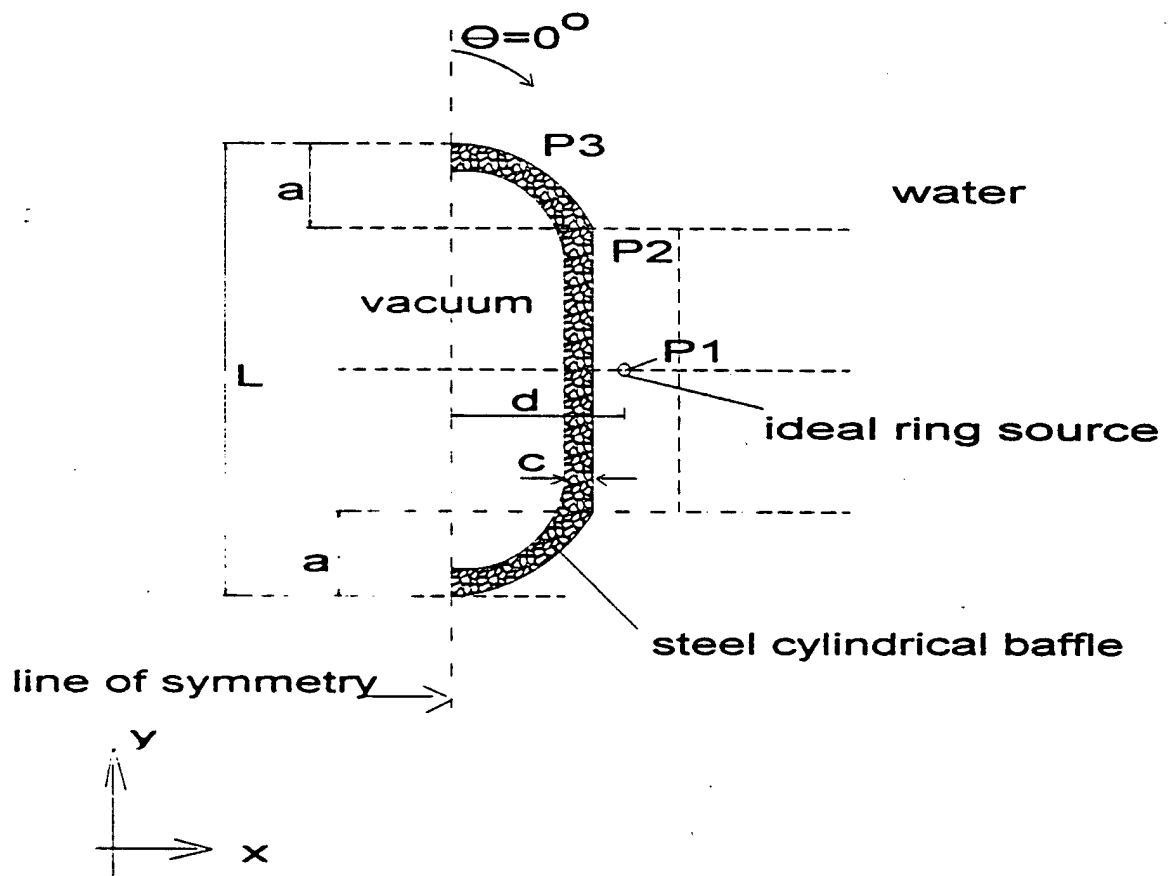


Figure 1.2b Axisymmetric model of an ideal ring source located in the vicinity of a cylindrical structure with hemispherical end caps.

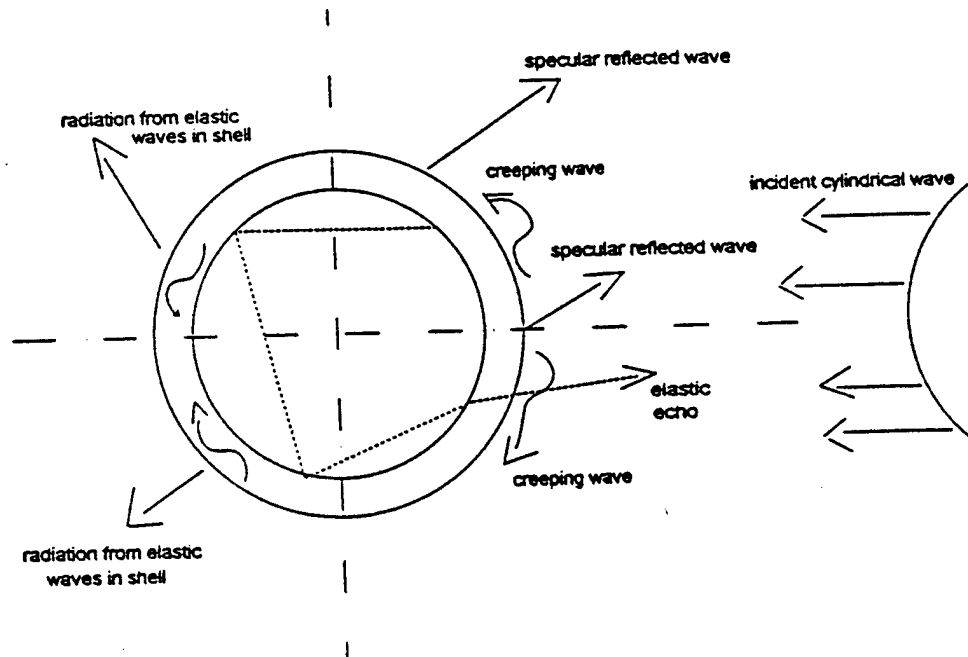


Figure 1.3 All of the components that will make up the scattered pressure field for the case of an incident cylindrical wave on an elastic cylindrical structure.

CHAPTER II

LITERATURE REVIEW

Much insight may be gained into transducer-baffle interaction by studying past publications on similar problems and investigating the method of solution. Perhaps the simplest elastic scattering problem is the scattering of a plane wave by curved elastic geometries. There have been many publications on this topic, and most have focused on cylindrical geometries. In 1951 Faran [4] looked at the scattering of a plane wave by a solid elastic cylinder. Ten years later Doolittle and Uberall [5] investigated scattering of a plane wave incident on an elastic cylindrical shell. The study presented general solutions for the sound fields obtained from a modal expansion. In 1967, Ugincius and Uberall [6] investigated scattering of a plane incident wave by a cylindrical shell immersed in a fluid and enclosing another fluid. The methodology that Ugincius and Uberall used in determining the scattered field is as follows: first they used a modal expansion [7] to obtain the normal mode solution for the scattered pressure, then they applied the Sommerfeld-Watson transformation [8] to the normal mode solution. Borovikov and Veksler [9] used a different approach in their study of scattering of sound waves by smooth elastic cylindrical shells. In determining the scattered field, the combination of two waves, the specular reflected wave and the symmetrical Lamb wave of zero order (also referred to as the quasi-longitudinal wave) were accounted for, and all other waves

were neglected. The authors used the Geometrical Theory of Diffraction [10] to obtain the far-field scattered pressure. All of the above references assumed that the cylinder (baffle) was infinite in length and that the source was located in the far-field, so the incident sound wave was planar.

Another class of research related to the present study is that of acoustic radiation from a source on a cylinder. In 1964 Greenspon and Sherman [11] derived expressions for the sound pressure generated by rectangular pistons on a rigid cylinder at large wave numbers. In this research the authors simplified the problem by neglecting the thickness of the pistons. In 1966, Junger [12] conducted a study of surface pressures generated by pistons on large cylindrical baffles for large ka . Junger also employed the Sommerfeld-Watson transformation for far-field calculations but for the analysis in the near-field he used the Kirchhoff approximation [13] because of the slow convergence of the Sommerfeld-Watson series for small distances from the source. In 1981, Liu and Rumerman [14] published a report on the effects of adjacent elastic structures on radiation by acoustic volume sources. In this report they investigated both point sources and line sources on several different baffle configurations. Their investigation of a point source on an infinite cylindrical shell relates directly to the present study. In the above reference, they mathematically modeled the pressure field as the sum of the pressure radiated when the shell is considered to be rigid and the pressure radiated due to the vibration of the shell. Their mathematical model began with the equations of motion for a thin elastic cylindrical shell. A displacement for the cylindrical shell was assumed, then substituted back into the equation of motion upon which a Fourier Transform [15] was applied. Their research was not concerned with the effects of the baffle on the source but investigated only the effects of the source on the baffle. More recently, in 1991, Butler and Porter [16]

studied the acoustic radiation from a source on the surface of an elastic cylinder. The authors used a Fourier Transform solution that was specialized for the case of "a transparent source or a transducer source small compared to the wavelength of sound in the medium" [16]. Numerical results for a 3-D study of a small source on a thin walled elastic infinite cylindrical tube were given. They studied the far-field scattered pressure for two primary source configurations: the first solution assumed that the source was transparent (this totally ignores the source's dimensions); the second solution assumed a small rigid source (this ignores the thickness of the source). Note that in all of the references mentioned above, many assumptions were made in order to solve the problem. The research presented here includes a piezoelectric source that has finite dimensions. The piezoelectric source is driven with a voltage and no assumptions were made about its vibration.

Although the above references were all concerned with infinite shells, many studies have been published on scattering from submerged finite shells. However, these studies do not include a realistic model for the acoustic source. A fairly recent publication in this group is that by Miller, Bao, and Uberall [17] in which they investigated acoustic scattering from elastic cylinders and cylindrical shells of finite length. Their investigation was both theoretical and experimental. For their theoretical model, they used a finite element code called SIERRAS that solved the coupled fluid-structure interaction problem. This study did not attempt to model any transduction process in the source or transducer-baffle interaction.

These are only a sampling of the publications on the scattering of a plane wave by a cylindrical elastic target, radiation from acoustic sources located on cylindrical geometries, and acoustic scattering from elastic cylindrical geometries of finite length.

Several different methods have been developed for determining the scattered pressure, and these methods may also be employed to solve the current transducer-baffle interaction problem. Four methods commonly used for determining the scattered pressure are: Modal Expansion, the Sommerfeld-Watson transformation, Fourier Transforms, and the Geometrical Theory of Diffraction.

A. Methodology

The modal expansion method begins with a modal decomposition of the incident wave in the coordinate system of the structure in which the wave is incident upon. Specifically for the plane strain model, each mode is a particular solution of the wave equation in cylindrical coordinates, with the coordinates r and θ separated. The θ dependence can also be considered as a Fourier series [18] which is the result of the periodic nature in the θ direction. With general expressions for the incident, scattered and transmitted pressure, which are in the form of modal expansions, the appropriate boundary conditions are applied and the unknown coefficients are solved for explicitly. The scattered pressure is a summation over the number of modes and an exact solution may be obtained with the aid of a computer. Additional terms are included in the summation until convergence is reached.

The Sommerfeld-Watson transformation converts the modal expansion for the scattered pressure into a residue series [19] at poles located at the zeroes of a determinant in the complex plane. This technique is used particularly at high frequencies where it takes many modes in the scattering summation for the function to converge while it only requires the contribution of a few poles in the residue series for convergence.

The Fourier Transform solution is similar to the modal expansion in that the radiated and scattered sound is expanded in a cylindrical coordinate system. A Fourier Transform with respect to the axial z coordinate is applied to the three-dimensional differential Helmholtz equation [20]. Upon integration over z , the transformed differential Helmholtz equation becomes two-dimensional. Taking advantage of the angular periodicity, the two-dimensional problem is further reduced to one dimension. Similar Fourier Transforms can be performed with respect to the z and θ coordinates for the elastic waves in the cylindrical shell. The boundary conditions can then be applied separately for each θ Fourier component. The inverse Fourier Transform is then used to obtain the scattered pressure.

The Geometrical Theory of Diffraction (GTD) is based on geometrical optics which describes the rays along which waves travel. When constructing the pressure field with a ray representation, one must determine all of the rays from the source location to a field point, including the direct ray, refracted rays, and reflected rays. The direct ray, refracted rays, and reflected rays are directly analogous to rays in optics. The Geometrical Theory of Diffraction introduces additional waves to approximately describe the spreading of waves, for example, GTD includes creeping waves. The laws of reflection and refraction are derived from Fermat's principle [21], also known as the Least Path principle and for each ray the optical length must be determined. This method gives insight into the behavior of the radiated and scattered fields; however, it is limited to high frequencies.

C. Summary

It has been shown that a lot of interest lies in this area of research and that in the past much effort has been placed on investigating the scattering of a plane wave by a cylindrical elastic target, radiation from acoustic sources located on cylindrical geometries, and acoustic scattering from elastic cylindrical geometries of finite length. Although much has been gained from the past works, there is still more to be gained from the present research.

CHAPTER III

MODELS

A. Introduction

In the study of transducer-baffle interactions two types of models will be utilized, an analytical model and a finite element model. Several configurations will be considered, but only the plane strain case of an ideal line source located in the vicinity of a water-loaded, thin, hollow, steel, cylindrical baffle will be solved with both an analytical and a finite element model. A confirmation of the finite element model will be accomplished by investigating the above case using the two different solution methods and comparing the results. The results predicted by the analytical model are used to verify the finite element results because this method of solution has been applied to similar geometries (as shown in the literature review) and the predictions were experimentally verified. All of the other configurations will be investigated with finite element models only. The following is a description of the theoretical basis of the analytic model:

B. Theory

The general wave equation for elastic waves in an extended homogeneous isotropic solid is expressed by Love [22] as:

$$(\lambda + 2G)\nabla\nabla \cdot \xi - G(\nabla \times \xi) = \rho_0 \frac{\partial^2 \xi}{\partial t^2} \quad (1)$$

where λ and G are the first two Lamé coefficients, $\vec{\xi}$ is the displacement vector and ρ_0 is the density of the material. The second Lamé coefficient, G , is the shear modulus.

The displacement is assumed to be the sum of two displacements, one associated with dilatational waves and the other associated with shear waves. Thus the displacement is of the form:

$$\vec{\xi} = -\nabla\phi + \nabla \times \vec{A} \quad (2)$$

where ϕ is a scalar potential and \vec{A} is a vector potential. From the Helmholtz theorem [23] which states that a vector field can be expressed as the sum of an irrotational field having a vanishing curl and a solenoidal field having a vanishing divergence, the wave equation can be separated into two components:

- (a) irrotational waves for which $\nabla \times \vec{\xi} = 0$
- (b) solenoidal waves for which $\nabla \cdot \vec{\xi} = 0$

For the irrotational wave one obtains

$$\nabla^2 \phi = \frac{1}{C_L^2} \frac{\partial^2 \phi}{\partial t^2} \quad (3)$$

where the dilatational wave speed in the solid is

$$C_L^2 = \frac{\lambda + 2\nu}{\rho_0} = \frac{B + \frac{4}{3}G}{\rho_0} \quad (4)$$

and B is the bulk modulus. This equation states there can be no transverse motion in the medium. For the solenoidal wave one obtains

$$\nabla^2 \vec{A} = \frac{1}{C_t^2} \frac{\partial \vec{A}}{\partial t^2} \quad (5)$$

where

$$C_t^2 = \frac{G}{\rho_o} \quad (6)$$

is the shear wave speed. This equation says that there will be no displacement in the direction in which the wave travels, i.e., the wave is entirely transverse. This wave is also referred to as a dilatationless wave.

For the line source in water, the sound field is a simple cylindrical wave which is expressed as a function of distance from the axis. However, in order to apply the appropriate boundary conditions later on, the equation for the field pressure must be translated to a (cylindrical) coordinate system whose axis coincides with the axis of the cylindrical baffle. The incident cylindrical wave and the scattered wave can each be expressed as a Fourier series in the polar angle θ as follows:

$$P_i = P_o \sum_n \varepsilon_n H_n^{(2)}(kd) \cos(n\pi) J_n(kr) \cos(n\theta) \quad (7)$$

$$P_s = P_o \sum_n \varepsilon_n C_n H_n^{(2)}(kr) \cos(n\theta) \quad (8)$$

where $\varepsilon_n = 1, n = 0$
 $\varepsilon_n = 2, n \geq 1$

and d is the distance from the center of the cylinder to the location of the line source, k is the wave number in the surrounding fluid, r is the distance to some field point referenced to the center of the cylinder, n is the number of modes of vibration, $H_n^{(2)}$ is the Hankel function of the second kind, J_n is the cylindrical Bessel function, and C_n is an unknown coefficient to be determined from the boundary conditions. P_o is the pressure amplitude and is related to the source volume velocity, Q_L , by:

$$P_o = \left| \frac{Q_L \omega \rho}{4} \right| \quad (9)$$

where ω is the angular frequency and ρ is the fluid density.

In the cylindrical layer there can exist both dilatational and shear waves. The scalar potential ϕ is symmetric about $\theta = 0$ degrees and is independent of z , as follows:

$$\phi = P_o \sum_n \varepsilon_n i^{-n} [A_n J_n(k_L r) + B_n Y_n(k_L r)] \cos(n\theta) \quad (10)$$

where A_n and B_n are unknown coefficients, k_L is the dilatational wave number, and Y_n is the cylindrical Neumann function. The vector potential \vec{A} is antisymmetric about $\theta = 0$ degrees so that the displacement derived from it will be symmetric about $\theta = 0$ degrees and is represented as follows:

$$A = P_o \sum_n \varepsilon_n i^{-n} [D_n J_n(k_s r) + E_n Y_n(k_s r)] \sin(n\theta) \quad (11)$$

where D_n and E_n are unknown coefficients and k_s is the shear wave number. Inside the cylinder (in the enclosed fluid medium) there is a compressional wave expressed as:

$$P_f = P_o \sum_n \epsilon_n i^{-n} M_n J_n(k_f r) \cos(n\theta) \quad (12)$$

where M_n is an unknown coefficient and k_f is the wave number in this fluid. The coefficient associated with the Neumann function (also referred as the Bessel function of the second kind) is zero because the origin is in the sound field domain and the solution must be bounded at $r=0$. The following boundary conditions are applied at the inner ($r=a$) and outer ($r=b$) surfaces of the cylinder.

- (i) normal displacements are continuous
- (ii) normal stresses are continuous
- (iii) tangential stresses are zero

After the boundary conditions are applied, there will be six equations and six unknowns (A_n, B_n, C_n, D_n, E_n , and M_n), and Cramers rule [24] may be employed to solve for the system of linear equations for the unknown coefficients. Once C_n is known the scattered pressure will be fully defined.

The scattered pressure is as follows:

$$P_s = P_o \sum_n \epsilon_n C_n H_n^{(2)}(kr) \cos(n\theta) \quad (13)$$

C_n can be written as the quotient of two 6x6 determinants, $C_n = \frac{|a_{ij}|}{|b_{ij}|}$. The expressions for these coefficients can be found in Neubauer's text on *Acoustic Reflection from Surfaces and Shapes* [25].

C. Analytical Model

For an ideal line source located near a hollow cylindrical baffle (figure 1.1b), an analytical model was developed based on the modal expansion technique. Existing FORTRAN code for back scattering of a plane incident wave from a hollow cylinder with air backing (written at Georgia Institute of Technology) was altered to describe a cylindrical incident wave because a line source is located near the baffle and the wave front curvature cannot be ignored. The analytical model assumes a time dependence of $e^{-i\omega t}$. From the analytical model one obtains the normal velocity on the outer and inner surface of the cylinder, far-field scattered pressure, far-field total pressure, and the pressure at any specified location, all as a function of θ . The following is the information necessary for the analytical model:

- the inner radius of the cylinder, 31.75 (cm)
- the outer radius of the cylinder, 34.29 (cm)
- the shear speed in the steel cylinder, 31060 (cm/s)
- the dilatational speed in the steel cylinder, 55940 (cm/s)
- the density of the inner fluid (air), 0.001293 (g/cm³)
- the density of the outer fluid (water), 1(g/cm³)
- the sound speed in the inner fluid (air), 34400 (cm/s)
- the sound speed in the surrounding fluid (water), 148200 (cm/s)
- excitation frequencies, f , of 1376 and 3439 (Hz)
- the location of the ideal line source referenced to the cylindrical axis, 36.83 (cm)
- the pressure amplitude of the source, $P_o = \left| \frac{Q_L \omega \rho}{4} \right|$ (Pa)
- θ start, finish and step are 0.0, 360.0, and 5.0 (deg), respectively

D. Finite Element Model

The finite element program SARA-2D [1] is used for the combined modeling of the finite baffle and the piezoelectric source, including the interaction between the two. The following description of SARA-2D is taken from information contained in a user's manual. SARA-2D solves the time harmonic problem of a structure submerged in an infinite fluid subjected to incident traveling waves or to displacements and/or forces within the structure. SARA stands for Structural Acoustics Response Analysis and the 2D refers to the two-dimensional version of the program. Finite elements are used to model both the structure and a portion of the fluid field (see appendix A); conventional displacement elements are used for the structure, and pressure-type acoustic elements are used for the external near-field. The remaining unbounded external fluid is modeled with infinite elements that include in their formulation the outward traveling and decaying wave. The coupled fluid-structure model results in a complex, symmetric, banded set of equations that can be efficiently solved by Gaussian elimination [26] for the structural displacements and fluid pressures. From the normal velocities and pressures at the fluid-structure interface, the near-field and far-field response is obtained using the Helmholtz integral equation [20]. All loading and response quantities are represented in a Fourier series [18] with a time dependence of $e^{i\omega t}$. The equations for the Fourier modes are uncoupled and each is solved separately for the coefficients of the response quantities. The actual response is obtained using superposition of modes. A frontal solver is used to process the equations element by element, alternating the assembly and elimination phases.

E. Elements

In both the axisymmetric and plane strain models quadrilateral elements were used for the baffle. Each node of a quadrilateral element has two translational degrees of freedom. For the near-field fluid and the infinite fluid, fluid and infinite fluid elements were used, each of these have only one degree of freedom, pressure. The sources are modeled with piezoelectric elements, each node of which has three degrees of freedom, two translations and one electric potential. Coupling elements were used at the fluid-structure interfaces. A coupling element translates between the displacement degree of freedom of the structure and the pressure degree of freedom of the fluid.

When constructing a finite element model it is important that the model contain enough elements to simulate the problem. On the other hand, if there are too many elements, the model is unnecessarily inefficient. As a rule of thumb, the number of elements required to accurately model the behavior is eight elements per wavelength at the highest frequency of interest. The current configurations contain several wavelengths and the acoustic wavelength will be used in determining the number of elements, then a mesh convergence study will be conducted to determine if the model accurately simulates the problem. The mesh convergence study is important because the acoustic wavelength is not the shortest wavelength in the system. In determining the number of elements needed for the plane strain model, first it is necessary to compute the mean circumference, c

$$c = 2\pi r \quad (14)$$

where r is the mean radius of the cylinder. In this model, $r = 0.3302$ m, thus $c = 2.075$ m. To have eight elements per wavelength at 3439 Hz,

$$\frac{\lambda}{8} = \frac{1500.0}{(3439.0)8.0} = 0.0545 \text{ m/elements}$$

Thus the necessary number of elements to accurately model the cylindrical baffle is $\frac{2.075}{0.0545} = 39$ elements. The method of determining the number of elements for the axisymmetric model is the same as above only there are two different regions to consider: the length of the cylinder wall, and the end caps. For this model, it was determined that 39 elements were needed for each end cap and 24 elements were needed for the cylindrical body. The results of the mesh convergence study are shown in Table 3.1 which represents the number of elements per every wavelength in the system for both the plane strain and axisymmetric models.

TABLE 3.1

Number of elements/wavelength used in the finite element models.

Plane Strain Model:

WAVE TYPE	CIRCUMFERENCE OF STRUCTURE	RADIALLY
Acoustic in water	16	6
Flexural in structure	10	
Extensional in structure	59	
Flexural in projector	5	
Extensional in projector	37	

Axisymmetric Model:

WAVE TYPE	CIRCUMFERENCE OF END CAPS	RADIALLY	LENGTH OF STRUCTURE
Acoustic in water	33	6	6
Flexural in structure	20		4
Extensional in structure	117		23
Flexural in projector			6
Extensional in projector			39

For the plane strain and axisymmetric finite element models, the following assumptions were made:

- material properties were linear
- no losses

In addition to the above assumptions, the plane strain model assumed no variation of displacement along the length (z-axis)- zero axial displacement and the axisymmetric model assumed no variation of displacement in x-direction at $x=0$ for any y position.

F. Material Properties

For the finite element model each piezoelectric source is Navy Type I, with material properties taken to be those found in Wilson [27]. The properties specified in the models that defined the piezoelectric sources are shown in Table 3.2. In Table 3.2, d_{ij} are the piezoelectric constants, s_{ij}^E are the elastic compliance constants measured at constant electric field, ρ is the density, ϵ_0 is the permittivity of free space (8.85×10^{-12} farads/meter), and $\frac{\epsilon_{ij}^s}{\epsilon_0}$ are the relative dielectric constants measured at constant strain.

The directivity of the 4.5 °, 9.0 °, and the 18.0 ° piezoelectric line sources in the free-field and driven with the voltages specified in Table 3.1 are shown in Figure 3.1, both for $ka=2$ and 5 respectively. All of the sources are omnidirectional at $ka=2$ and 5, except for the 18.0 ° piezoelectric line source which begins to show some directivity at $ka=5$. The introduction of directivity is due to the arc length of the source, it is a quarter of the acoustic wavelength. The free-field directivity was obtained from the plane strain finite element model in which the cylindrical baffle was replaced with fluid and the interior vacuum was filled in with fluid (see appendix A for drawing).

TABLE 3.2

The material properties of Navy Type I used in the finite element model.

PARAMETER	VALUE	UNITS
d_{31}	-123×10^{-12}	C/N
d_{33}	289×10^{-12}	C/N
d_{15}	496×10^{-12}	C/N
s_{11}^E	12.3×10^{-12}	m^2/N
s_{12}^E	-4.05×10^{-12}	m^2/N
s_{13}^E	-5.31×10^{-12}	m^2/N
s_{33}^E	15.5×10^{-12}	m^2/N
s_{44}^E	39.0×10^{-12}	m^2/N
$\frac{\epsilon_{11}^r}{\epsilon_0}$	730	unitless
$\frac{\epsilon_{33}^r}{\epsilon_0}$	635	unitless
ρ	7500.0	kg/m^3

The other materials used in the finite element model were found in Kinsler and Frey [28]; these values are shown in Table 3.3.

TABLE 3.3

The material properties of steel and water used in the finite element model.

MATERIAL	PARAMETER	VALUE	UNITS
Steel	E	19.5X10 ¹⁰	Pa
	ν	0.28	unitless
	ρ	7700.0	kg/m ³
Water	ρ	1000.0	kg/m ³
	c	1500.0	m/s

G. Source Drive

For the plane strain finite element model one of the sound sources is an ideal line source that is infinite in length, radially dimensionless, and uniformly pulsating. In the free-field, there will only be an outward traveling wave. The magnitude of the pressure at any distance r from the source in the free-field is expressed as:

$$|P(r)| = \left| \frac{Q_L \omega \rho}{4} H_0^{(2)}(kr) \right|, \quad (15)$$

where $H_0^{(2)}(kr) = \frac{1}{\sqrt{r}} e^{ikr}$, so that the magnitude of the pressure in the far-field is found to be

$$|P_f(r)| = \frac{1}{\sqrt{r}} \left| \frac{Q_L \omega \rho}{4} \right|. \quad (16)$$

Extrapolating the far-field pressure to a reference distance of $r = 1$ meter gives

$$|P_o| = |P_r(1m)| = \left| \frac{Q_L \omega \rho}{4} \right|. \quad (17)$$

The volume velocity of the line source, Q_L , required to produce a specified sound pressure at 1 meter (extrapolated from the far-field) for a 1000 Hz signal is determined as follows:

$$|Q_L| = \left| \frac{4P_o}{\omega \rho} \right|, \quad (18)$$

where P_o is the extrapolated pressure at $r=1$ meter. A pressure of 20 Pa was chosen to define Q_L because it is a typical pressure used in the experimental work at Georgia Tech. Resulting in a value of $Q_L = 31.73 \times 10^{-06} \text{ m}^3 / \text{s}$. This volume velocity is used to define the ideal line source in both the analytical and finite element model. The following information will be used to determine the required voltage for each piezoelectric source to produce the same volume velocity as that of the ideal line source.

- the angular frequency ω (rad/sec)
- the change in volume, $\Delta V_o = \frac{Q_L}{\omega}$ (m^3)
- the mean radius of the source, $R = 0.3302$ (m)
- the angle the source subtends, θ_s , (the three cases observed are 4.5, 9.0, and 18.0 deg)
- the thickness of the sources, $t=0.0127$ (m)

- the arc length of the source, $s = \frac{R\theta\pi}{180.0}$ (m)
- the average cross-sectional area of each source, $a = st$ (m²)
- the volume per unit length of each source, $V_o = a \cdot 1$ (m³)
- the electric field in the poled direction, $E_3 = \frac{\phi_o}{t}$ (C/m²)
- the piezoelectric coefficients, $d_{31} = -123 \times 10^{-12}$ and $d_{33} = 289 \times 10^{-12}$ (C/N)
- the strain in the x, y, and z direction, $S_1 = d_{31}E_3$, $S_2 = d_{31}E_3$, and $S_3 = d_{33}E_3$
- the volumetric strain $\frac{\Delta V_o}{V_o} = S_1 + S_2 + S_3$

Definition (11) assumes that the stresses and corresponding strains due to the fluid loading are negligible. This is a reasonable assumption since the strain is predominately due to the electric field. The voltage is determined to be

$$\phi_o = \frac{\left[\frac{\Delta V_o}{V_o} \right] t}{2d_{31} + d_{33}} \text{ (volts).} \quad (19)$$

The required voltage to produce the same volume velocity as that of the ideal line source is shown for each finite piezoelectric source at the two frequencies of interest in Table 3.4. Note that the ideal line source is specified by a volume velocity and the piezoelectric sources are driven with a voltage. The velocity of the piezoelectric surface and the applied voltage are related by

$$\text{velocity} = d_{33} V_o j\omega \quad (20)$$

where V_0 is the voltage amplitude. The relationship between the ideal line source drive and that of the finite piezoelectric drive shows a 90° phase difference. This 90° phase difference will be taken into account in presenting the results.

TABLE 3.4

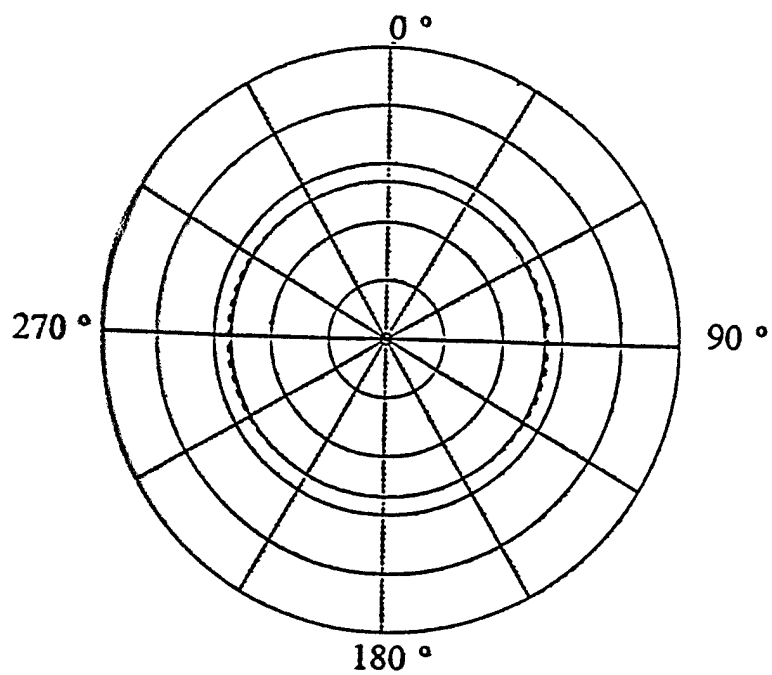
The required voltage for each source to produce the same volume velocity as the ideal line source.

INCLUDED ANGLE OF SOURCE (degrees)	ELECTRIC DRIVE (Volts)	FREQUENCY (Hertz)
4.5	1706.0	1376
4.5	682.0	3439
9.0	853.0	1376
9.0	342.0	3439
18.0	427.0	1376
18.0	172.0	3439

H. Verification of the Finite Element Model

Comparisons are made between the analytical model and the finite element model, which is plane strain, that contains the ideal line source. The following data will show the normal velocity and the total pressure on the outer surface of the cylinder due to the line source excitation. All of the above mentioned results are at the two frequencies, 1376 and 3439 Hz. The geometry for both the analytical and finite element model is shown in figure 1.1b, which shows that the source is symmetric about zero degrees. The line source used to predict the following data is dimensionless, it is an ideal line source. Figures 3.2 through 3.5 show the normal velocity on the outer surface of the cylinder, Figures 3.6

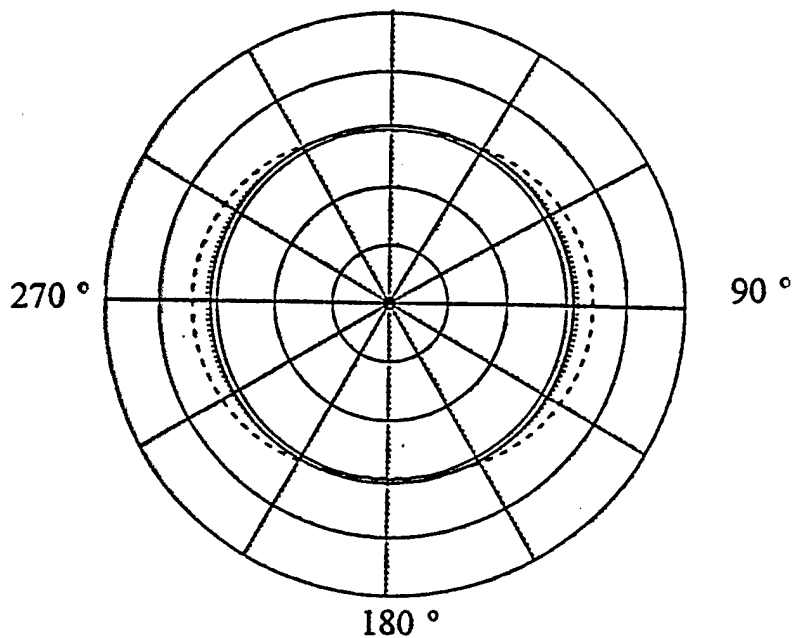
through 3.9 show the total pressure on the outer surface of the cylinder. The finite element and analytical results differ the most at zero degrees and this percent difference remains within 1 dB. A good error estimate for the analytical and finite element models is not known hence an explanation of the difference at zero degrees between that of the finite element and analytical results cannot be given. However, this error is small and the results from the finite element model correlate well with the results from the analytical model. Therefore, from the data it is safe to say that the finite element model is accurate and the remainder of the research will be based on the finite element results.



180 °

(a)

0 °



180 °

(b)

Figure 3.1 Directivity pattern of three piezoelectric line sources under free-field conditions at $ka=2$ (a) and $ka=5$ (b). The piezoelectric line sources are: 4.5° (solid line), 9.0° (dotted line), and an 18.0° (dashed line). 10 dB/division.

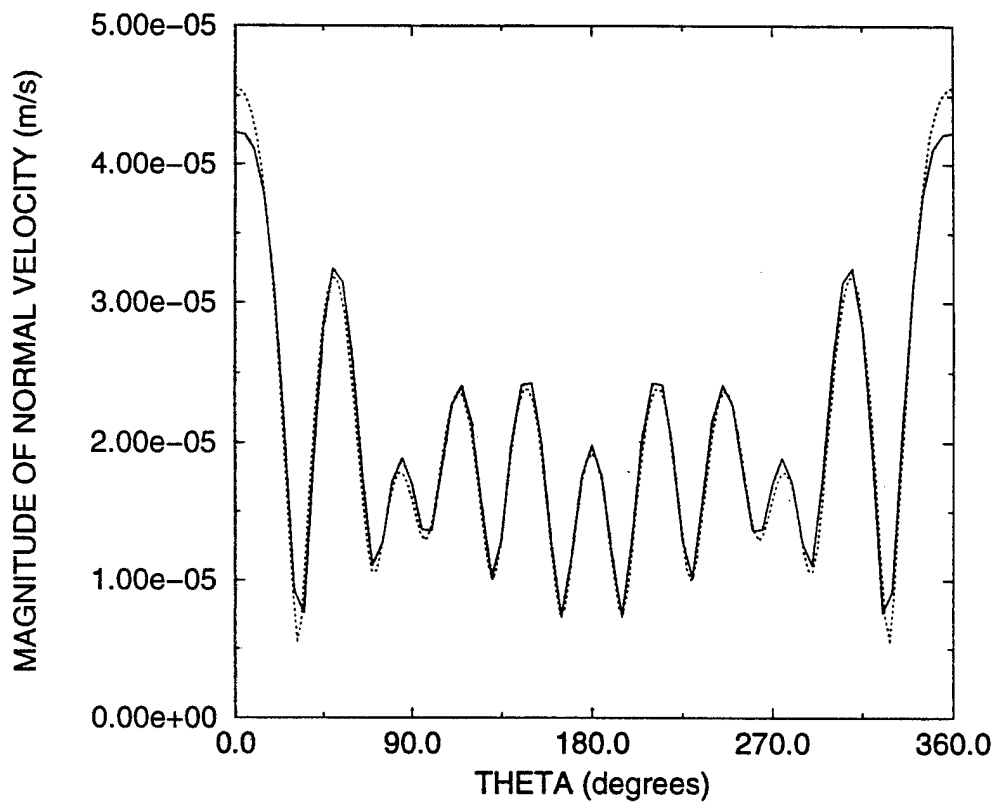
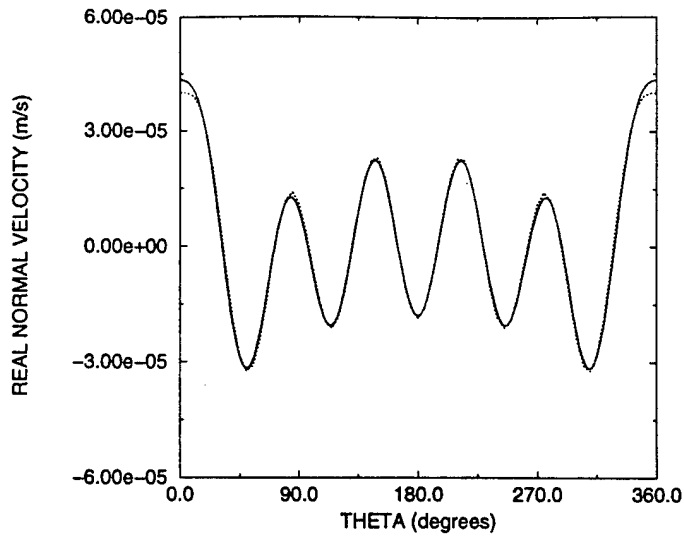
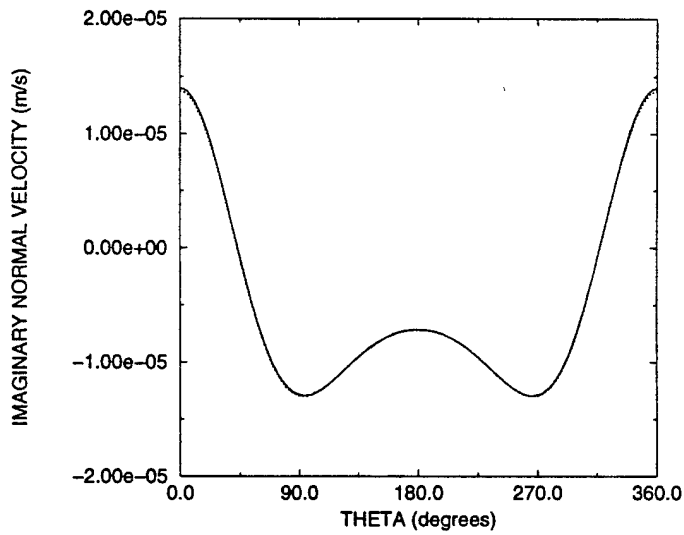


Figure 3.2 Magnitude of normal velocity on the outer surface of the cylinder versus theta at $ka=2$, for an ideal line source excitation located at zero degrees. The solid line is the analytical solution and the dotted line is the finite element solution.



(a)



(b)

Figure 3.3 (a) real normal velocity on the outer surface of the cylinder (b) imaginary normal velocity on the outer surface of the cylinder, both are at $ka=2$ and are due to an ideal line source excitation located at zero degrees. The solid line is the analytical solution and the dotted line is the finite element solution.

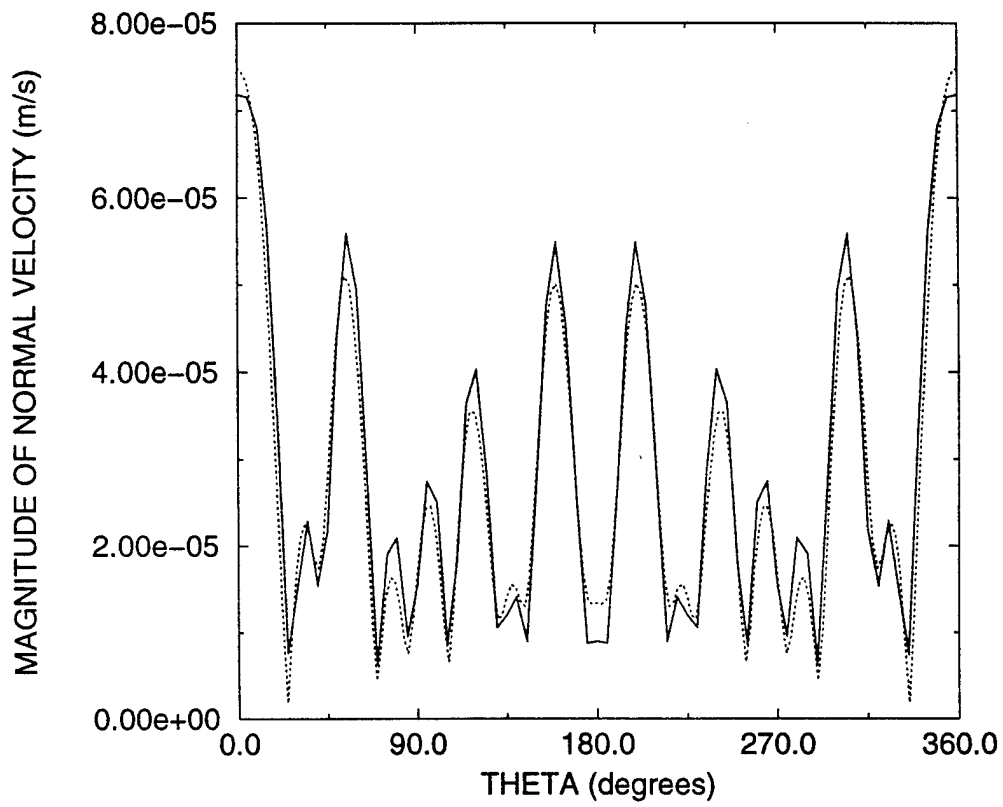
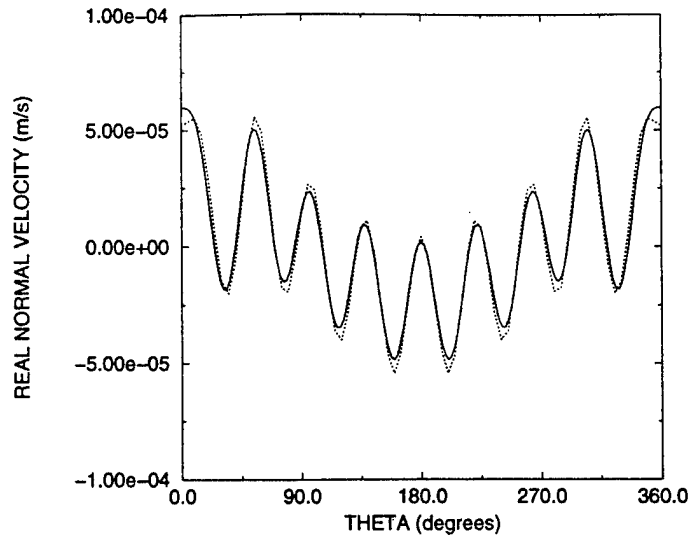
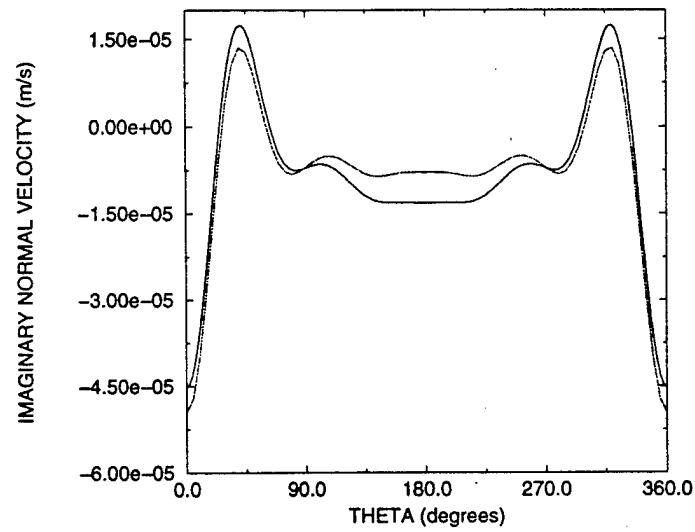


Figure 3.4 Magnitude of normal velocity on the outer surface of the cylinder at $ka=5$ for an ideal line source excitation located at zero degrees. The solid line is the analytical solution and the dotted line is the finite element solution.



(a)



(b)

Figure 3.5 (a) real normal velocity on the outer surface of the cylinder, (b) imaginary normal velocity on the outer surface of the cylinder, both are at $ka=5$ for an ideal line source excitation located at zero degrees. The solid line is the analytical solution and the dotted line is the finite element solution.

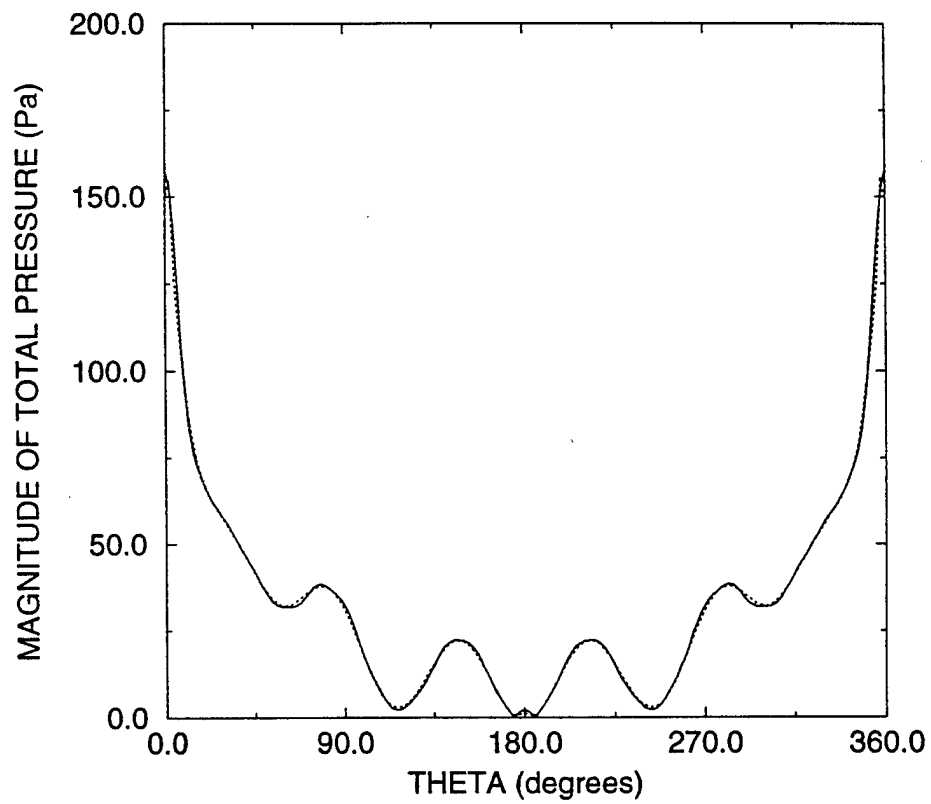
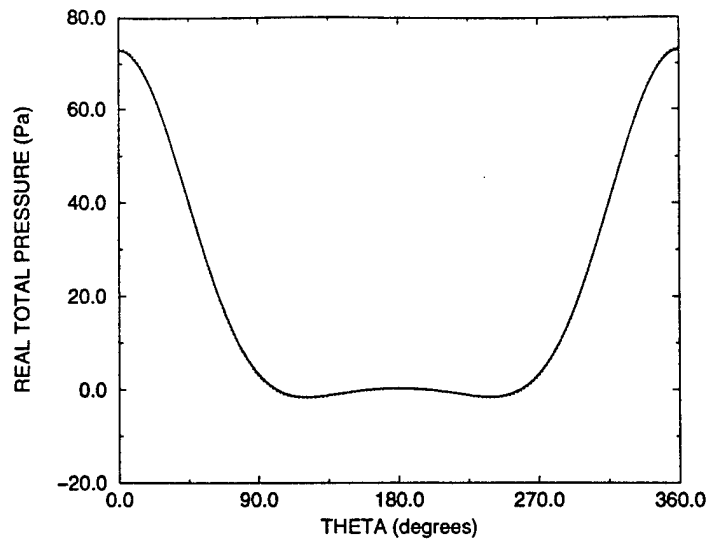
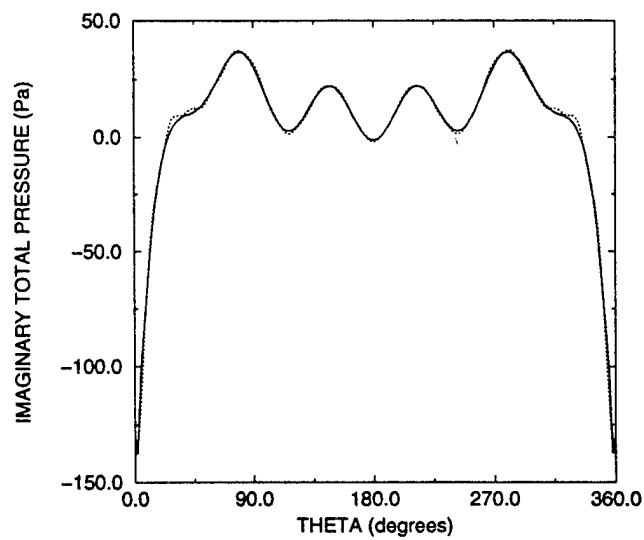


Figure 3.6 Magnitude of total pressure on the outer surface of the cylinder at $ka=2$ for an ideal line source excitation located at zero degrees. The solid line is the analytical solution and the dotted line is the finite element solution.



(a)



(b)

Figure 3.7 (a) real total pressure on the outer surface of the cylinder, (b) imaginary total pressure on the outer surface of the cylinder, both are at $ka=2$ for an ideal line source excitation located at zero degrees. The solid line is the analytical solution and the dotted line is the finite element solution.

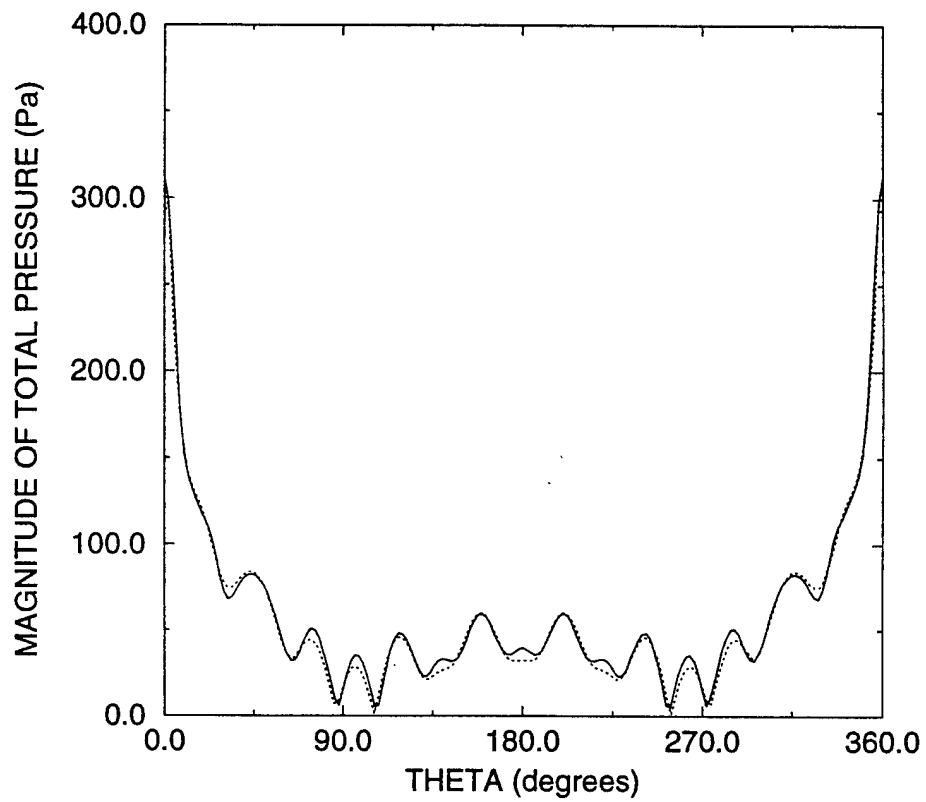
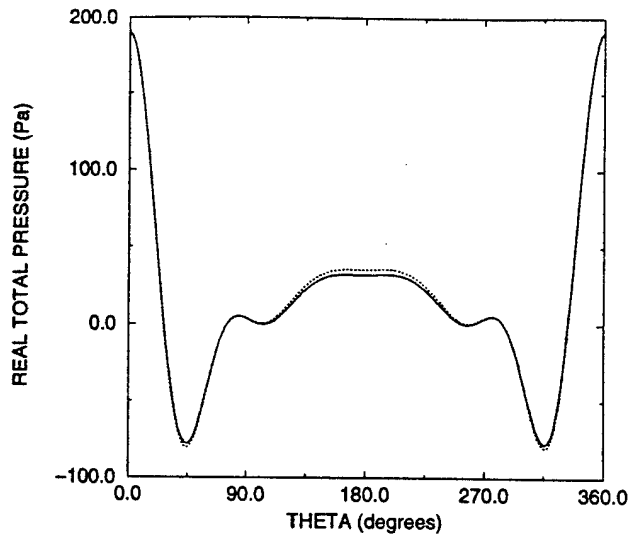
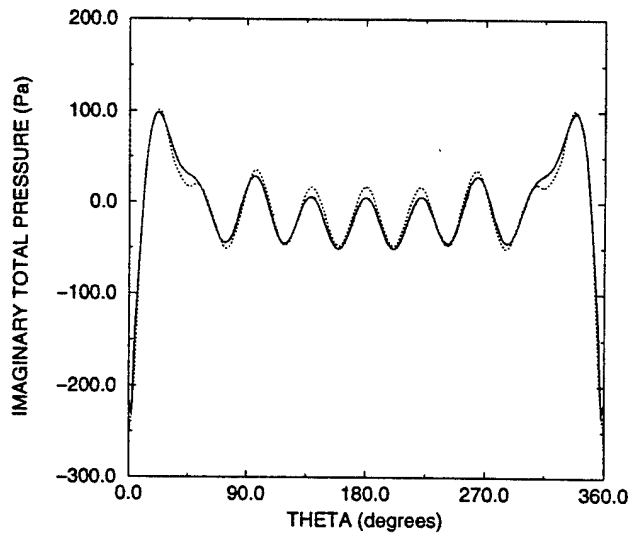


Figure 3.8 Magnitude of total pressure on the outer surface of the cylinder at $ka=5$ for an ideal line source excitation located at zero degrees. The solid line is the analytical solution and the dotted line is the finite element solution.



(a)



(b)

Figure 3.9 (a) real total pressure on the outer surface of the cylinder, (b) imaginary total pressure on the outer surface of the cylinder, both are at $ka=5$ for an ideal line source excitation located at zero degrees. The solid line is the analytical solution and the dotted line is the finite element solution.

CHAPTER IV

RESULTS and DISCUSSION

A. Introduction

The results and discussion presented in this chapter for the plane strain model are arranged under the following main topics:

(1) The normal velocity and the acoustic pressure at the surface of the baffle, and the use of this data to determine what elastic waves are excited in the baffle by the adjacent projector;

(2) The far-field pressure directivity patterns for the projector-baffle system and comparison with the directivity patterns for the same projector under free-field conditions;

(3) The transmitting voltage response (TVR) of the projector in the vicinity of the baffle and comparison with the corresponding TVR of the projector under free-field conditions;

(4) Comparison of the ideal source to the finite piezoelectric source.

B. Plane Strain Model

The elastic waves excited in the baffle are determined from analysis of the calculated normal velocity on the baffle surface. Plots of the velocity data show a standing wave pattern which is analyzed as follows:

(1) The separation between adjacent velocity magnitude peaks is determined and compared with estimated values of $\frac{\lambda}{2}$ for flexural and extensional waves in the baffle.

(2) The wavenumber spectrum for the normal velocity is calculated and peak wavenumbers in the spectrum are related to elastic waves in the baffle.

It is useful for this analysis to estimate the flexural and extensional wavelengths in both the baffle and the projector. Here we assume that the flexural and extensional waves have approximately the same phase speeds in the cylinder as in an equivalent thin plate. This approximation was introduced in chapter I, section B. The phase velocity of extensional and flexural waves in a thin plate [2] are:

$$c_E = \left(\frac{E}{\rho(1-\nu^2)} \right)^{\frac{1}{2}} \quad (21)$$

$$c_F = \left(\frac{Eh^2}{12\rho(1-\nu^2)} \right)^{\frac{1}{4}} \omega^{\frac{1}{2}} \quad (22)$$

where E is Young's modulus, ν is Poisson's ratio, ρ is the density, and h is the plate thickness. The wavelengths calculated from c_E and c_F are presented in Table 4.1 in which the material properties from Table 3.2 and 3.3 were used.

TABLE 4.1

Calculated wavelengths.

WAVE TYPE	ka=2	ka=5
acoustic in water	1.09 (m)	0.436 (m)
flexural (in structure)	0.419 (m)	0.265 (m)
extensional (in structure)	3.81 (m)	1.52 (m)
flexural (in projector)	0.242 (m)	0.153 (m)
extensional (in projector)	2.51 (m)	1.00 (m)

In Figure 4.1 one finds the angle between two adjacent magnitude peaks in the cylinder to be approximately 35° , which gives an arc length of 0.209 meters. The arc length is equivalent to a half-wavelength because it is the distance between two peaks on a magnitude plot. The corresponding real and imaginary velocities are shown in Figure 4.2. For the case of $ka=5$ the angle between two velocity peaks in Figure 4.3 is found to be approximately 20° , which gives an arc length of 0.120 meters. Again the arc length represents a half-wavelength and the corresponding real and imaginary velocities are shown in Figure 4.4. By doubling these values, we find that the wavelength at each of the two frequencies is approximately equivalent to the flexural wavelength calculated in a one-inch thick, infinite steel plate.

Another factor to investigate in the results obtained from the velocity profile is the number of wavelengths along the circumference. By dividing the circumference of the cylinder by the appropriate wavelength we can determine the number of flexural and extensional wavelengths that can exist in the cylinder. For $ka=2$, there can be five flexural wavelengths and one-half of an extensional wavelength around the circumference. For $ka=5$, there can be eight flexural and one-and-one-half extensional wavelengths. From the data presented, it is seen that the real normal velocity for $ka=2$ and 5 (Figures 4.2 and 4.4) contains five and eight wavelengths respectively. The above analysis could also be done with the total pressure on the baffle surface (Figures 4.5 through 4.8). Therefore, it is believed that the dominant waves propagating in the cylinder are flexural.

An alternate way of analyzing the velocity data is to determine the wavenumber spectrum for the normal velocity standing wave pattern. The wavenumber spectrum is a result of wave vector analysis and is determined by taking the spatial Fourier Transform [15] of the normal velocity profile. A wavenumber spectrum is a representation of wave amplitude versus wavenumber and may be used with any type of wave that is a function of

space. The result of the wave vector analysis is a wavenumber spectrum in which the peaks represent the dominant propagating waves. This analysis was only performed for the plane strain case, in which the Fourier Transform is carried out with respect to the circumference of the shell. Figures 4.9 through 4.14 show the results of the wave vector analysis. At $ka=2$ the flexural and the extensional wavenumbers are 14.9 and 1.73 m^{-1} respectively. From Figures 4.9, 4.10, and 4.11 it is seen that the greatest wavenumber is approximately 15 m^{-1} and that the extensional wave is not significant. At $ka=5$ the flexural and the extensional wavenumber are 23.7 and $4.32 \text{ (m}^{-1}\text{)}$ respectively; Figures 4.12, 4.13, and 4.14 show that the flexural wave is definitely the dominant propagating wave. When comparing the wave amplitude as a function of wavenumber for $ka=2$ and 5 it is seen that the extensional wave is significant at $ka=5$ and hardly detectable at $ka=2$. This is because at $ka=5$, the circumference of the cylinder can support a complete extensional wavelength and at $ka=2$, it cannot. A wavenumber of zero corresponds to the breathing mode. The modes of vibration in the cylinder are only a function of circumferential length because the model is plane strain and therefore there will be no coupling between axial and circumferential modes. At both frequencies there are other small peaks appearing with k values that lie between that of the extensional and flexural waves. The small peaks in the wavenumber spectrum do not correspond to physical waves. These peaks are side lobes in the Fourier transform due to the finite length of the data window, where the finite length is the circumference of the shell. It should be noted that the spectrum is not symmetrical about the main peak. The wavenumber amplitudes are larger in the low k region. Therefore it is possible that in this region the spectrum includes other physical waves such as the fast, extensional wave, or an evanescent wave. The loss in resolution due to the side lobes is a limitation of the Fourier transform. Possibly a better resolution for the wavenumber spectrum can be obtained by using a

different signal processing procedure, for example, the Prony method. The present analysis is limited to only investigating the dominant waves. It is concluded that the waves propagating circumferentially in the cylinder are predominantly flexural.

The modes of vibration of the baffle depend on the types of waves that propagate in it. The combination of flexural and extensional waves (which are the two lowest Lamb waves) in the baffle provide its displaced shape. To have a basis for comparison of the displaced shape of the cylinder for the different finite sources, the undisplaced mesh is presented in Figure 4.15. Figures 4.16 through 4.21 show the displaced shape of the cylinder. The predominant motion of the cylinder is bending, although some stretching is detectable. The bending motion of the cylinder is due to the flexural wave, which is subsonic. The stretching motion of the cylinder is due to the extensional wave, which is supersonic. As was discussed in chapter I, section B, subsonic waves decay exponentially with distance. Although the extensional wave is supersonic, it produces a much smaller displacement than the flexural wave, hence, an extensional mode is not very good at producing a large net volume change. The relative contributions of these elastic waves in the cylinder, to the scattered far-field pressure cannot be concluded from these results.

The scattered far-field pressure can be seen in Figures 4.22 and 4.23 for $ka=2$ and 5, respectively. At $ka=2$ the scattered far-field pressure is somewhat omnidirectional. The scattered far-field pressure at $ka=5$ is directive. As shown in Figure 4.23, it is seen that the majority of the sound is in the back ($\theta=180^\circ$) and there is no significant nulls. To understand what portion of the scattered far-field pressure is due to the elasticity of the cylinder two additional directivity patterns are included (Figures 4.24 and 4.25). These figures show the scattered far-field pressure due to an ideal line source excitation from an elastic cylinder and from an equivalent rigid cylinder at $ka=2$ and 5 respectively. From these figures it is concluded that the scattered far-field pressure is dominated by the

elasticity of the cylinder. In both cases there is symmetry about zero degrees and the scattered far-field pressure is relatively the same for each source excitation.

The total far-field pressure (Figures 4.26 and 4.27) is the combination of the scattered pressure and that radiated from the source in the far-field, extrapolated to one meter. For comparison, the directivity patterns of the finite projectors are relatively omnidirectional (see Figures 3.1a and 3.1b). At $ka=2$ there is a null at $\theta=0^\circ$. This is caused by the cancellation of the source radiation and the structure scattering in this direction. The total far-field pressure at $ka=5$ is directive, as shown in Figure 4.27. It is seen that the 4.5° and the 9.0° piezoelectric sources have essentially the same effect on the cylinder; however, the results for the 18.0° piezoelectric source are different. This is caused by the interaction between the baffle and the transducer. The transducer's size is now apparent; the 18.0° piezoelectric source cannot be considered to be transparent.

In the process of studying the effect of the structure on the source it is important to observe the Transmitting Voltage Response (TVR) because it is an important parameter for a projector transducer. The TVR describes how efficient the transducer is in radiating sound in any specified direction. The Transmitting Voltage Response is

$$TVR = \frac{\text{Far - field sound pressure in specified direction}}{\text{Voltage applied across electrical input terminals}} = \frac{P_f(R_o, \theta, \phi)}{V_d} \quad (23)$$

where the far-field pressure P_f is extrapolated from the far-field to a reference distance R_o . Usually $R_o=1$ meter. The angles θ and ϕ specify the direction along which the pressure is measured. For the plane strain model, the TVR is presented in Tables 4.2 through 4.7. The tables show the TVR of the source radiation only as a function of the size of the source, for the source under both free-field conditions and while in the vicinity

of the cylinder. Also included in the tables is the TVR of the combined radiation and scattering of the source and baffle.

TABLE 4.2

Transmitting voltage response of a 4.5° piezoelectric source under free-field conditions, while in the vicinity of the structure, and of the source-baffle system, at $ka=2$.

THETA (degrees)	TVR (dB re 1Pa/V @ 1m) source-baffle system	TVR (dB re 1Pa/V @ 1m) source near structure	TVR (dB re 1Pa/V @ 1m) source in free- field
0	-33.970	-37.707	-37.644
15	-34.056	-37.701	-37.639
30	-34.107	-37.687	-37.625
45	-34.257	-37.669	-37.607
60	-34.869	-37.652	-37.591
75	-36.058	-37.641	-37.579
90	-38.158	-37.638	-37.576
105	-42.559	-37.646	-37.581
120	-55.273	-37.661	-37.595
135	-47.901	-37.681	-37.613
150	-40.945	-37.700	-37.630
165	-37.967	-37.713	-37.642
180	-37.170	-37.717	-37.646

TABLE 4.3

Transmitting voltage response of a 9.0° piezoelectric source under free-field conditions, while in the vicinity of the structure, and of the source-baffle system, at $ka=2$.

THETA (degrees)	TVR (dB re 1Pa/V @ 1m) source-baffle system	TVR (dB re 1Pa/V @ 1m)so source near structure	TVR (dB re 1Pa/V @ 1m) source in free- field
0	-27.490	-31.730	-31.678
15	-27.569	-31.714	-31.664
30	-27.833	-31.671	-31.624
45	-28.081	-31.613	-31.570
60	-27.939	-31.556	-31.517
75	-27.638	-31.516	-31.478
90	-27.478	-31.505	-31.465
105	-27.613	-31.527	-31.480
120	-28.571	-31.576	-31.520
135	-30.651	-31.642	-31.574
150	-33.418	-31.706	-31.629
165	-35.870	-31.754	-31.669
180	-36.877	-31.771	-31.684

TABLE 4.4

Transmitting voltage response of a 18.0° piezoelectric source under free-field conditions, while in the vicinity of the structure, and of the source-baffle system, at $ka=2$.

THETA (degrees)	TVR (dB re 1Pa/V @ 1m) source-baffle system	TVR (dB re 1Pa/V @ 1m) source near structure	TVR (dB re 1Pa/V @ 1m) source in free-field
0	-22.616	-25.697	-25.821
15	-22.543	-25.650	-25.767
30	-22.646	-25.522	-25.621
45	-23.473	-25.351	-25.426
60	-24.910	-25.182	-25.236
75	-25.893	-25.063	-25.099
90	-25.775	-25.026	-25.047
105	-25.456	-25.081	-25.092
120	-25.771	-25.216	-25.223
135	-26.501	-25.399	-25.407
150	-27.457	-25.581	-25.596
165	-28.707	-25.715	-25.739
180	-29.363	-25.764	-25.792

TABLE 4.5

Transmitting voltage response of a 4.5° piezoelectric source under free-field conditions, while in the vicinity of the structure, and of the source-baffle system, at $ka=5$.

THETA (degrees)	TVR (dB re 1Pa/V @ 1m) source-baffle system	TVR (dB re 1 Pa/V @ 1m) source near structure	TVR (dB re 1Pa/V @ 1m) source in free-field
0	-22.920	-26.125	-25.953
15	-23.434	-26.086	-25.917
30	-24.461	-25.911	-25.832
45	-22.880	-25.869	-25.724
60	-21.760	-25.753	-25.621
75	-22.641	-25.674	-25.551
90	-26.006	-25.655	-25.534
105	-27.873	-25.699	-25.574
120	-36.352	-25.798	-25.662
135	-32.817	-25.927	-25.778
150	-24.998	-26.053	-25.890
165	-22.855	-26.141	-25.969
180	-21.938	-26.167	-25.993

TABLE 4.6

Transmitting voltage response of a 9.0° piezoelectric source under free-field conditions, while in the vicinity of the structure, and of the source-baffle system, at $ka=5$.

THETA (degrees)	TVR (dB re 1Pa/V @ 1m) source-baffle system	TVR (dB re 1 Pa/V @ 1m) source near structure	TVR (dB re 1Pa/V @ 1m) source in free-field
0	-16.515	-20.493	-20.152
15	-16.720	-20.365	-20.057
30	-17.795	-20.024	-19.804
45	-17.616	-19.580	-19.473
60	-16.043	-19.163	-19.159
75	-15.502	-18.874	-18.942
90	-17.181	-18.777	-18.873
105	-18.673	-18.892	-18.969
120	-21.220	-19.196	-19.213
135	-29.838	-19.624	-19.555
150	-29.433	-20.072	-19.912
165	-23.376	-20.413	-20.184
180	-21.164	-20.483	-20.285

TABLE 4.7

Transmitting voltage response of a 18.0° piezoelectric source under free-field conditions, while in the vicinity of the structure, and of the source-baffle system, at $ka=5$.

THETA (degrees)	TVR (dB re 1Pa/V @ 1m) source-baffle system	TVR (dB re 1 Pa/V @ 1m) source near structure	TVR (dB re 1Pa/V @ 1m) source in free-field
0	-19.474	-9.352	-14.974
15	-14.886	-9.437	-14.556
30	-11.079	-9.669	-13.525
45	-7.787	-9.989	-12.326
60	-7.624	-10.306	-11.311
75	-8.984	-10.497	-10.658
90	-12.450	-10.439	-10.436
105	-13.199	-10.107	-10.658
120	-16.711	-9.604	-11.331
135	-17.847	-9.081	-12.326
150	-12.004	-8.649	-13.524
165	-10.449	-8.370	-14.554
180	-10.412	-8.273	-14.972

At $ka=2$, the source in the free-field and the source when operating near the structure for all three piezoelectric sources result in approximately the same sound pressure (± 0.2 dB). At $ka=5$, the TVR of the 4.5° and the 9.0° piezoelectric sources, under free-field conditions and while in the vicinity of the baffle, produce the same sound pressure (± 1.0 dB). The TVR of the 18.0° piezoelectric source is significantly different when operating under free-field conditions and in the vicinity of the baffle. This difference again points out the effect of the baffle on the transducer. The sound scattered from the baffle "sees" the projector. In all cases, the TVR originating from the source radiation and the baffle scattering is unlike the TVR of the source under free-field conditions. The combined radiation of the source and the baffle is directive; this directivity is induced by the scattering of the baffle.

The last topic to be discussed involves the modeling of the source, i.e., under what conditions can a finite source be treated as an ideal source. To determine if there exists a limiting condition in which the source may be idealized, we review the data once again and take note of any trends. One very noticeable trend in the magnitude of the normal velocity versus theta and the magnitude of the total pressure versus theta (Figures 4.1, 4.3, 4.5, and 4.7) for both frequencies, is that as the source increases in size, the peaks are amplified. The magnitude data does not show the entire picture; we must also look at the real and imaginary data individually. Figures 4.2, 4.4, 4.6, and 4.8 show the real and imaginary normal velocity and total pressure at $ka=2$ and 5. The real and imaginary results are similar for all of the sources.

To determine the conditions in which the source can be modeled ideally, a comparison is made of each source size to the wavelengths within the system. Table 4.8 presents the arc length of each source.

TABLE 4.8

Sources' arc length

SOURCES' INCLUDED ANGLE (deg)	ARC LENGTH (m)
4.5	0.027
9.0	0.054
18.0	0.108

Tables 4.1 and 4.8 show that the arc length of the 4.5 ° and the 9.0 ° piezoelectric sources are much less than (an order of magnitude) all of the defined wavelengths calculated in the system. Because the 4.5 ° and the 9.0 ° piezoelectric sources influence the baffle in the same manner as the ideal line source and these piezoelectric sources have the same Transmitting Voltage Response when operating in the free-field and while in the vicinity of the structure, it is concluded that the 4.5 ° and the 9.0 ° piezoelectric sources can be modeled as an ideal line source. On the other hand, when comparing results from the 18.0° piezoelectric source and that of the ideal line source, the only discrepancy is seen in the total far-field pressure at $ka=5$. This difference is because the 18.0 ° source produces a significantly different sound field when operating under free-field conditions compared to operating in the vicinity of the baffle as was shown in the TVR tables. The 18.0 ° piezoelectric source was significantly influenced by the baffle and therefore it cannot be modeled ideally. Thus, the determining criteria for when one may model the source ideally is the arc length of the piezoelectric source. For a source located a fixed distance of 2.54 cm out from the outer surface of the baffle, the arc length of the source must be at least an order of magnitude smaller than the shortest wavelength in the system at the highest frequency of interest in order to be modeled ideally. Note the above conclusion on modeling a finite source ideally is based on that source being held at a fixed

distance ~~out~~ from the baffle and that the variation of distance between the source and the baffle has ~~not~~ been included in this study.

C. Axisymmetric Model

The results and discussion presented in this section are arranged under the following main topics:

(1) The normal velocity and the acoustic pressure at the surface of the baffle, and the use of this data to determine what elastic waves are excited in the baffle by the adjacent projector,

(2) The far-field pressure directivity patterns for the projector-baffle system;

(3) The far-field pressure directivity patterns of the finite piezoelectric ring projector and comparison with the directivity patterns for the same projector under free-field conditions.

The standing wave pattern of the vibrations generated by the projector transducer in the axisymmetric baffle is more complicated than the vibration pattern generated in the plane strain case. This is partly due to the difference in phase velocities of the bending waves in the straight, cylindrical and the end, spherical portions of the baffle. Also, there may be some mode conversion, from bending to extensional waves, at the junction between the straight and the spherical regions of the baffle.

For a cylindrical shell the phase velocity for the Lamb modes is a function of the direction of propagation as was introduced in chapter I, section B. Propagation along the axial direction is much more complicated than that around the circumference. The waves that propagate axially depend on whether you are operating above or below the ring frequency of the structure. The ring frequency [4] is defined as

$$f_a = \frac{c_{E,p}}{2\pi a} \quad (24)$$

where a is the mean radius of the baffle. Well below the ring frequency, the structure vibrates equivalently to low frequency vibrations in a thin bar, the displacement caused by this longitudinal wave is predominantly axial but is coupled to the radial direction by Poisson's ratio. In the proximity of the ring frequency there is no simple expression for the phase velocity in the shell $c_{E,s}$ because the vibration is undergoing a transition, and $c_{E,s}$ is determined by numerically solving the shell equations. Above the ring frequency both Lamb modes exist, and the plate approximation can be used to estimate $c_{E,s}$ and $c_{f,s}$. The baffle in the current study has a ring frequency of 2527 Hz. Therefore at $ka=2$ we are operating below the ring frequency and at $ka=5$ we are operating above the ring frequency.

The elastic waves excited in the baffle are determined from analysis of the calculated normal velocity on the baffle surface. The separation between adjacent velocity magnitude peaks is determined and compared with estimated values of $\frac{\lambda}{2}$ for flexural and extensional waves in the baffle. Although torsional modes are also supported, at our frequencies, their displacements are small and their contribution is insignificant, so they will not be discussed. The flexural and extensional wavelengths determined from numerically solving the axisymmetric shell equations are tabulated in Table 4.9, these values were obtained from the mechanical engineering department at Georgia Institute of Technology [29].

TABLE 4.9

Wavelengths in the cylindrical baffle determined from the axisymmetric shell equations.

WAVELENGTH	ka=2	ka=5
flexural wavelength	not present	0.223 (m)
extensional wavelength	1.75 (m)	1.60 (m)

The axisymmetric model (Figure 2) was used to investigate:

(1) The effects of an adjacent ring source on an elastic cylindrical structure with hemispherical end caps as a function of vertical position.

(2) The effects of a finite piezoelectric ring projector located at position P1 on an elastic cylindrical structure with hemispherical end caps.

(3) Comparisons between the ideal ring projector to that of the piezoelectric ring projector located at position P1.

The normal velocity and total pressure on the outer surface of the baffle for different ideal ring source locations are shown in Figures 4.28 through 4.39, where $z=0$ corresponds to the position midway along the axis of the baffle. At $ka=5$ there are substantial standing waves in the baffle with which one can determine the wavelength. At $ka=2$, the normal velocity data shows one complete wavelength in the baffle for an ideal ring source excitation located at P1. At $ka=2$, the normalized distance between two adjacent peaks is 0.7, i.e., 70 % of half the total length of the baffle (0.684 m). The wavelength at $ka=2$ is therefore found to be 1.37 m, this is 22% different than the numerical value of the extensional wavelength. This large percent difference is due to the coupling between the extensional and radial modes, the velocity profile of the structure does not contain a pure extensional mode. At $ka=5$, the distance between two adjacent peaks was determined to be approximately 0.12, which corresponds to 0.117 meters. This was the same for the three different source locations. The wavelength at $ka=5$ was determined to be 0.235 meters, which is within 5% of the value for the flexural wavelength determined

numerically. For $ka=5$, the data shows 8 wavelengths when the source excitation is located at position P1. Numerically the baffle may support 8 complete wavelengths of an axially propagating flexural wave. It is concluded that the dominant wave in the baffle is an axial propagating flexural wave when the source is driven above the ring frequency of the structure. The amplitude of the data shows that the largest displacement is at the point closest to the source location. Each source induces a standing wave with a varying amplitude, this fluctuation in amplitude is due to the interference of the flexural and extensional waves.

The scattered far-field pressure data is shown in Figures 4.40 through 4.45. The structure can be thought of as many point sources each with its own complex vibration and the far-field pressure is due to the contributions of all the sources. The far-field pressure is determined both by the pressures and the velocities on the surface of the structure and is computed using the Kirchoff Helmholtz integral. All of the data displayed for the ideal ring source located at P1 is symmetric about $z=0$ due to the symmetry of the configuration. For the ring source located at P2 and P3, the greatest vibration is seen at the top and bottom of the end caps. The large pressure seen at the top and bottom of the end caps is due to the end caps acting as reflectors, this is caused by the symmetry in the structure, there are no displacements in the x direction at the symmetry line.

In the second part of the axisymmetric analysis, a finite piezoelectric ring projector was located at position P1. The effect of this source on the structure was compared to that of the ideal ring source located at the same position. The effect of the structure on the piezoelectric ring source was also investigated. Figures 4.46 and 4.47 show the total far-field pressure and the scattered far-field pressure due to a finite piezoelectric ring source excitation. The scattered pressure is made up of the specular reflection, elastic echo, diffraction echo, and scattering due to the elastic waves inside the shell. While the

total pressure is the scattered pressure plus the radiation of the source. When comparing the above data to the free-field directivity of the finite piezoelectric ring projector, in Figure 4.48, one can see the effect of the structure on the output of the projector. At $ka=2$, the scattered pressure is more directive than the total pressure. The nulls in the scattered pressure occur at the beginning of the end caps and these nulls are absent in the total pressure because the source is adding a pressure here. At $ka=5$, the scattered pressure is basically the same shape as that at $ka=2$, however, the length of the cylindrical body is beginning to approach that of the acoustic wavelength which gives rise to the two dips in the center lobe. The total pressure at $ka=5$ again shows the combined radiation of the source and the scattering of the structure.

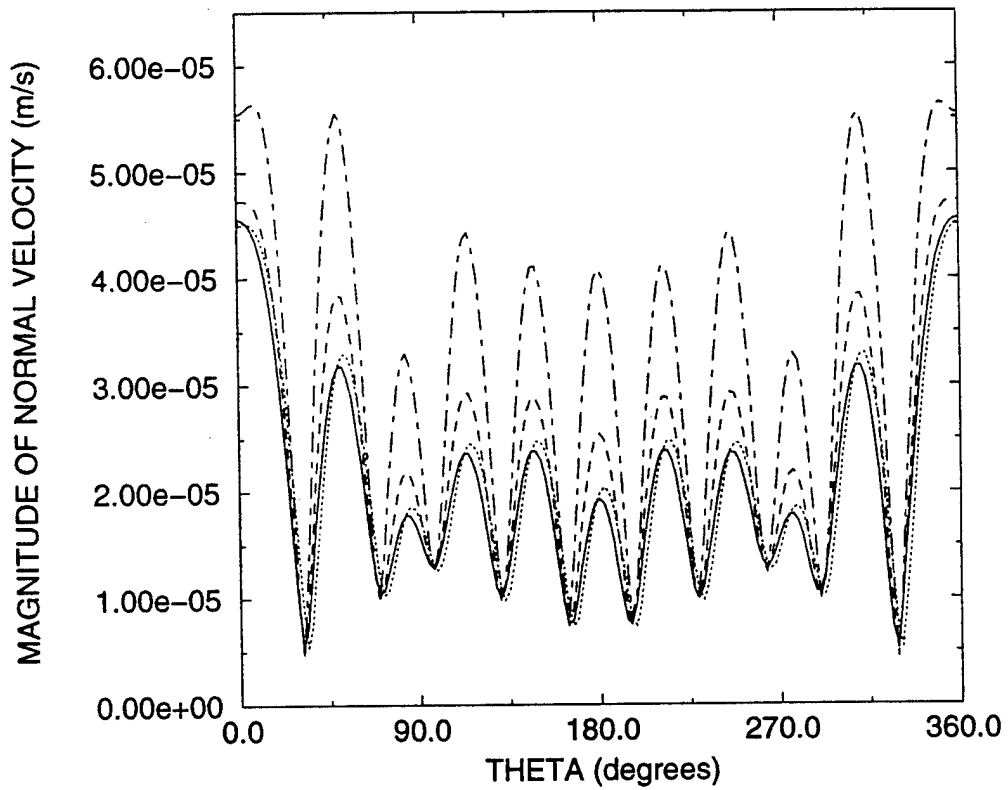
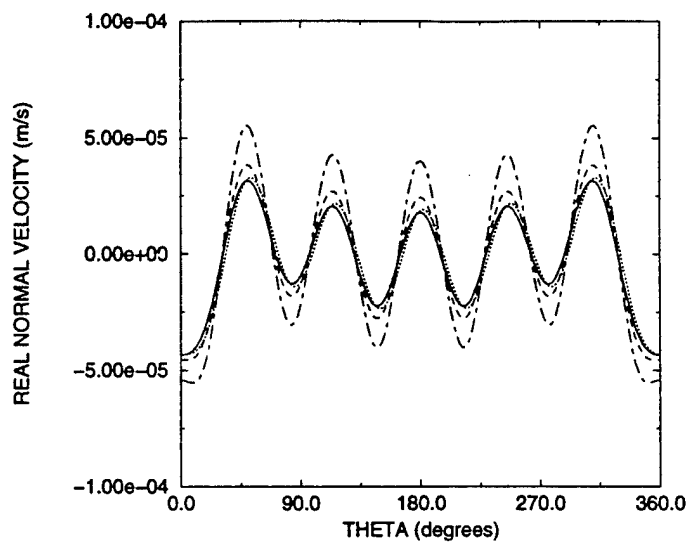
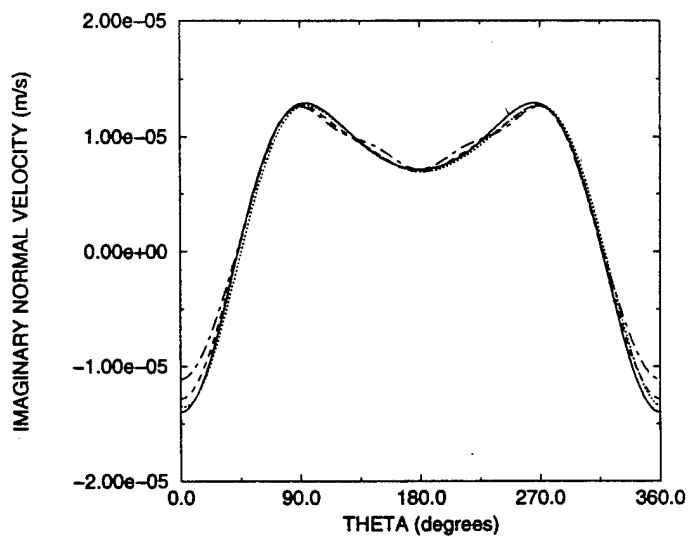


Figure 4.1 Magnitude of normal velocity on the outer surface of the cylinder versus theta at $ka=2$, for four different sources located at zero degrees: an ideal line source (solid line), a 4.5° piezoelectric source (dotted line), a 9.0° piezoelectric source (dashed line), and an 18.0° piezoelectric source (dash-dot line).



(a)



(b)

Figure 4.2 (a) real normal velocity on the outer surface of the cylinder versus theta, (b) Imaginary normal velocity on the outer surface of the cylinder versus theta; both are at $ka=2$ for four different sources located at zero degrees: an ideal line source (solid line), a 4.5° piezoelectric source (dotted line), a 9.0° piezoelectric source (dashed line), and an 18.0° piezoelectric source (dash-dot line).

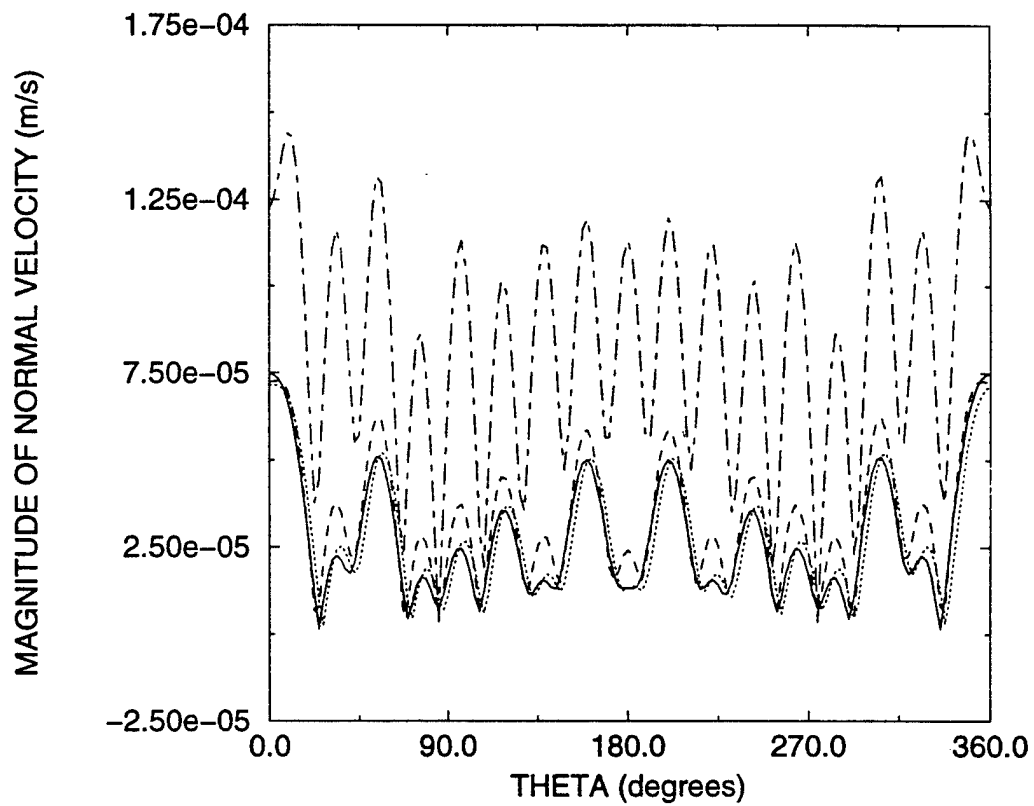
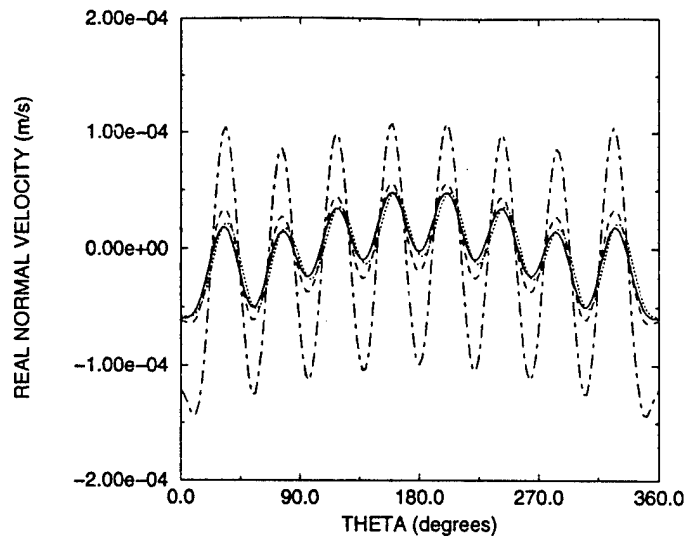
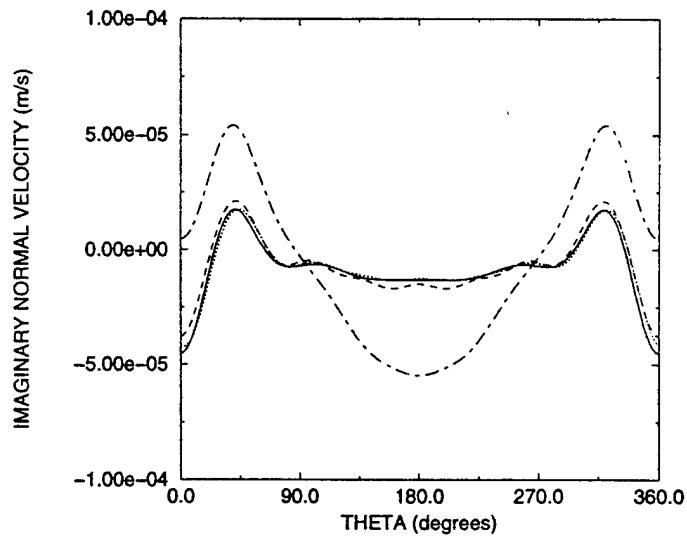


Figure 4.3 Magnitude of normal velocity on the outer surface of the cylinder versus theta at $ka=5$, for four different sources located at zero degrees: an ideal line source (solid line), a 4.5° piezoelectric source (dotted line), a 9.0° piezoelectric source (dashed line), and an 18.0° piezoelectric source (dash-dot line).



(a)



(b)

Figure 4.4 (a) real normal velocity on the outer surface of the cylinder versus theta, (b) imaginary normal velocity on the outer surface of the cylinder versus theta; both are at $ka=5$ for four different source excitations located at zero degrees: an ideal line source (solid line), a 4.5° piezoelectric source (dotted line), a 9.0° piezoelectric source (dashed line), and an 18.0° piezoelectric source (dash-dot line).

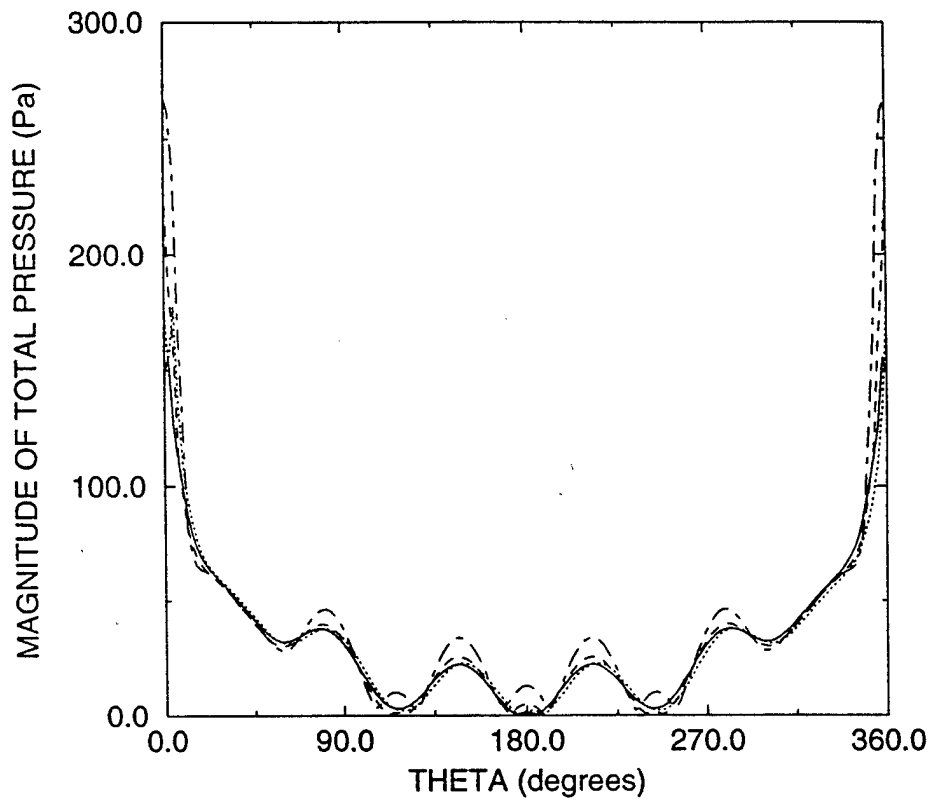


Figure 4.5 Magnitude of the total pressure on the outer surface of the cylinder versus theta at $ka=2$, for four different sources located at zero degrees: an ideal line source (solid line), a 4.5° piezoelectric source (dotted line), a 9.0° piezoelectric source (dashed line), and an 18.0° piezoelectric source (dash-dot line).

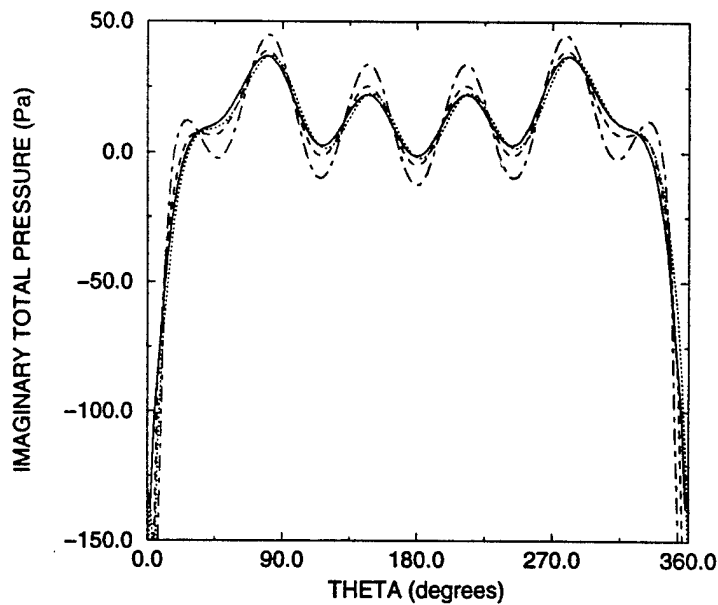
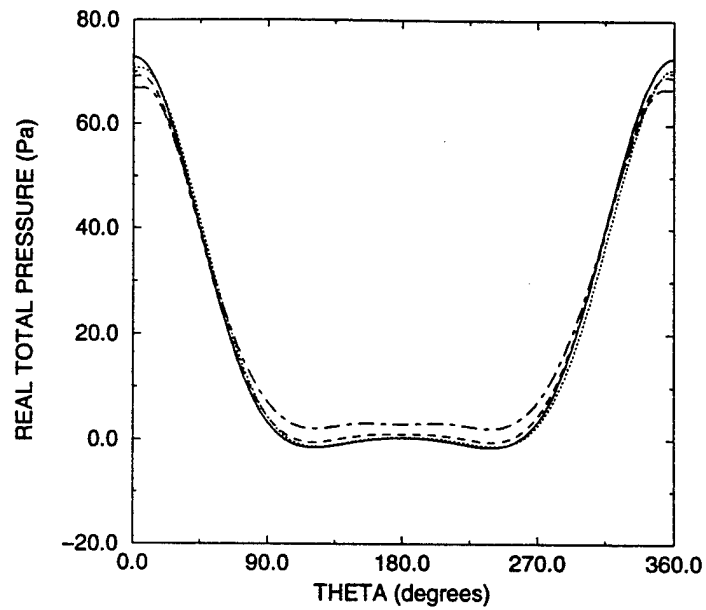


Figure 4.6 (a) real total pressure on the outer surface of the cylinder versus theta, (b) imaginary total pressure on the outer surface of the cylinder versus theta; both are at $ka=2$ for four different source excitations located at zero degrees: an ideal line source (solid line), a 4.5° piezoelectric source (dotted line), a 9.0° piezoelectric source (dashed line), and an 18.0° piezoelectric source (dash-dot line).

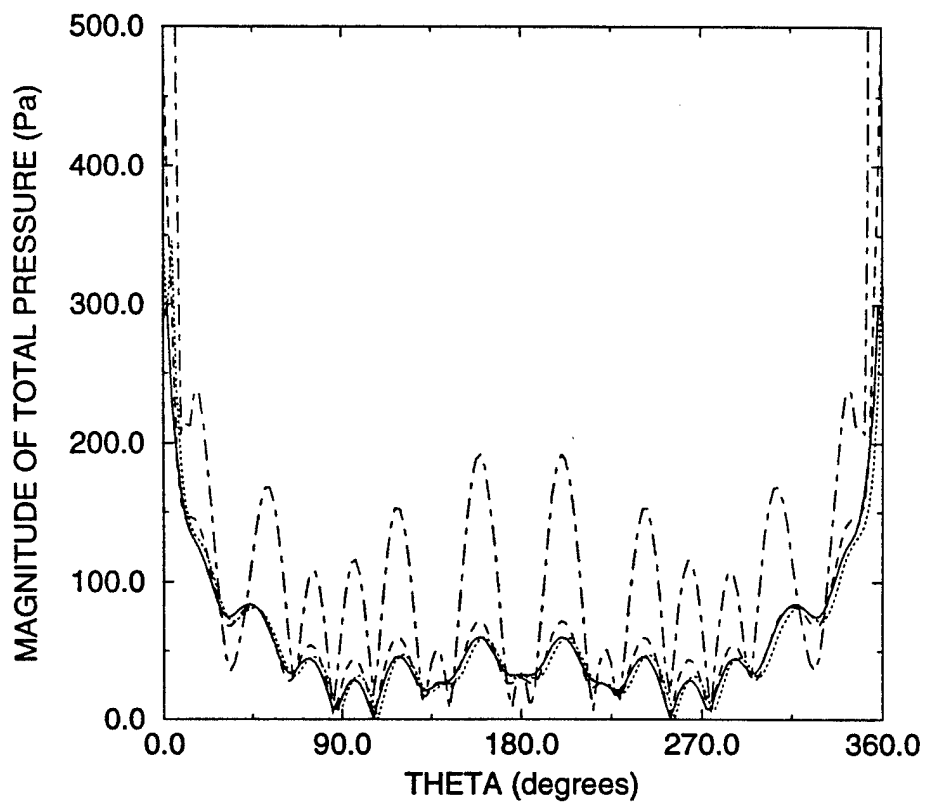
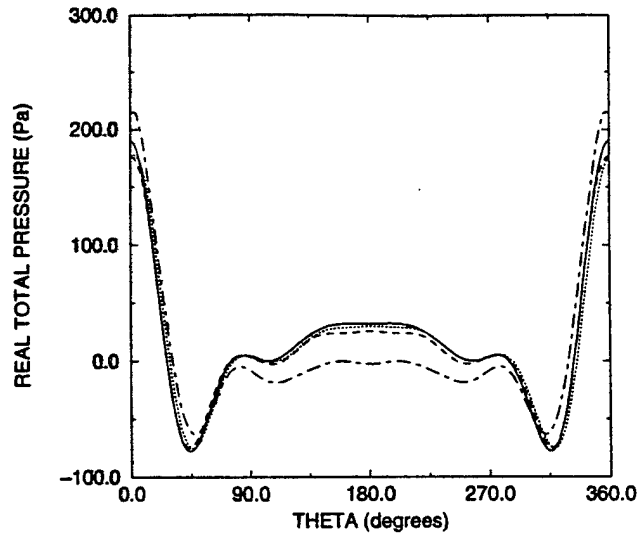
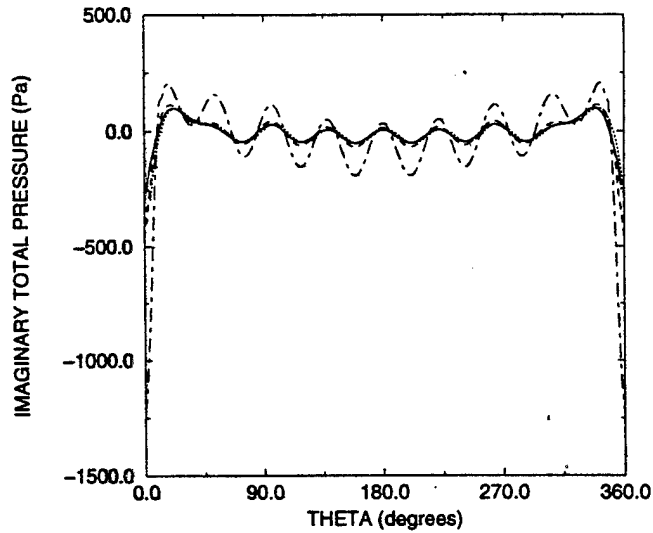


Figure 4.7 Magnitude of the total pressure on the outer surface of the cylinder versus theta at $ka=5$, for four different sources located at zero degrees: an ideal line source (solid line), a 4.5° piezoelectric source (dotted line), a 9.0° piezoelectric source (dashed line), and an 18.0° piezoelectric source (dash-dot line).



(a)



(b)

Figure 4.8 (a) real total pressure on the outer surface of the cylinder versus theta (b) imaginary total pressure on the outer surface of the cylinder versus theta; both are at $ka=5$ for four different source excitations located at zero degrees: an ideal line source (solid line), a 4.5° piezoelectric source (dotted line), a 9.0° piezoelectric source (dashed line), and an 18.0° piezoelectric source (dash-dot line).

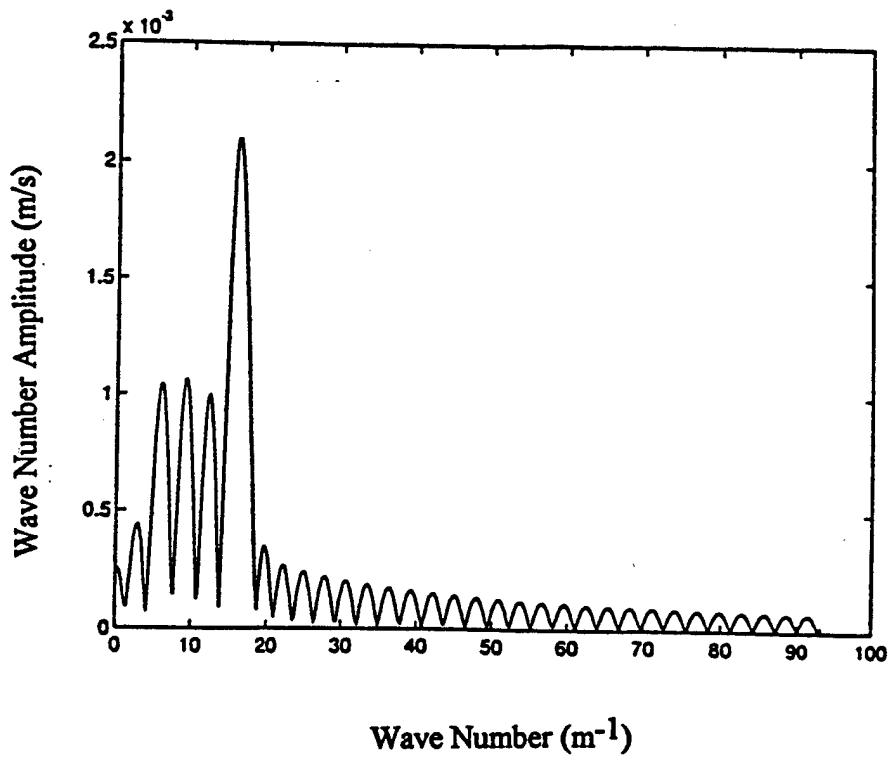


Figure 4.9 Wave number spectrum for the normal surface velocity. The spectrum was determined from the normal velocity versus theta on the outer surface of the cylinder which was excited by a 4.5° piezoelectric source located at zero degrees for $ka=2$.

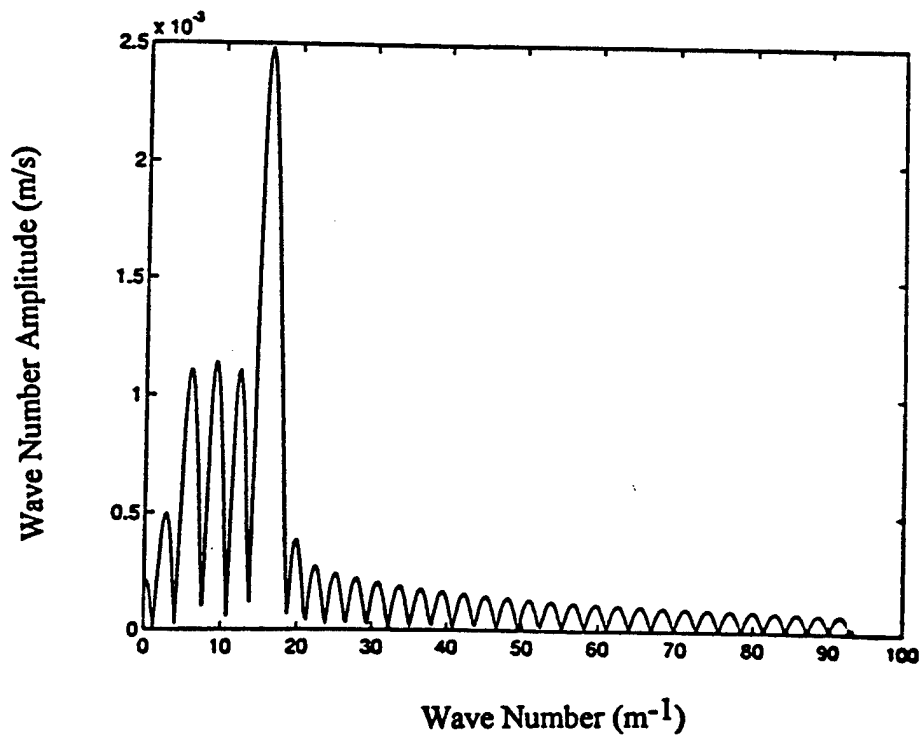


Figure 4.10 Wave number spectrum for the normal surface velocity. The spectrum was determined from the normal velocity versus theta on the outer surface of the cylinder which was excited by a 9.0° piezoelectric source located at zero degrees for $ka=2$.

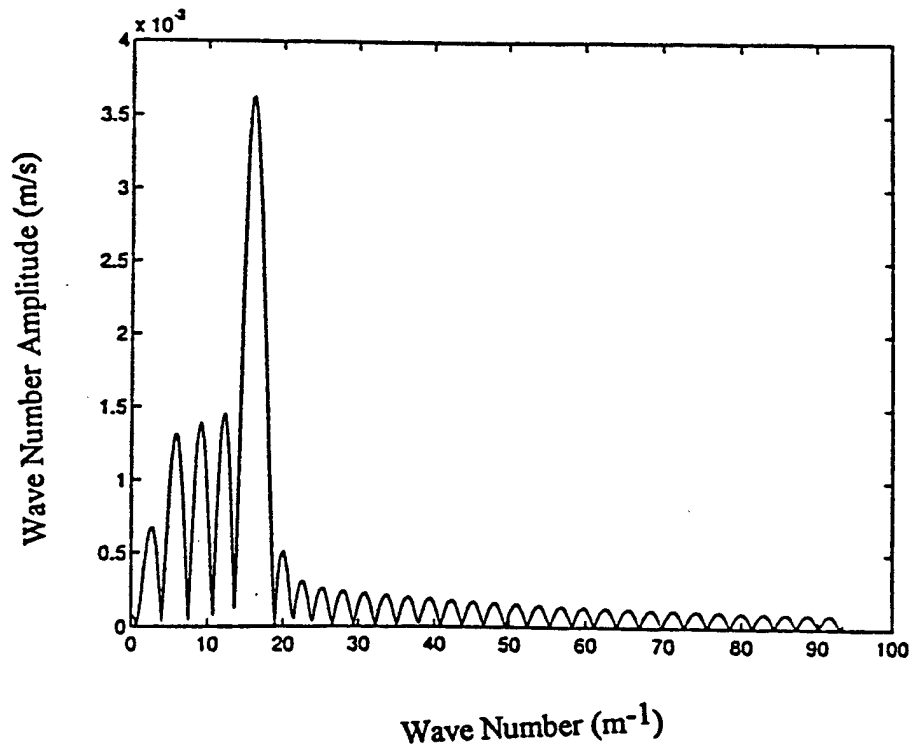


Figure 4.11 Wave number spectrum for the normal surface velocity. The spectrum was determined from the normal velocity versus theta on the outer surface of the cylinder which was excited by a 18.0° piezoelectric source located at zero degrees for $ka=2$.

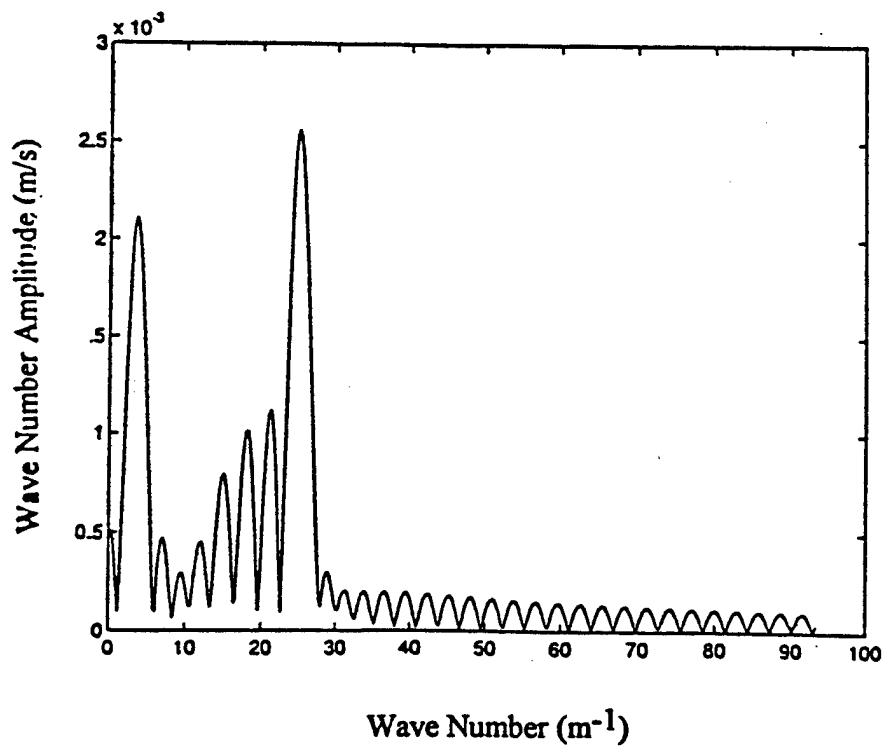


Figure 4.12 Wave number spectrum for the normal surface velocity. The spectrum was determined from the normal velocity versus theta on the outer surface of the cylinder which was excited by a 4.5° piezoelectric source located at zero degrees for $ka=5$.

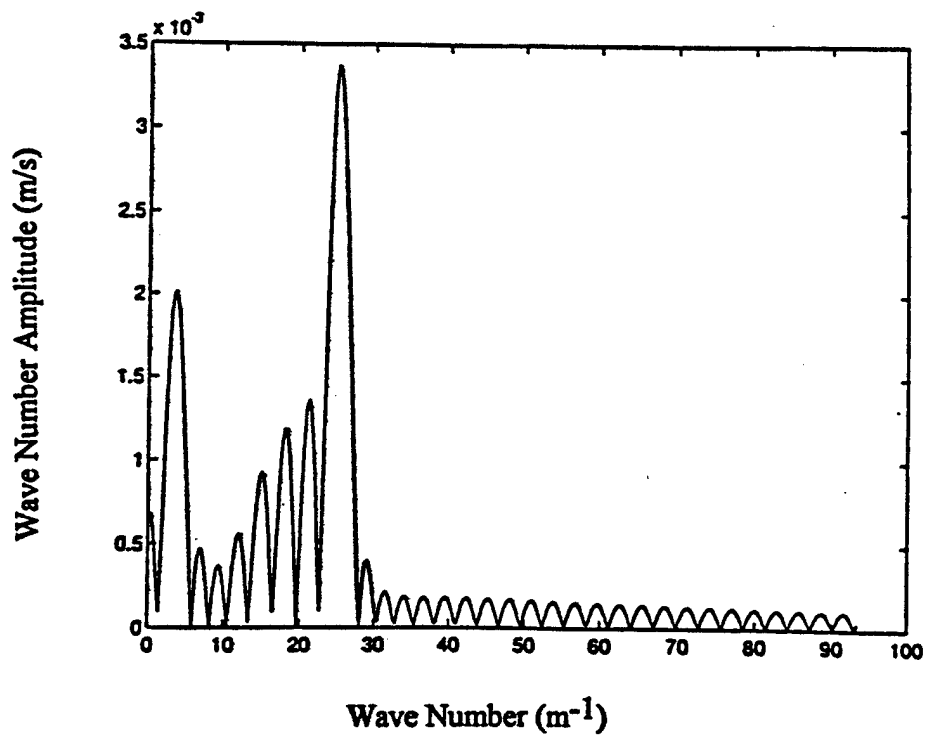


Figure 4.13 Wave number spectrum for the normal surface velocity. The spectrum was determined from the normal velocity versus theta on the outer surface of the cylinder which was excited by a 9.0° piezoelectric source located at zero degrees for $ka=5$.

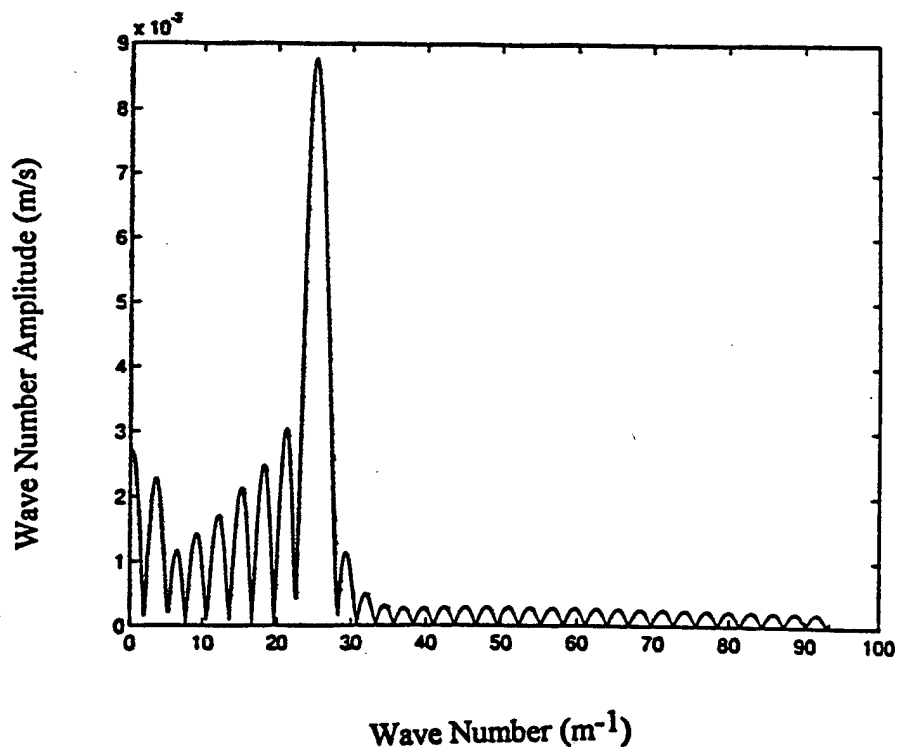


Figure 4.14 Wave number spectrum for the normal surface velocity. The spectrum was determined from the normal velocity versus theta on the outer surface of the cylinder which was excited by a 18.0° piezoelectric source located at zero degrees for $ka=5$.

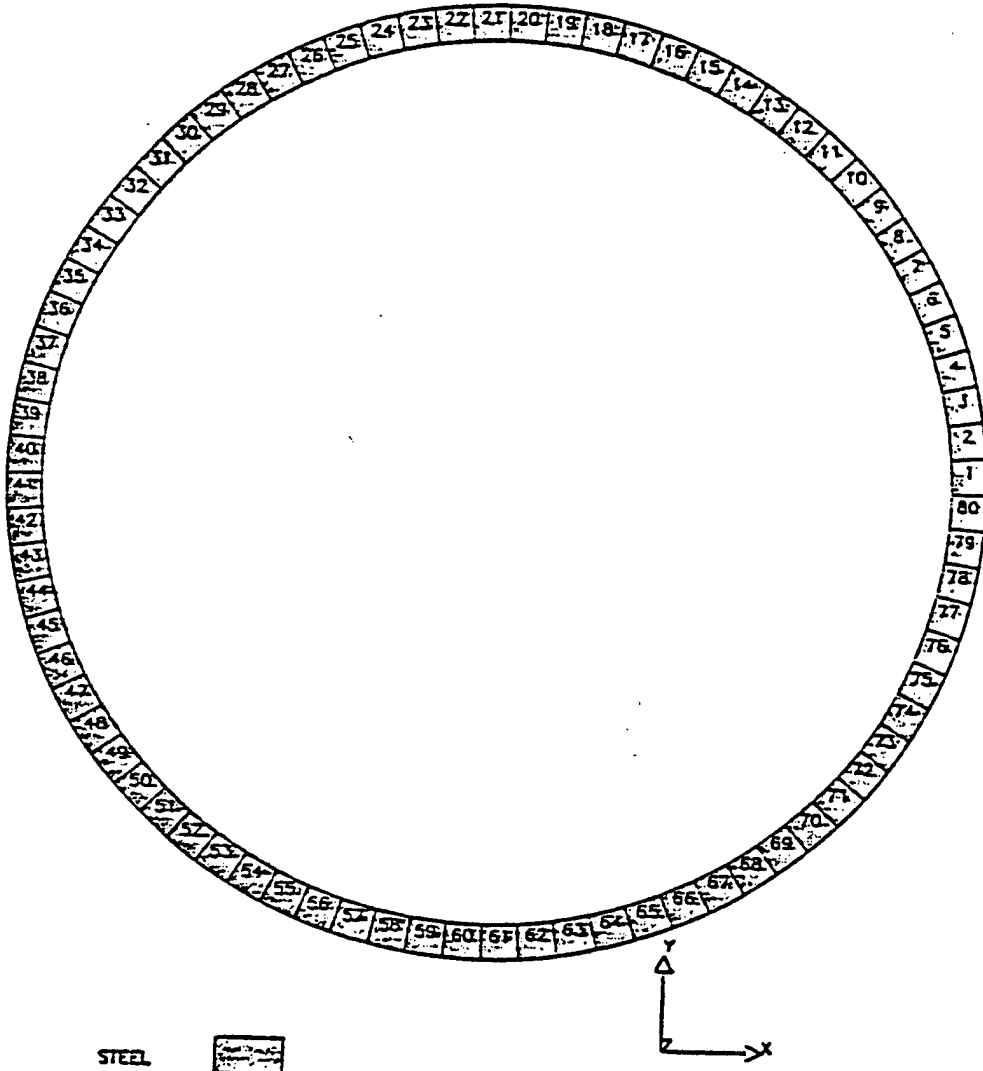


Figure 4.15 Static shape of the plane strain cylinder with each element numbered.

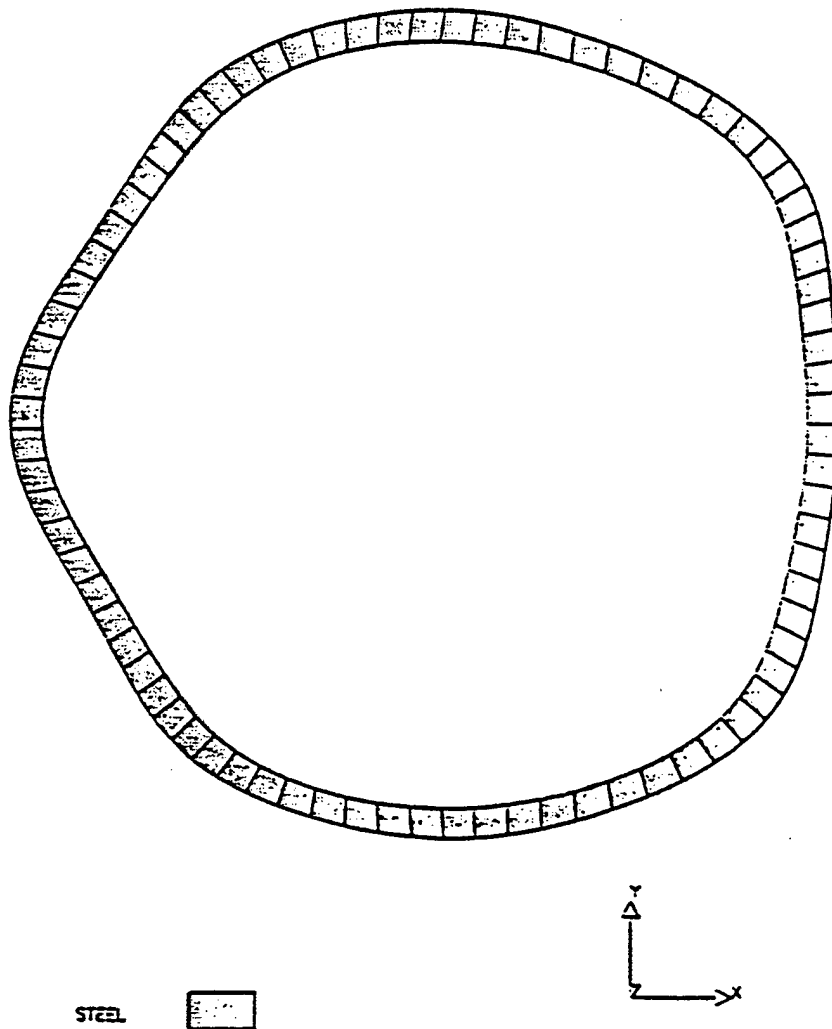


Figure 4.16 Displaced shape (magnified 20 times) of the cylinder due to a 4.5° piezoelectric source excitation at $ka=2$.

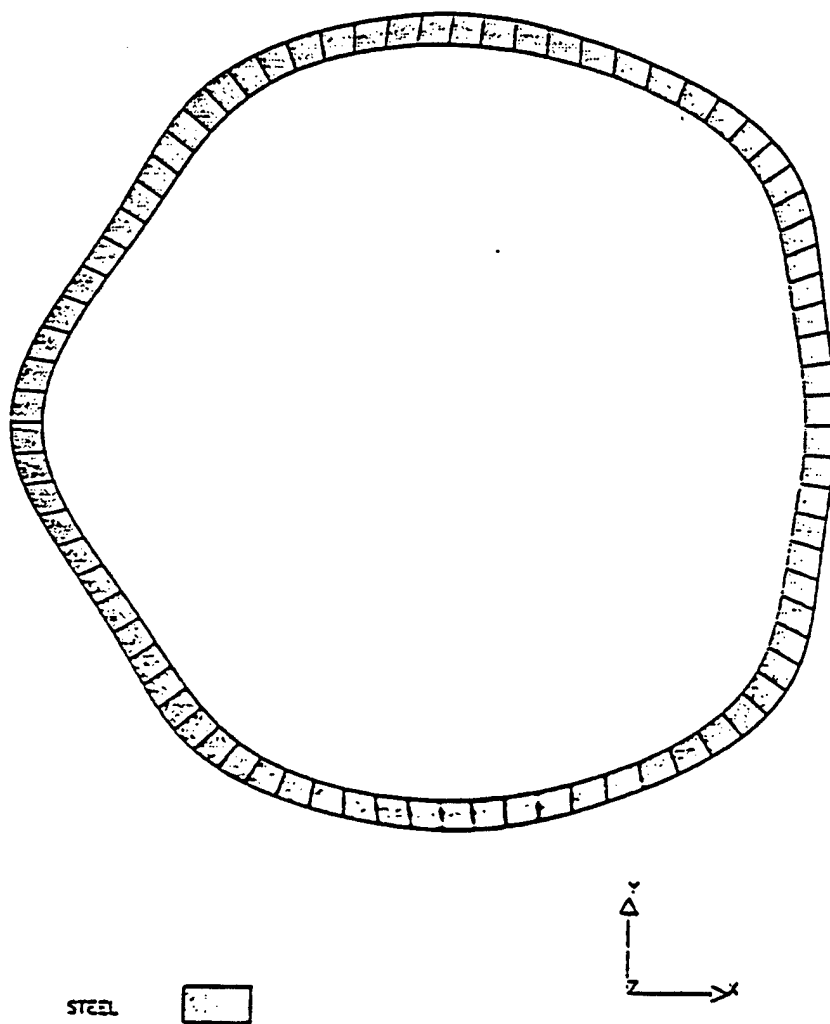


Figure 4.17 Displaced shape (magnified 20 times) of the cylinder due to a 9.0° piezoelectric source excitation at $ka=2$.

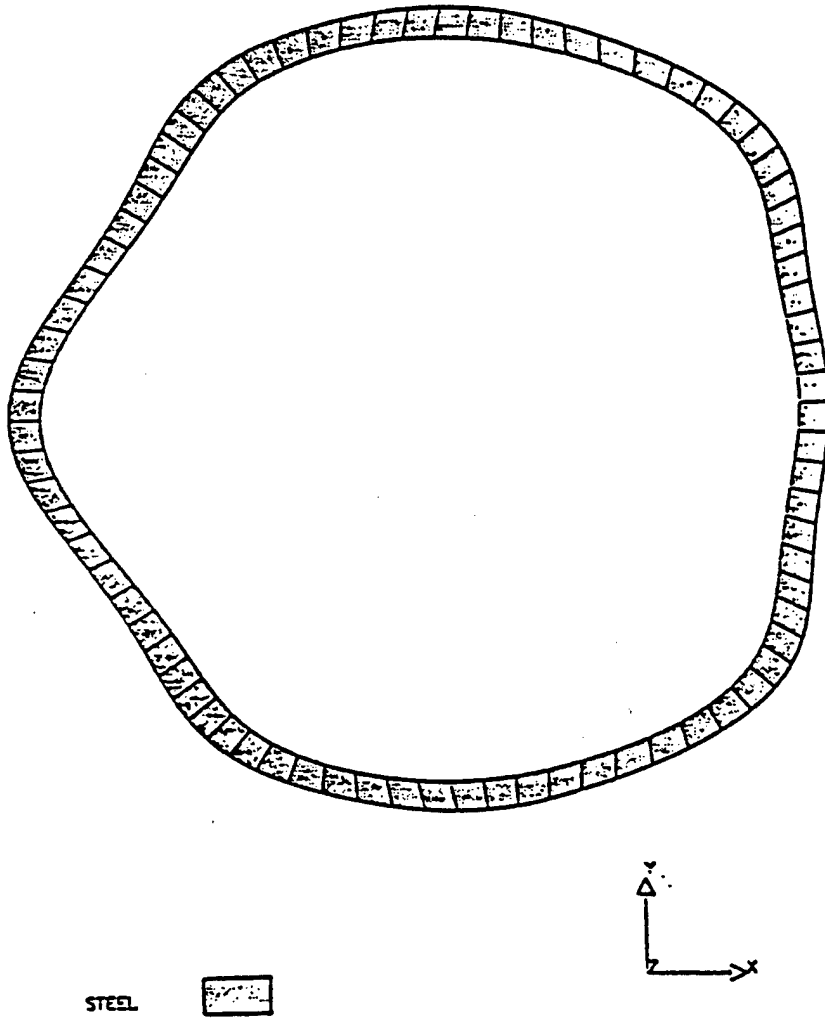


Figure 4.18 Displaced shape (magnified 20 times) of the cylinder due to a 18.0° piezoelectric source excitation at $ka=2$.

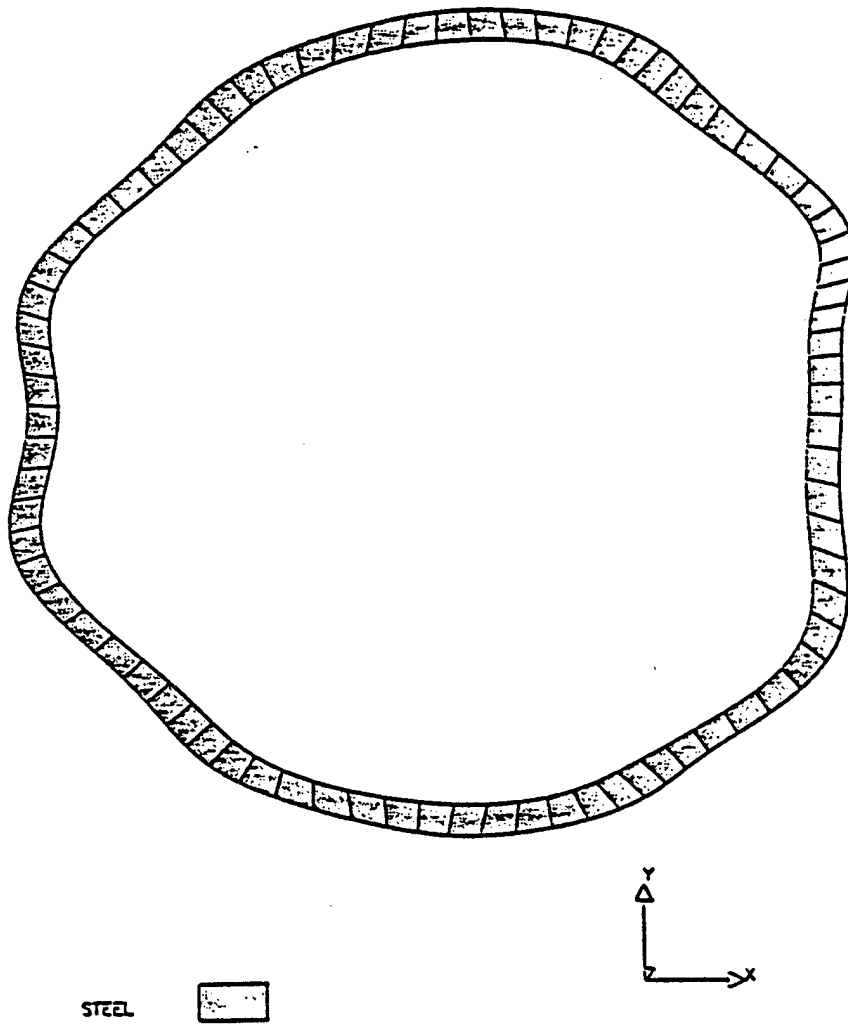


Figure 4.19 Displaced shape (magnified 20 times) of the cylinder due to a 4.5° piezoelectric source excitation at $ka=5$.

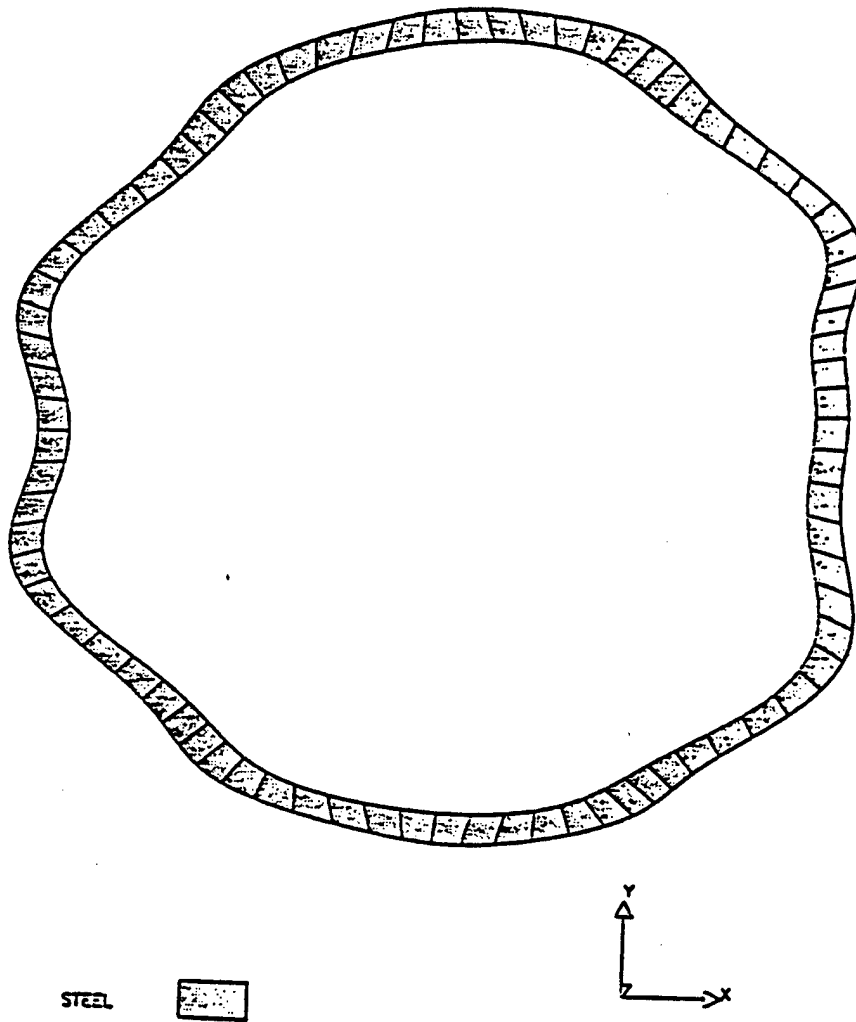


Figure 4.20 Displaced shape (magnified 20 times) of the cylinder due to a 9.0° piezoelectric source excitation at $ka=5$.

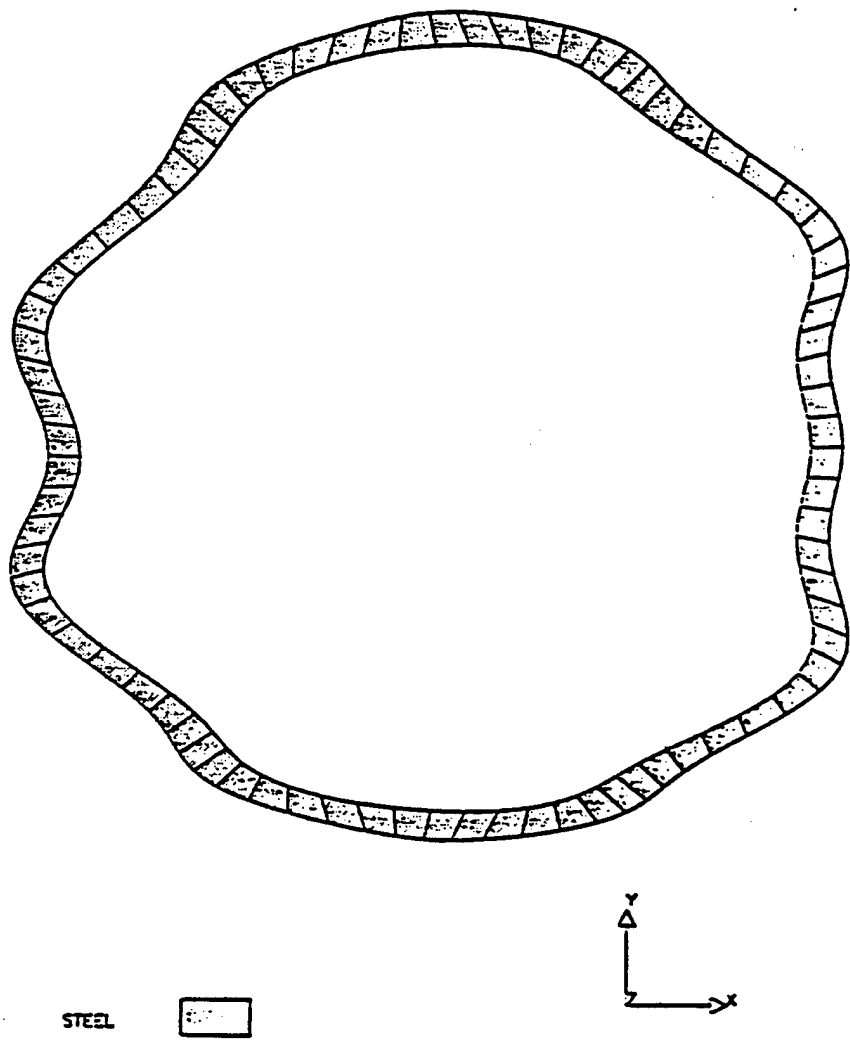


Figure 4.21 Displaced shape (magnified 20 times) of the cylinder due to a 18.0° piezoelectric source excitation at $ka=5$.

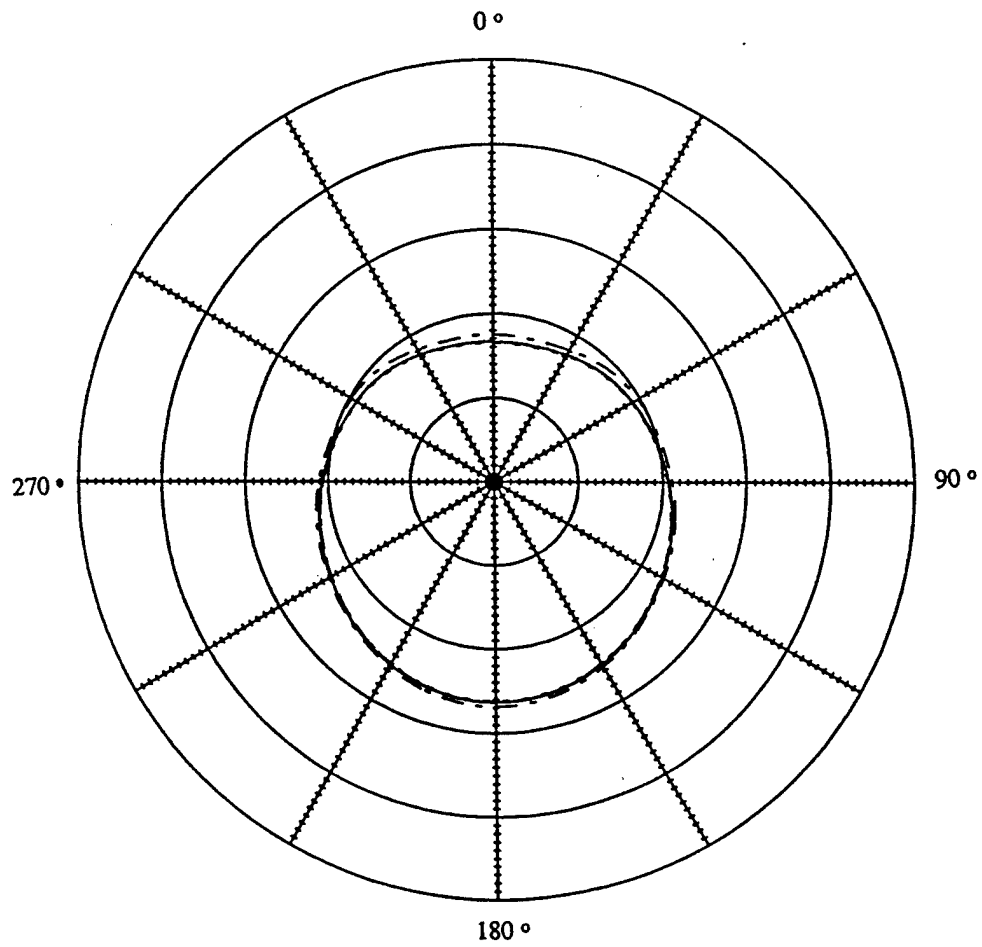


Figure 4.22 Far-field scattered pressure (dB) at $ka=2$, due to four different sources located at zero degrees: an ideal line source (solid line), a 4.5° piezoelectric source (dotted line), a 9.0° piezoelectric source (dashed line), and an 18.0° piezoelectric source (dash-dot line). 10 dB/division

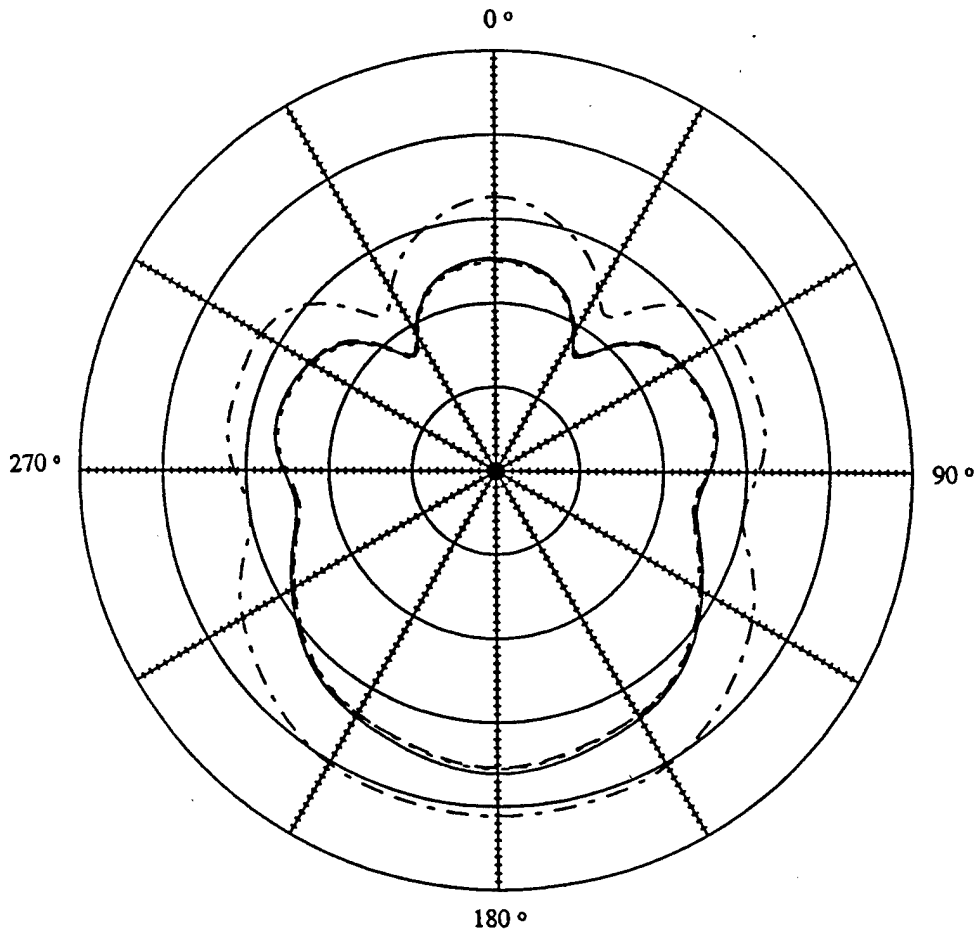


Figure 4.23 Far-field scattered pressure (dB) at $ka=5$, due to four different source excitations located at zero degrees: an ideal line source (solid line), a 4.5° piezoelectric source (dotted line), a 9.0° piezoelectric source (dashed line), and an 18.0° piezoelectric source (dash-dot line). 10 dB/division

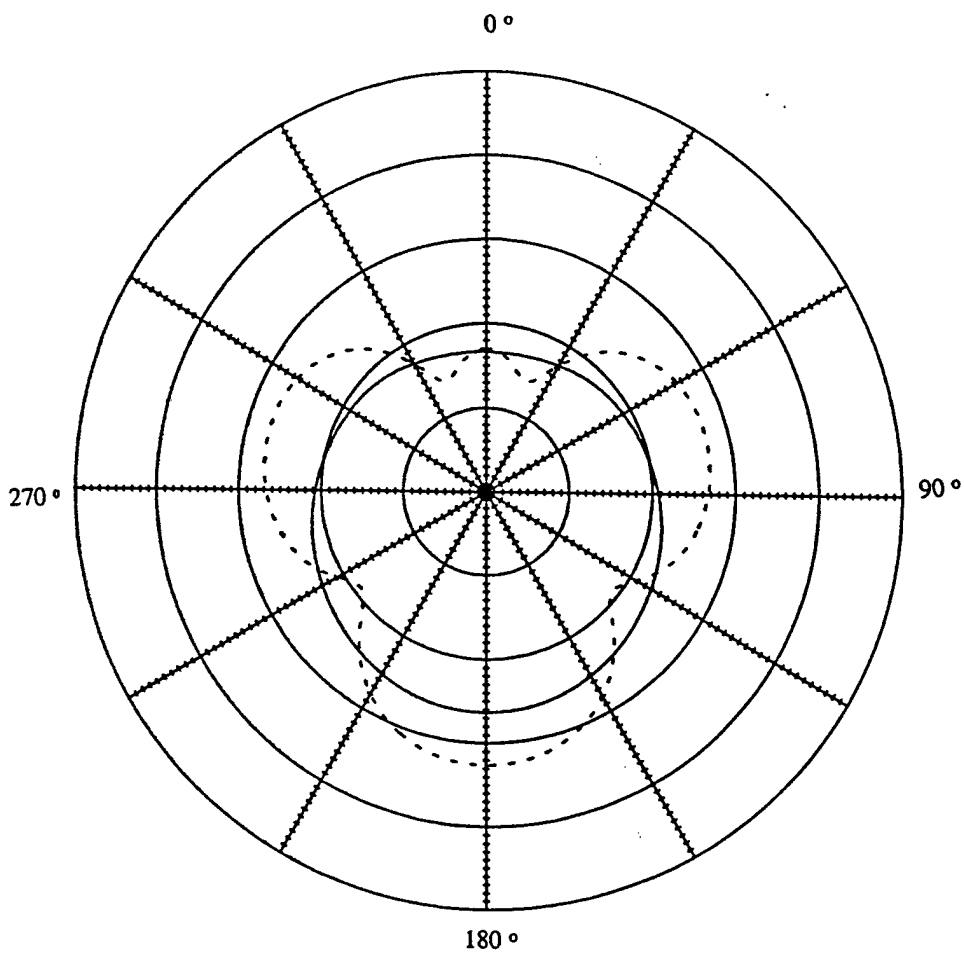


Figure 4.24 Far-field scattered pressure at $ka=2$ from an elastic cylindrical shell (solid line) and from a rigid cylindrical shell (dotted line) due to an ideal line source excitation located at zero degrees.

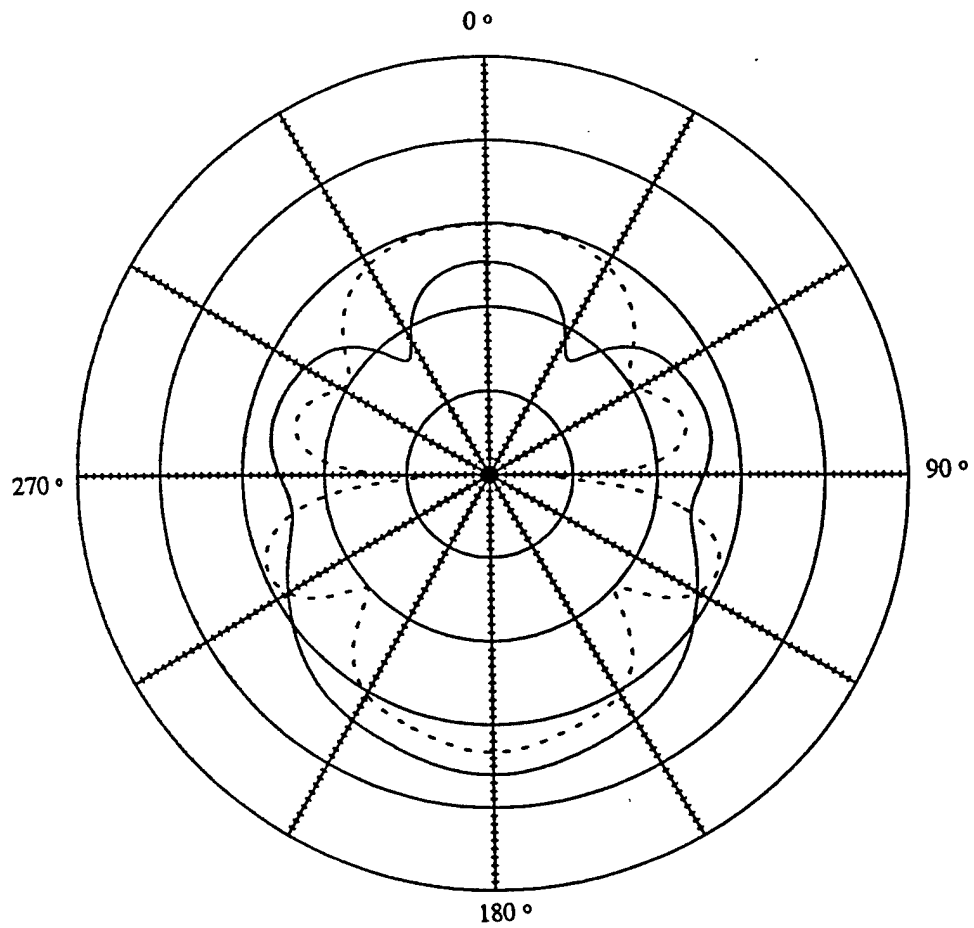


Figure 4.25 Far-field scattered pressure at $ka=5$ from an elastic cylindrical shell (solid line) and from a rigid cylindrical shell (dotted line) due to an ideal line source excitation located at zero degrees.

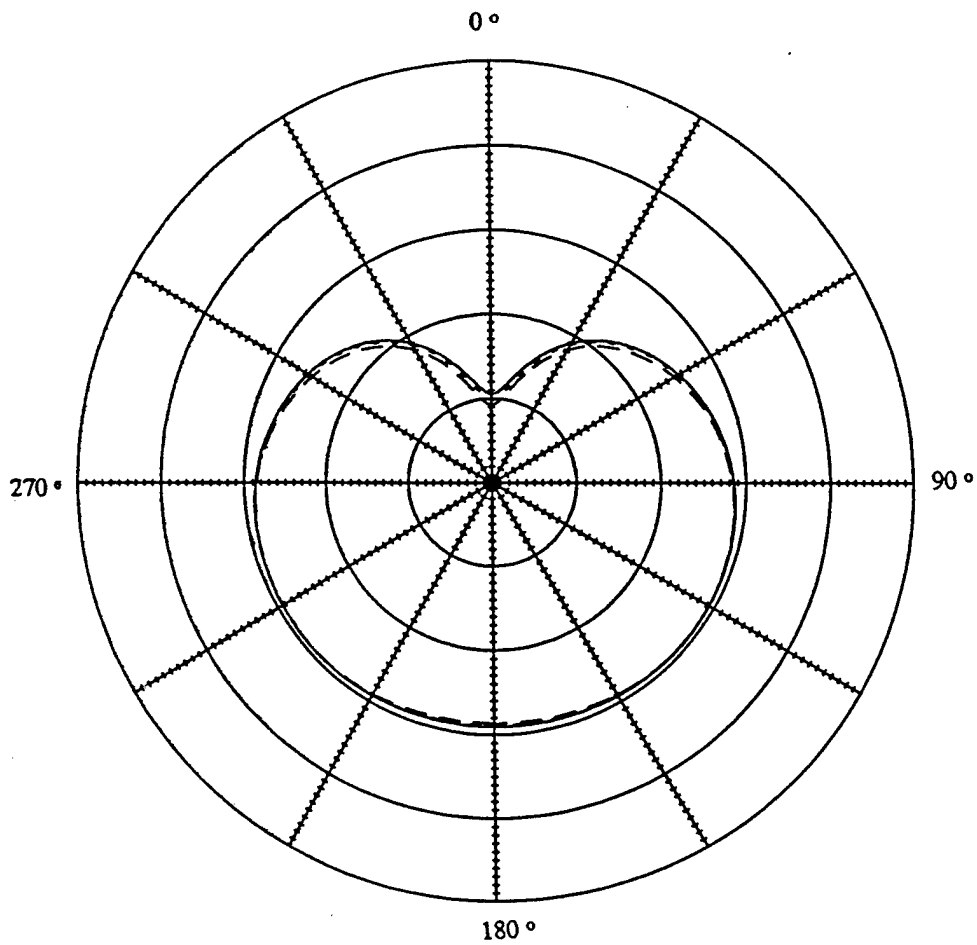


Figure 4.26 Far-field total pressure (dB) at $ka=2$, due to three different sources located at zero degrees: a 4.5° piezoelectric source (solid line), a 9.0° piezoelectric source (dotted line), and an 18.0° piezoelectric source (dash-dot line). 10 dB/division

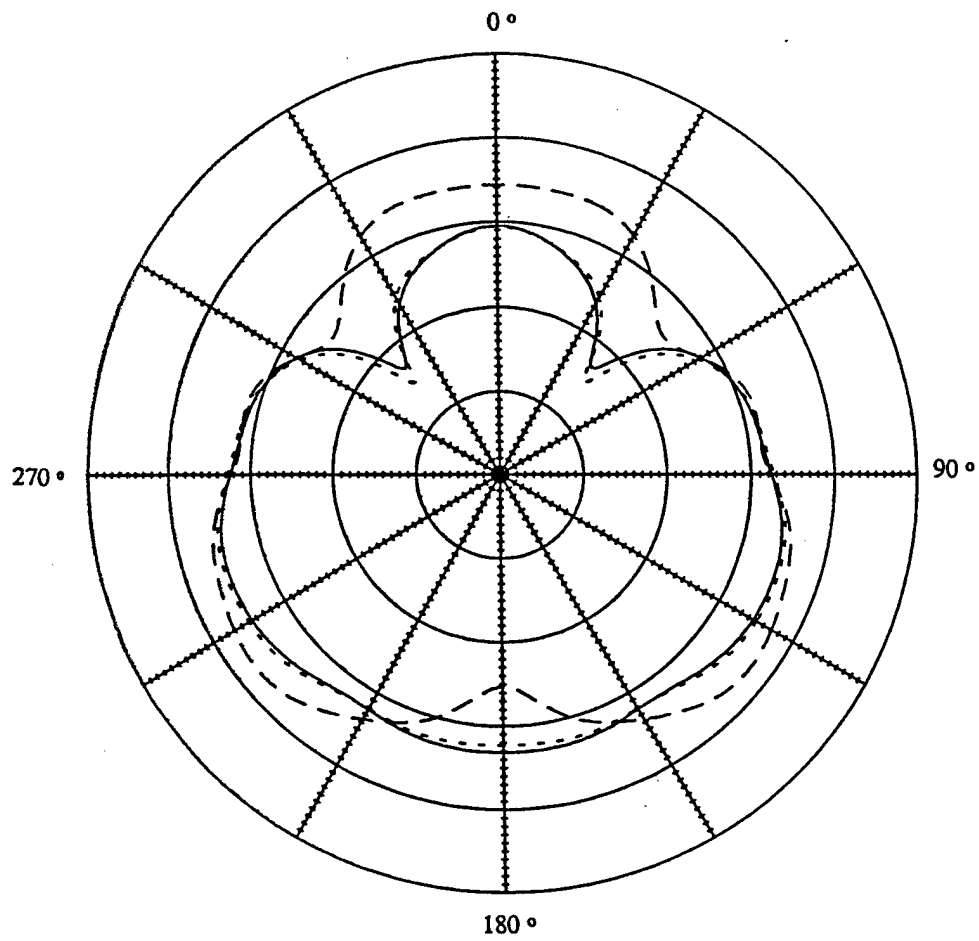


Figure 4.27 Far-field total pressure (dB) at $ka=5$ due to three different source excitations located at zero degrees: a 4.5° piezoelectric source (solid line), a 9.0° piezoelectric source (dotted line), and an 18.0° piezoelectric source (dash-dot line). 10 dB/division

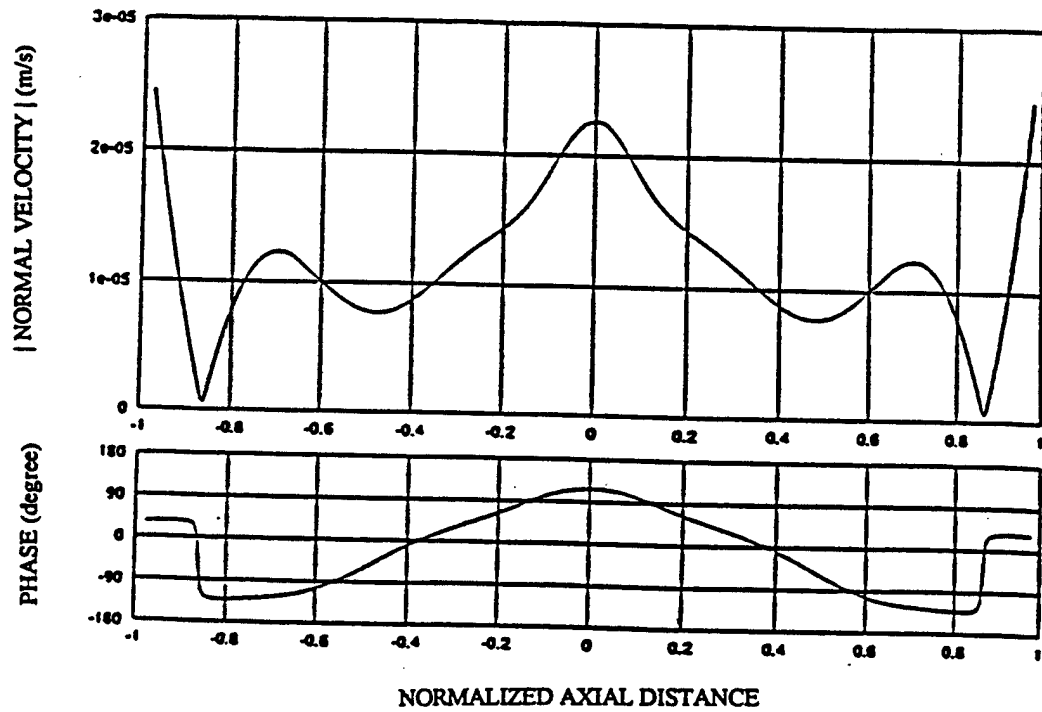


Figure 4.28 Magnitude and phase of the normal velocity on the outer surface of the cylindrical shell with hemispherical end caps, at $ka=2$. The excitation is due to an ideal ring source located at position P1.

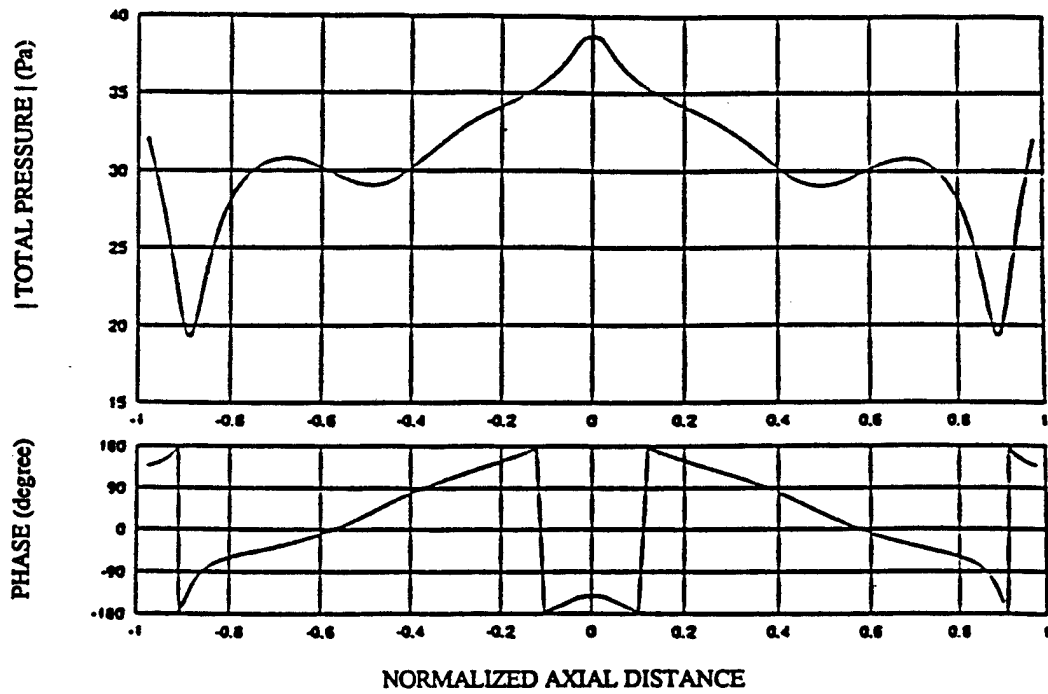


Figure 4.29 Magnitude and phase of the total pressure on the outer surface of the cylindrical shell with hemispherical end caps, at $ka=2$. The excitation is due to an ideal ring source located at position P1.

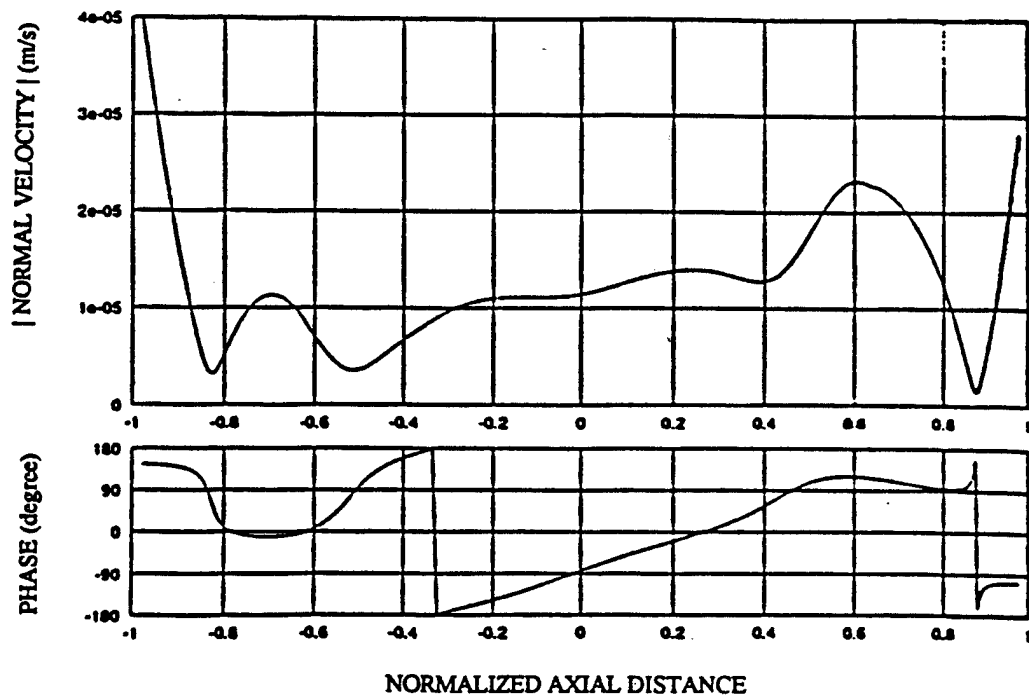


Figure 4.30 Magnitude and phase of the normal velocity on the outer surface of the cylindrical shell with hemispherical end caps, at $ka=2$. The excitation is due to an ideal ring source located at position P2.

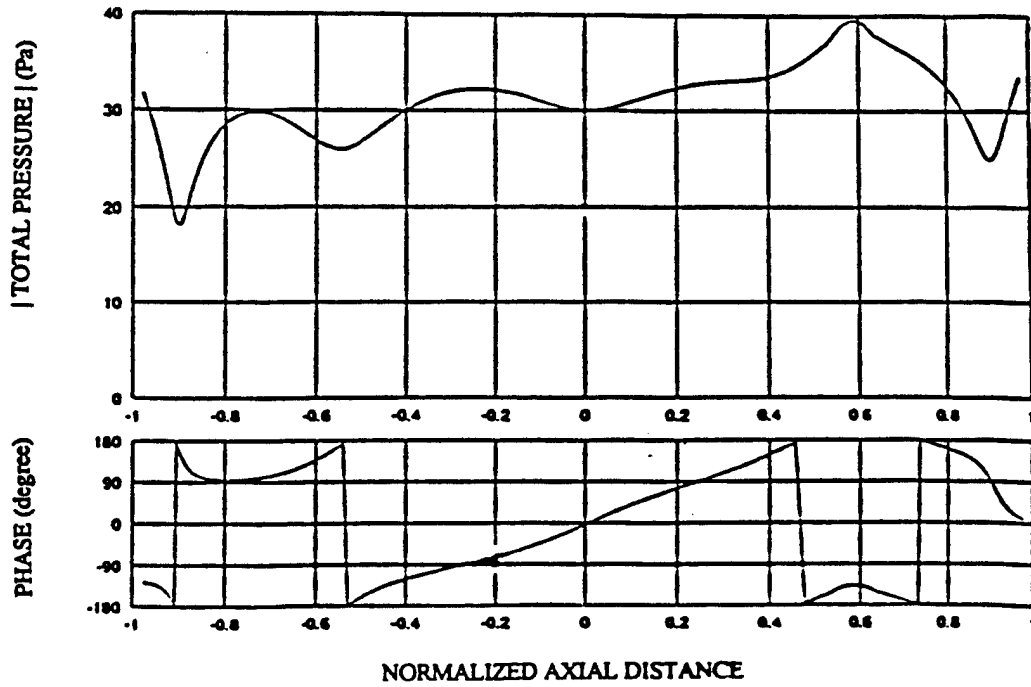


Figure 4.31 Magnitude and phase of the total pressure on the outer surface of the cylindrical shell with hemispherical end caps, at $ka=2$. The excitation is due to an ideal ring source located at position P2.

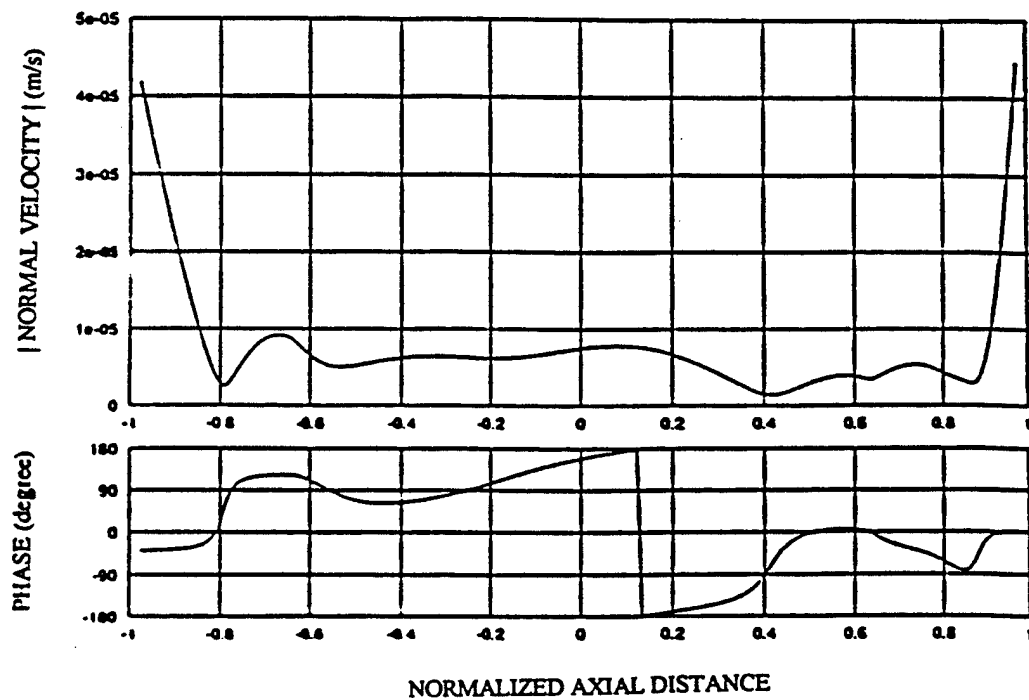


Figure 4.32 Magnitude and phase of the normal velocity on the outer surface of the cylindrical shell with hemispherical end caps, at $ka=2$. The excitation is due to an ideal ring source located at position P3.

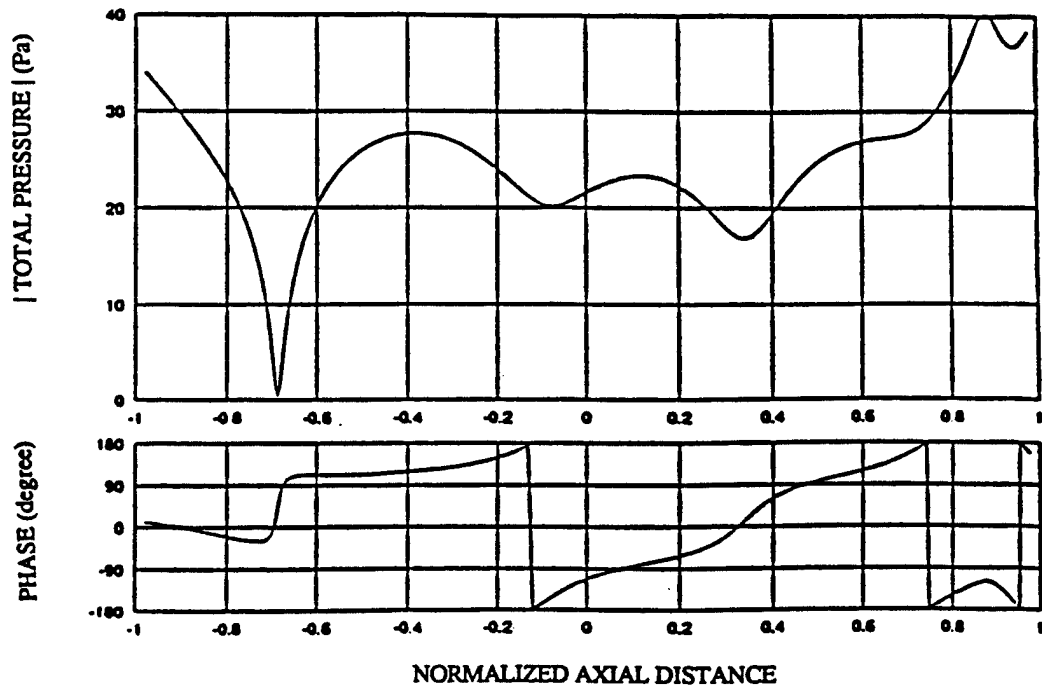


Figure 4.33 Magnitude and phase of the total pressure on the outer surface of the cylindrical shell with hemispherical end caps, at $ka=2$. The excitation is due to an ideal ring source located at position P3.

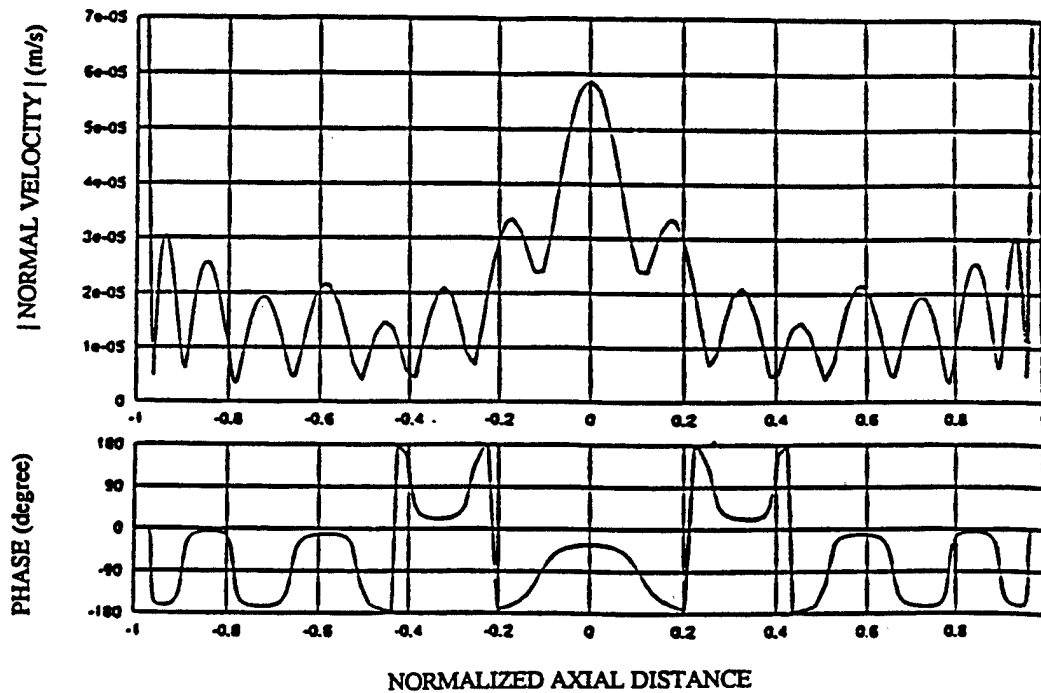


Figure 4.34 Magnitude and phase of the normal velocity on the outer surface of the cylindrical shell with hemispherical end caps, at $ka=5$. The excitation is due to an ideal ring source located at position P1.

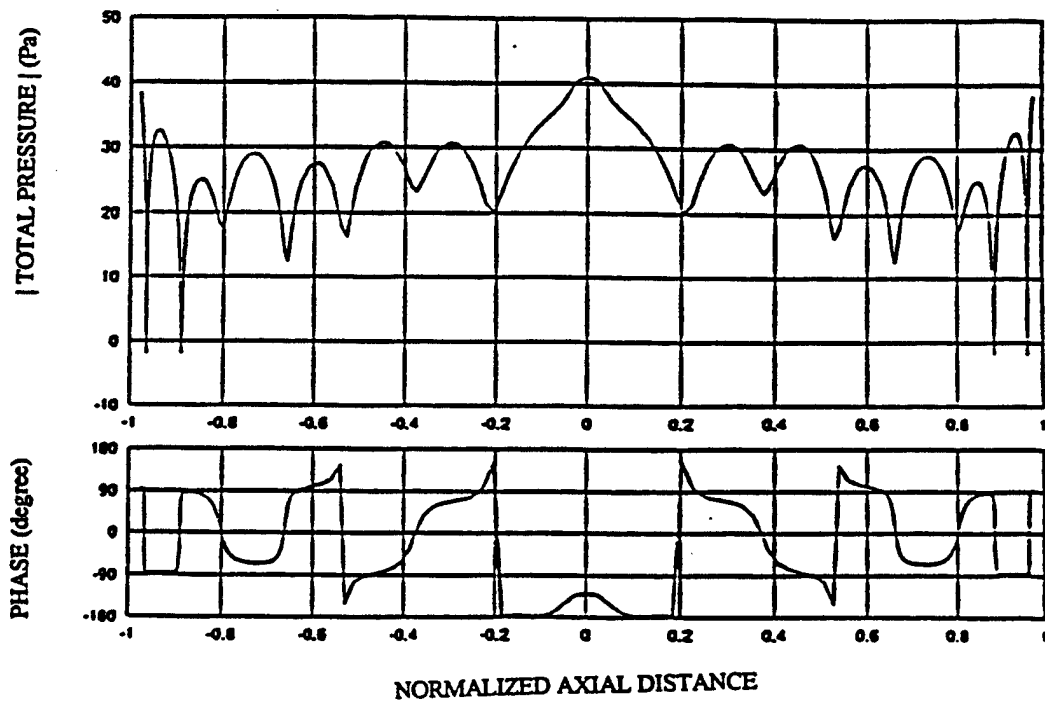


Figure 4.35 Magnitude and phase of the total pressure on the outer surface of the cylindrical shell with hemispherical end caps, at $ka=5$. The excitation is due to an ideal ring source located at position P1.

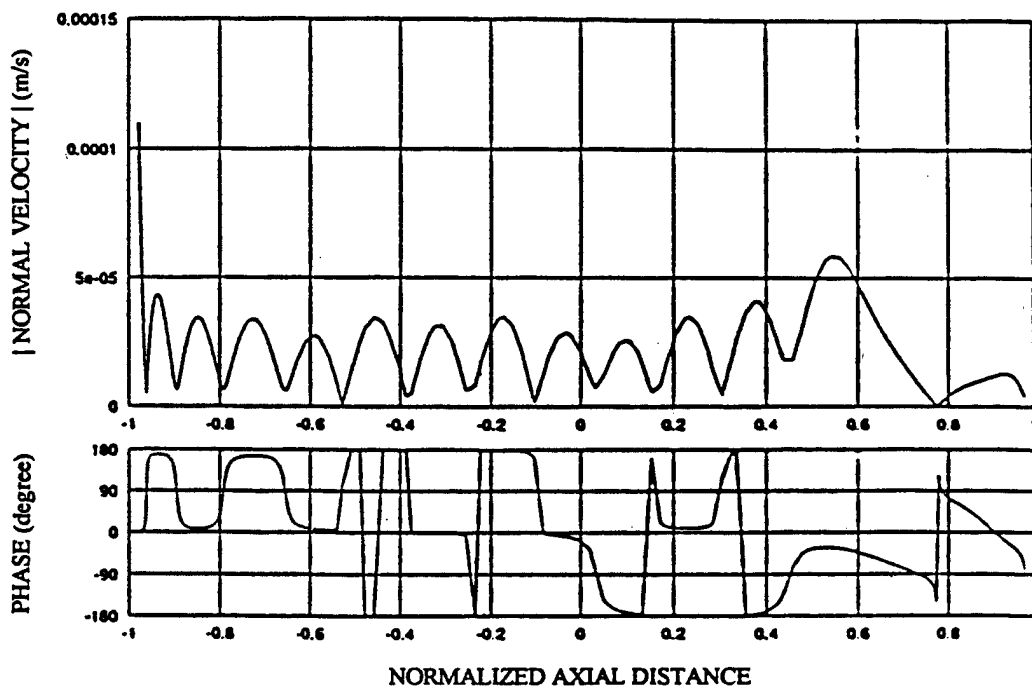


Figure 4.36 Magnitude and phase of the normal velocity on the outer surface of the cylindrical shell with hemispherical end caps, at $ka=5$. The excitation is due to an ideal ring source located at position P2.

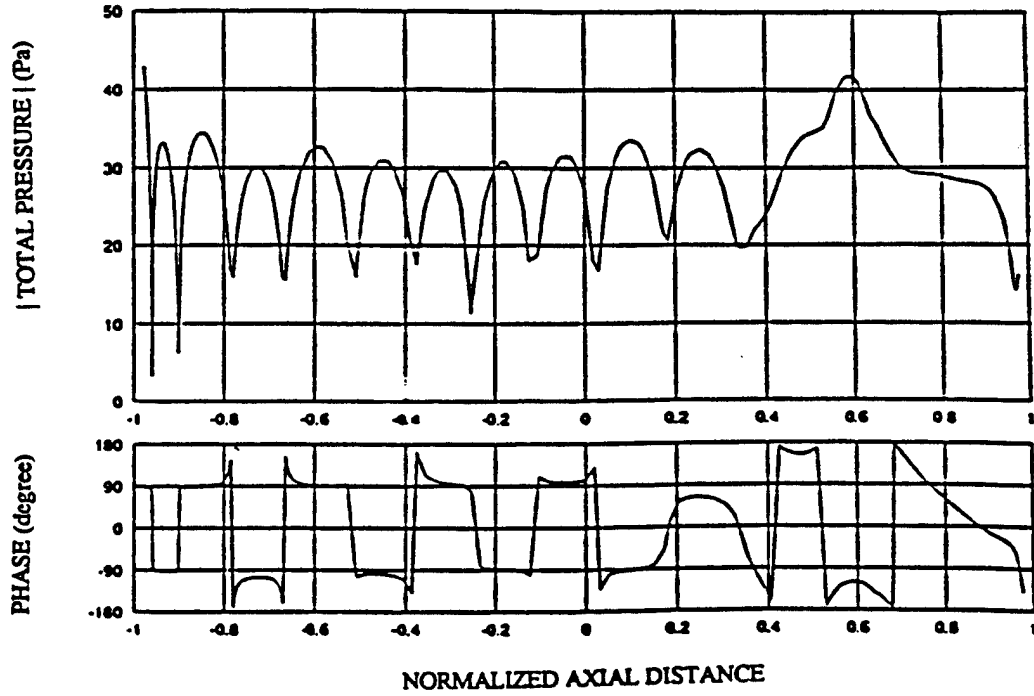


Figure 4.37 Magnitude and phase of the total pressure on the outer surface of the cylindrical shell with hemispherical end caps, at $ka=5$. The excitation is due to an ideal ring source located at position P2.

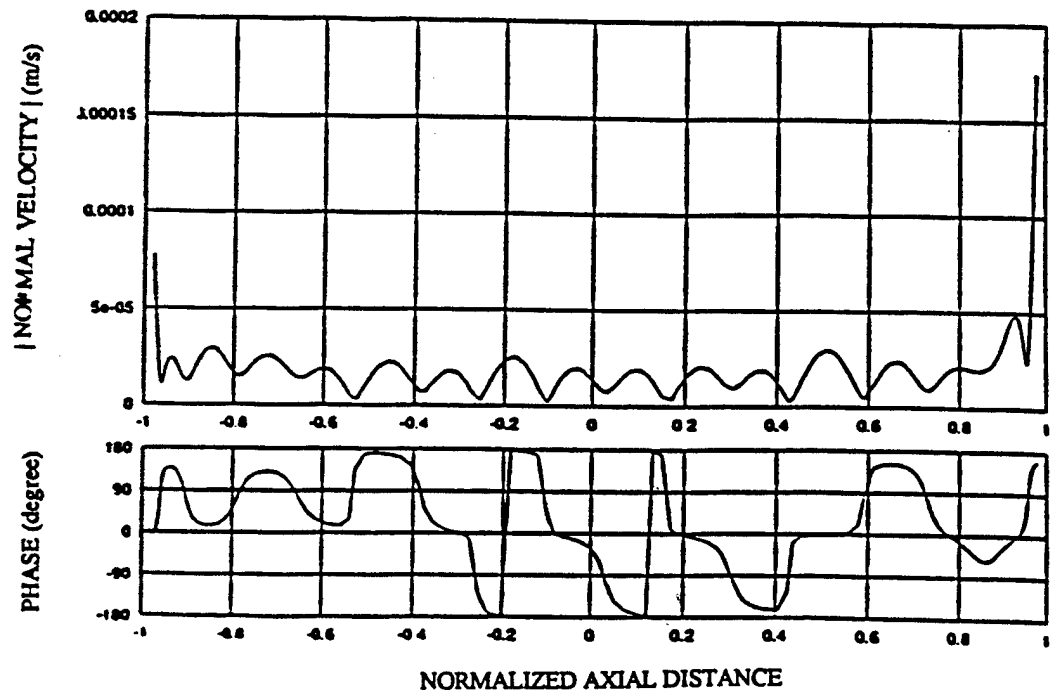


Figure 4.38 Magnitude and phase of the normal velocity on the outer surface of the cylindrical shell with hemispherical end caps, at $ka=5$. The excitation is due to an ideal ring source located at position P3.

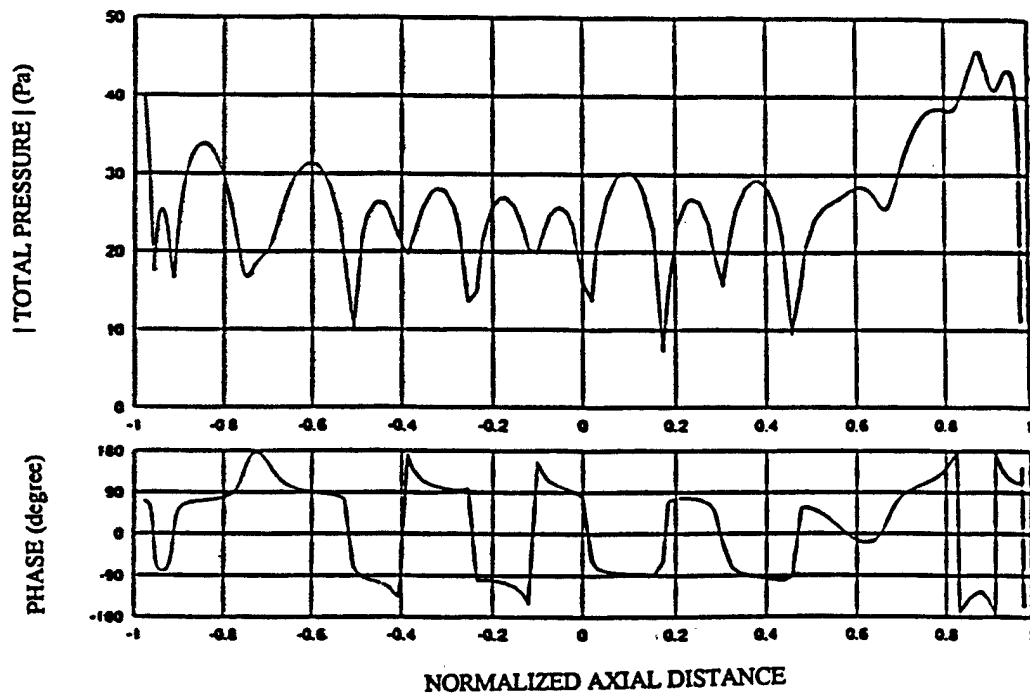


Figure 4.39 Magnitude and phase of the total pressure on the outer surface of the cylindrical shell with hemispherical end caps, at $ka=5$. The excitation is due to an ideal ring source located at position P3.

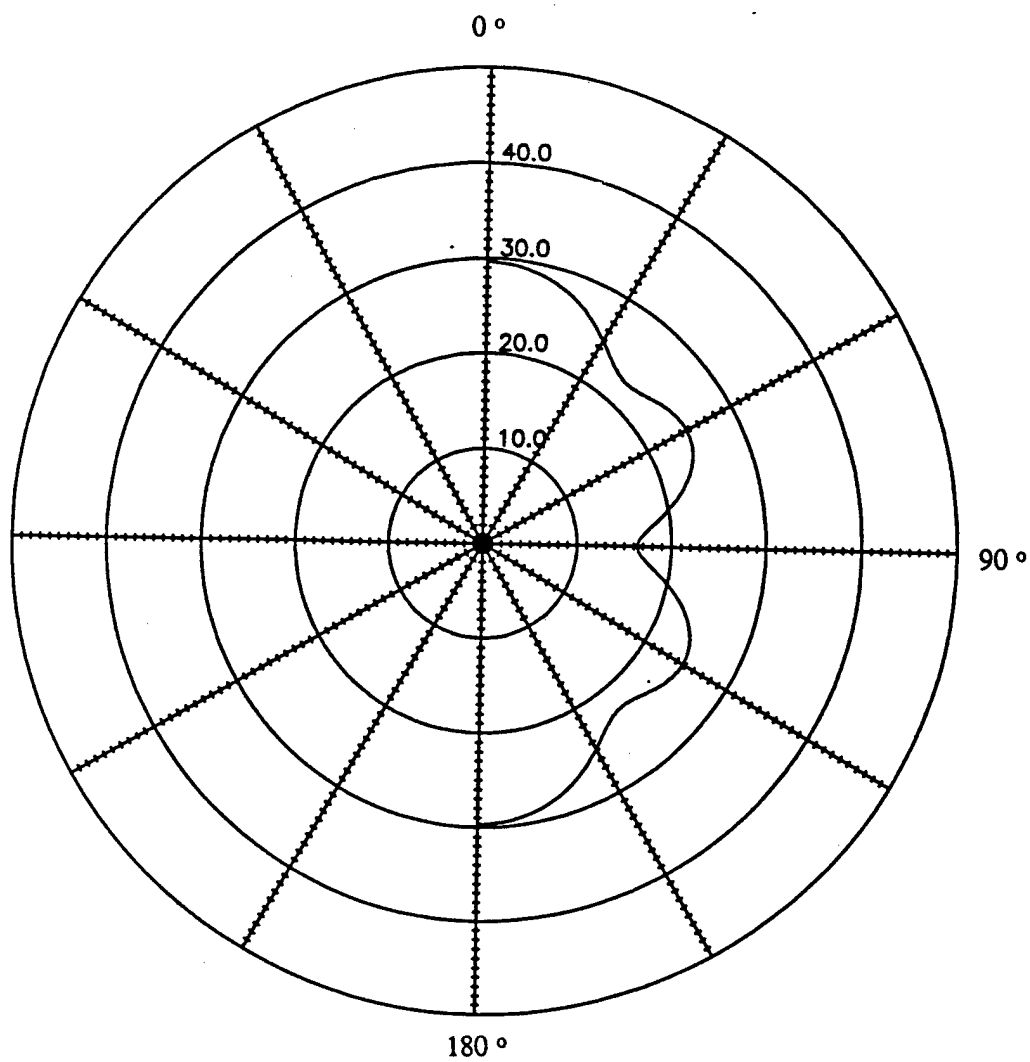


Figure 4.40 Far-field scattered pressure from the cylindrical shell with hemispherical end caps at $ka=2$. The excitation is due to an ideal ring source located at position P1.

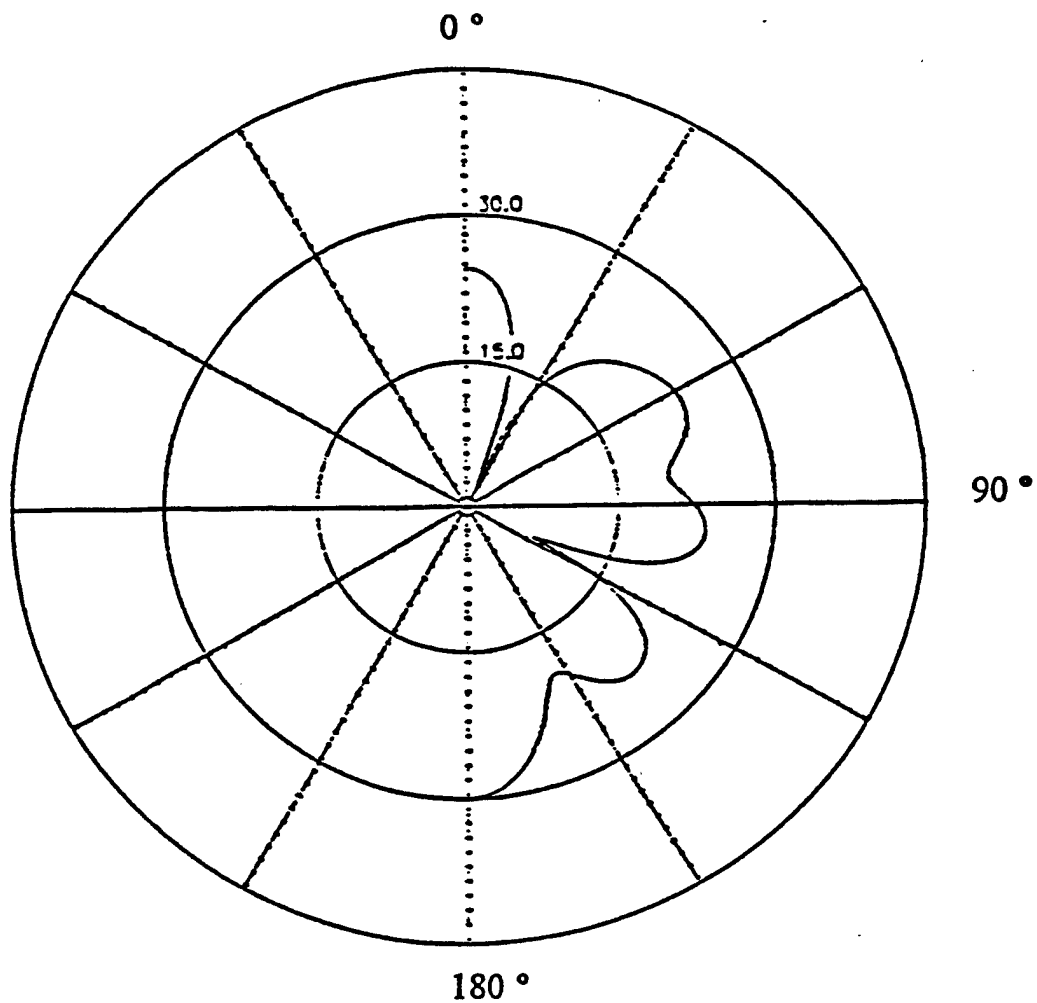


Figure 4.41 Far-field scattered pressure from the cylindrical shell with hemispherical end caps at $ka=2$. The excitation is due to an ideal ring source located at position P2.

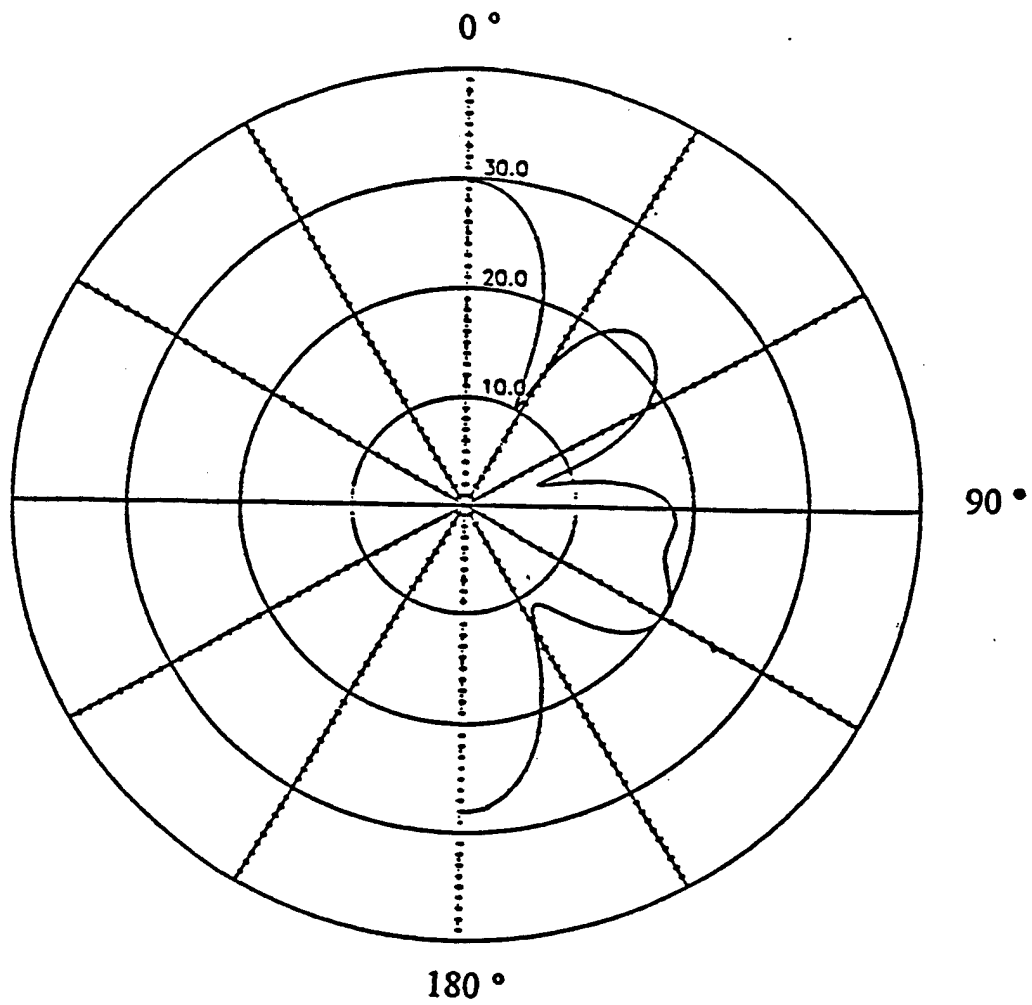


Figure 4.42 Far-field scattered pressure from the cylindrical shell with hemispherical end caps at $ka=2$. The excitation is due to an ideal ring source located at position P3.

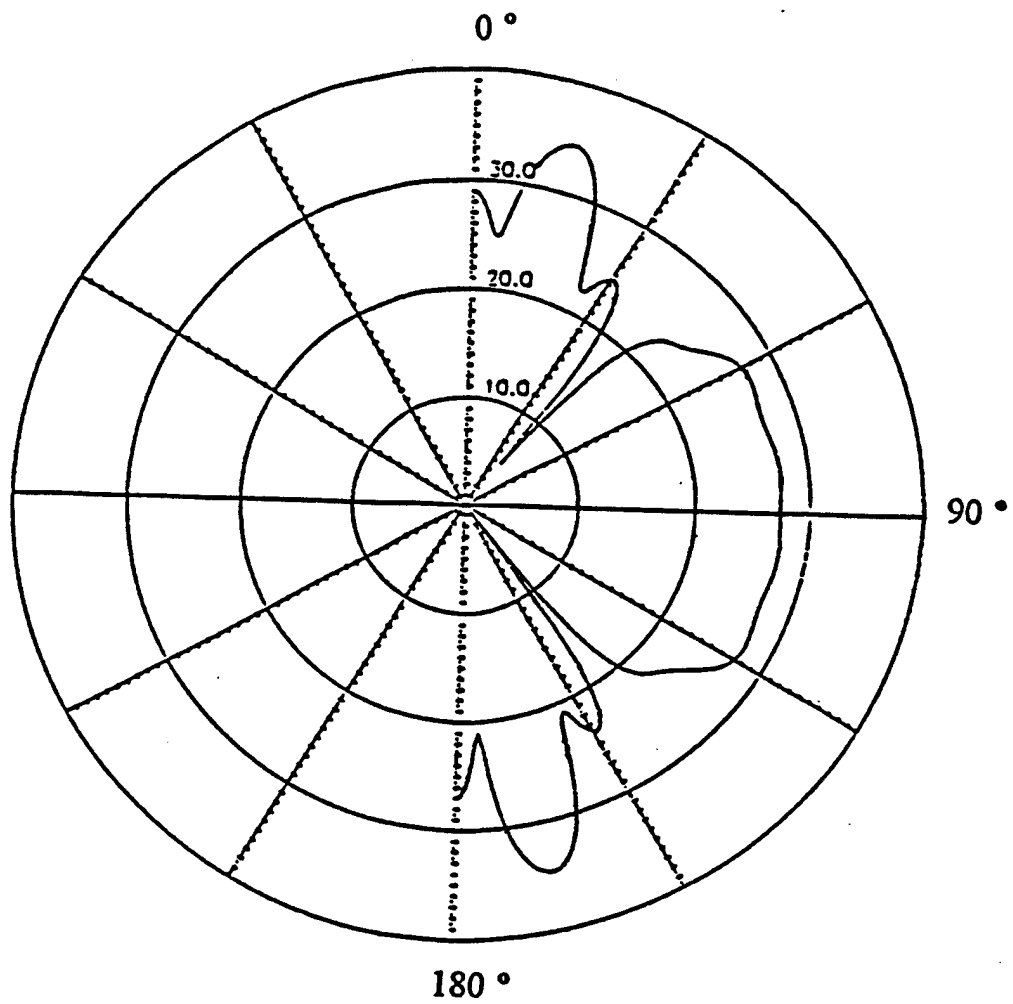


Figure 4.43 Far-field scattered pressure from the cylindrical shell with hemispherical end caps at $ka=5$. The excitation is due to an ideal ring source located at position P1.

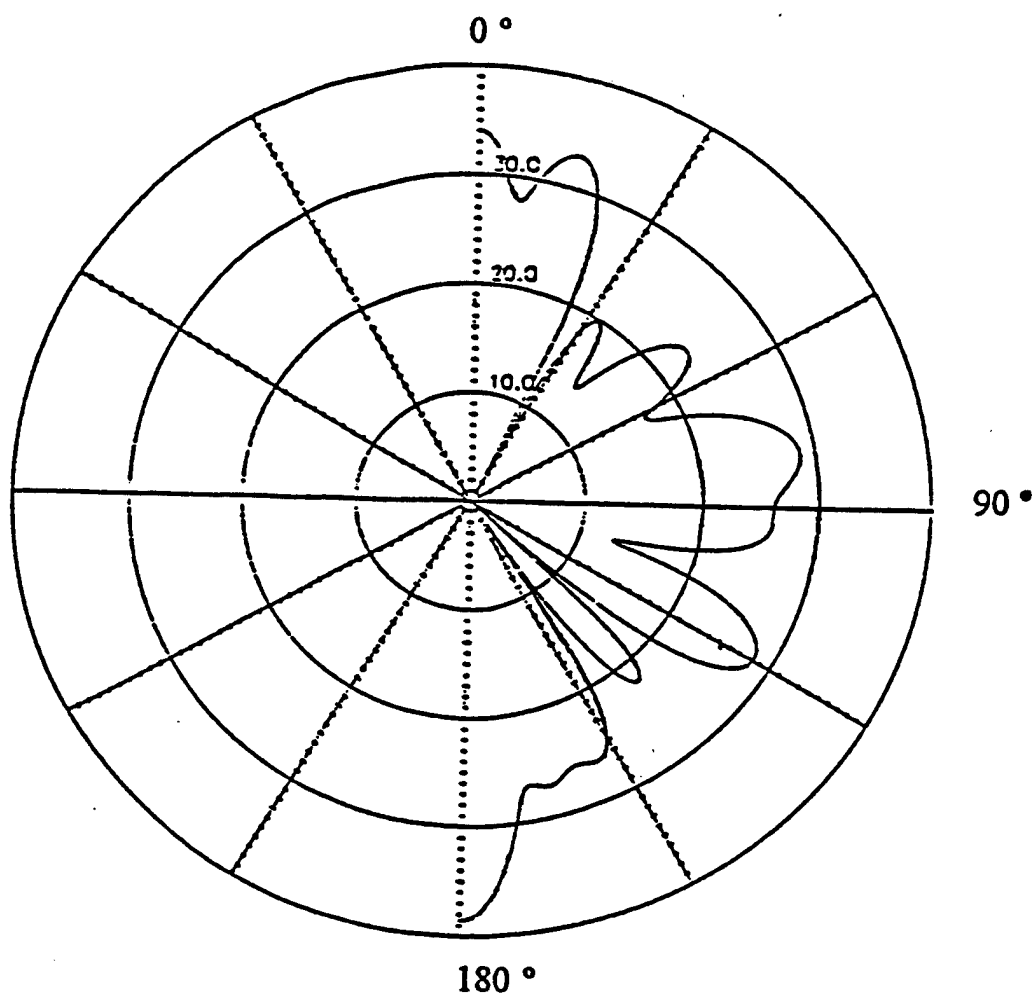


Figure 4.44 Far-field scattered pressure from the cylindrical shell with hemispherical end caps at $ka=5$. The excitation is due to an ideal ring source located at position P2.

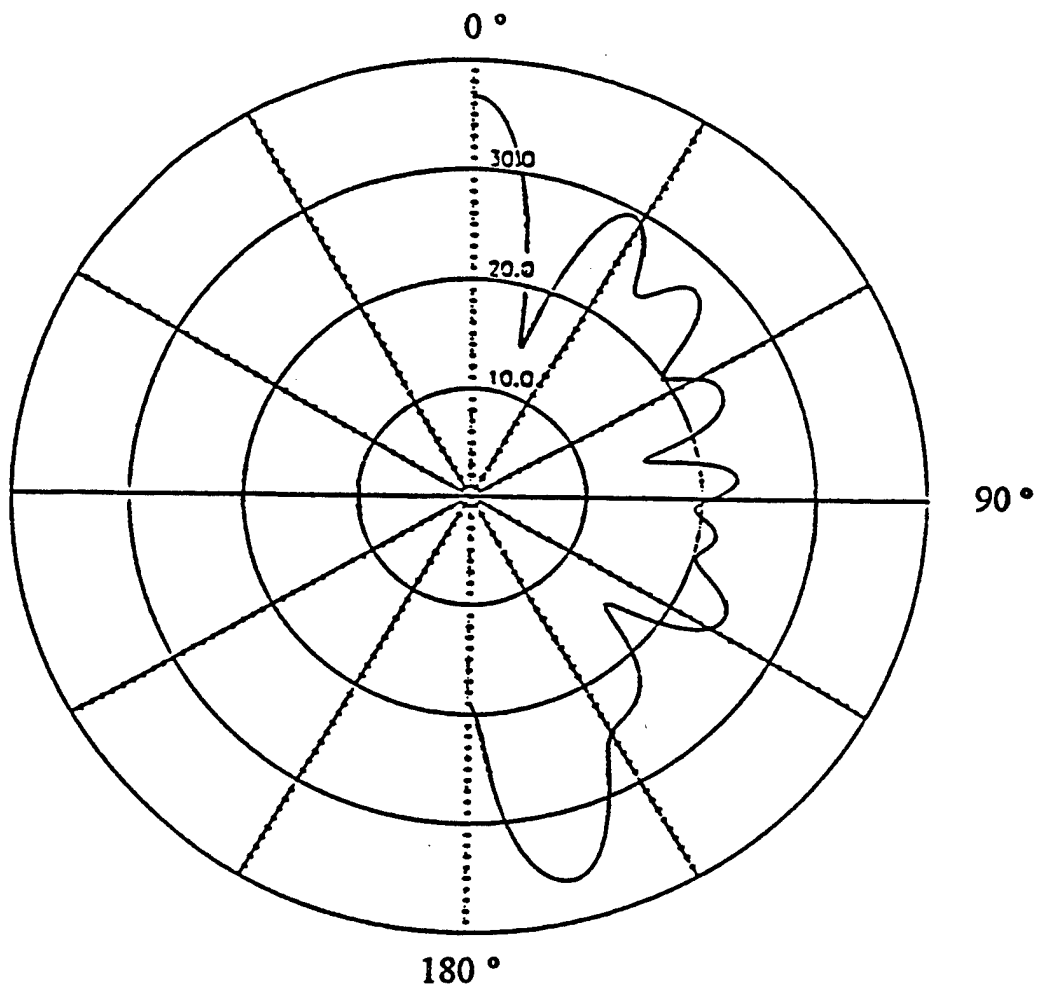


Figure 4.45 Far-field scattered pressure from the cylindrical shell with hemispherical end caps at $ka=5$. The excitation is due to an ideal ring source located at position P3.

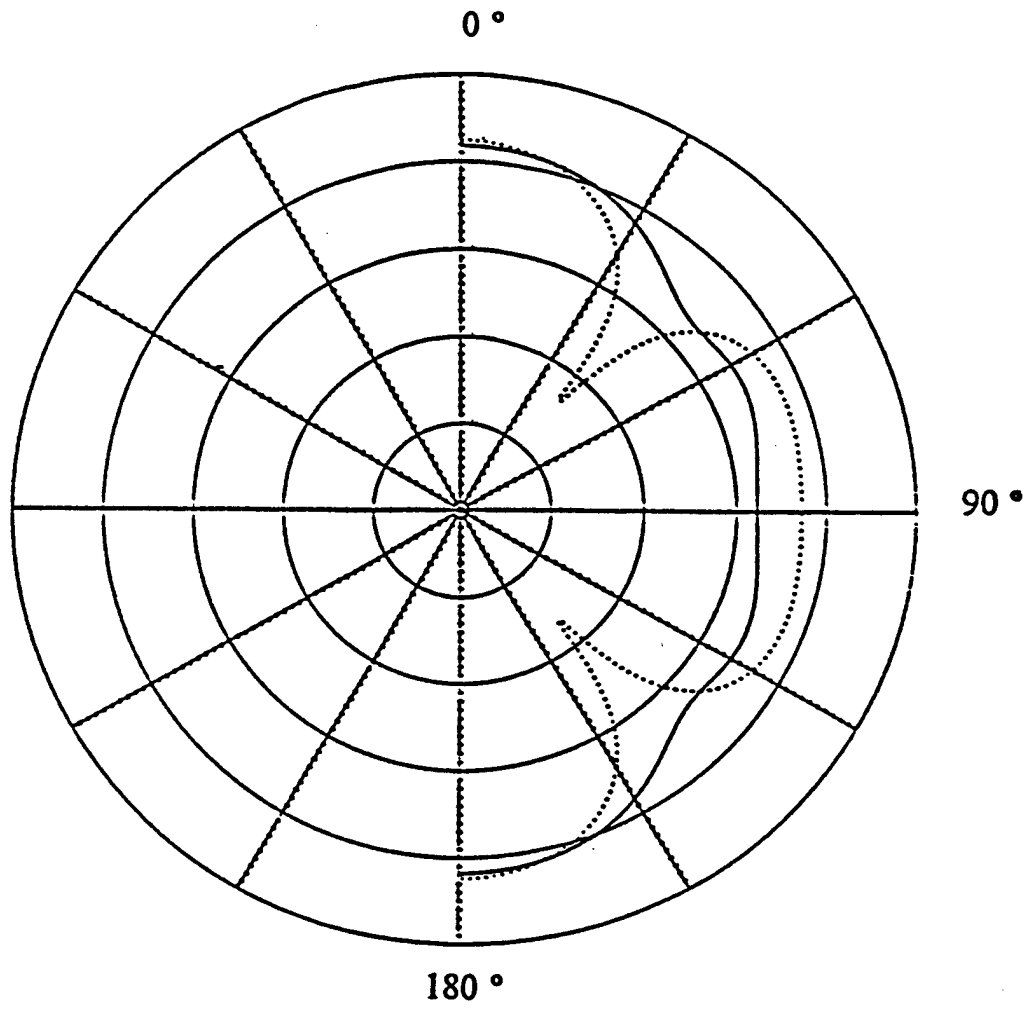


Figure 4.46 Total far-field pressure (solid line) and scattered far-field pressure (dotted line) at $ka=2$. The finite cylindrical structure with hemispherical end caps is excited by a finite piezoelectric ring source located at position P1. 10 dB/division.

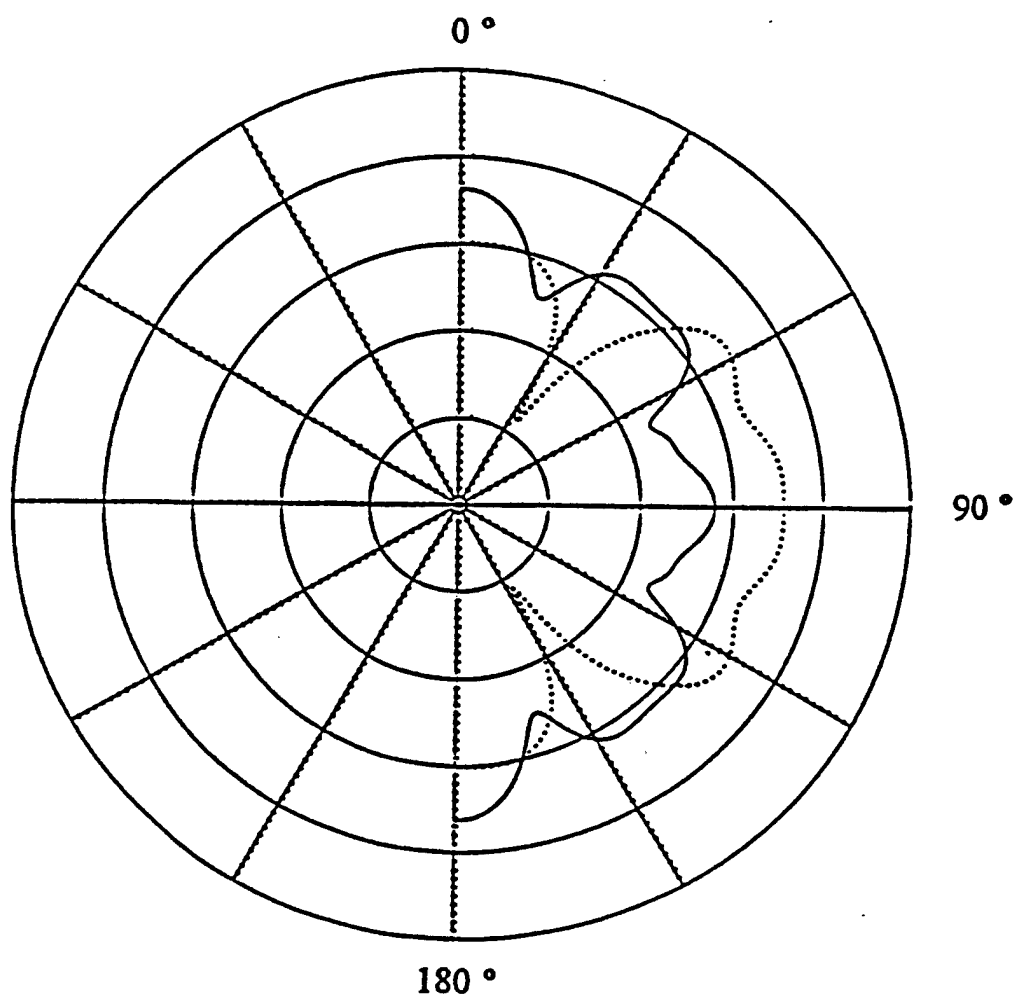


Figure 4.47 Total far-field pressure (solid line) and scattered far-field pressure (dotted line) at $ka=5$. The finite cylindrical structure with hemispherical end caps is excited by a finite piezoelectric ring source located at position P1. 10 dB/division.

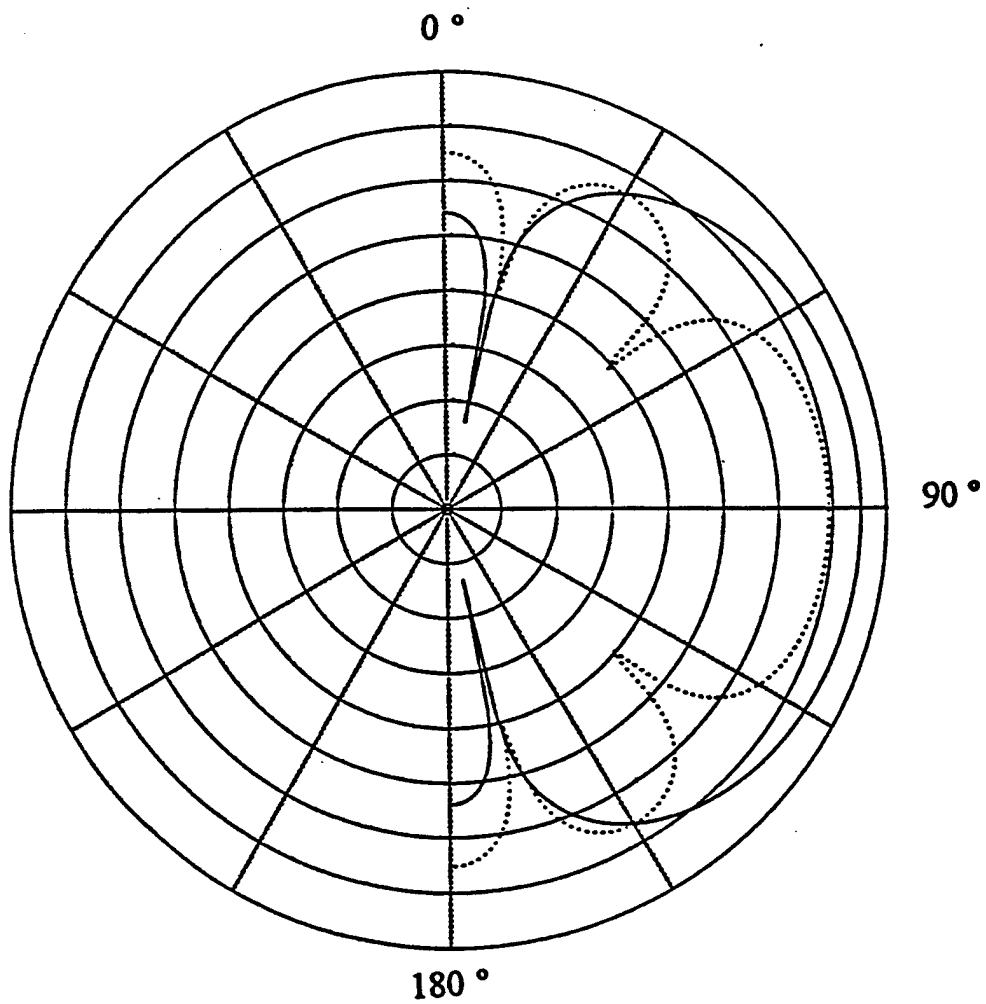


Figure 4.48 Free-field directivity pattern of a finite piezoelectric ring source at $ka=2$ (solid line) and at $ka=5$ (dotted line).

CHAPTER IV

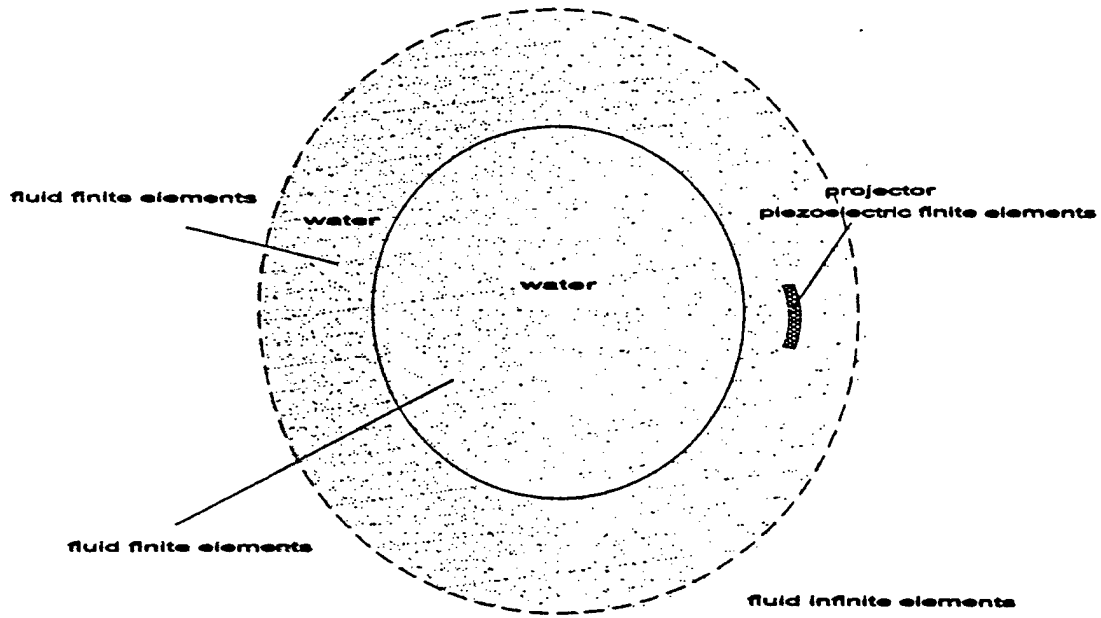
CONCLUSIONS

- Analysis of the normal velocity pattern at the surface of the baffle shows that the projector excites mainly flexural waves in the baffle. There is some evidence of weak excitation of the fast, extensional wave at $ka=5$.
- The main differences between the far-field pressure from the projector near the baffle and the projector in the free-field are probably due to interference between the direct sound from the projector and the sound reflected from the baffle.
- Three different sizes of piezoelectric projector were modeled, with 4.5° , 9.0° , and 18.0° angular extent. For the 4.5° and 9.0° projectors the TVR in the forward direction is not significantly affected by the presence of the baffle. This indicates that the source strength of the projector is not significantly changed by the presence of the baffle. The main differences between baffle and free-field conditions along other directions are probably due to interference between the direct and reflected sound signals.
- The 18.0° projector was the only source which showed significant deviations from ideal source performance. In particular, the TVR for this projector in the vicinity of the baffle is significantly different from the TVR under free-field conditions. The 18.0° projector is the only source modeled whose dimensions (width) are comparable to the flexural (shortest) wavelength in the baffle, and in the piezoelectric projector.

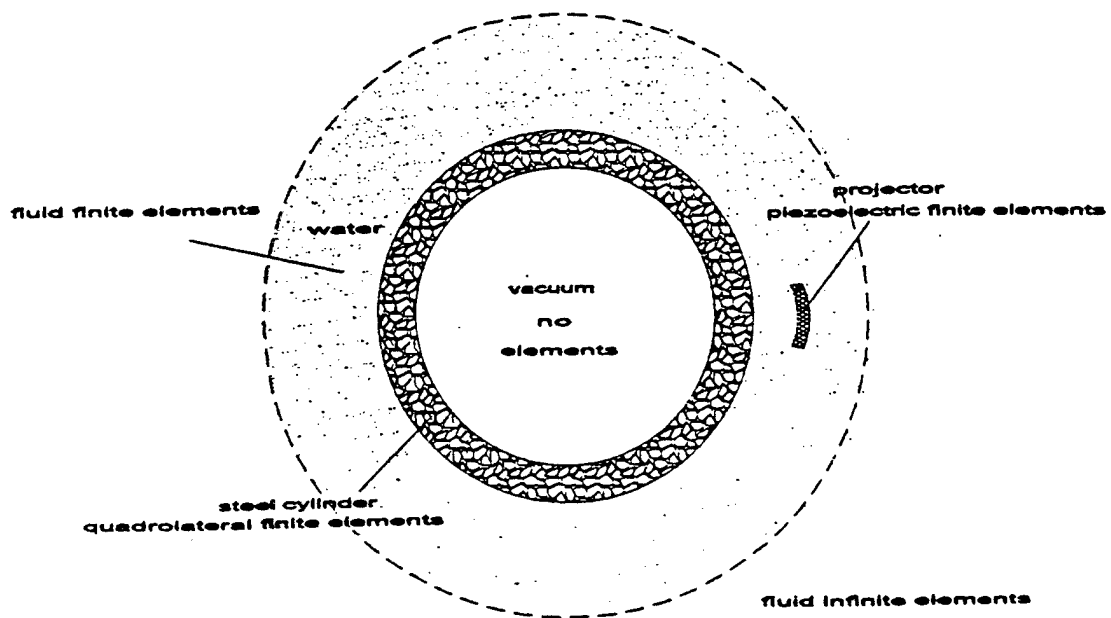
Therefore, the present calculations suggest that the projector near a baffle can be modeled as an ideal, acoustically transparent source as long as its dimensions are less than about one quarter of the shortest elastic wavelength in the system (baffle or projector). The above conclusion applies for projectors at the single, fixed distance from the baffle which was used in this study. The distance of the projector from the baffle is an important parameter which should be investigated.

APPENDIX I

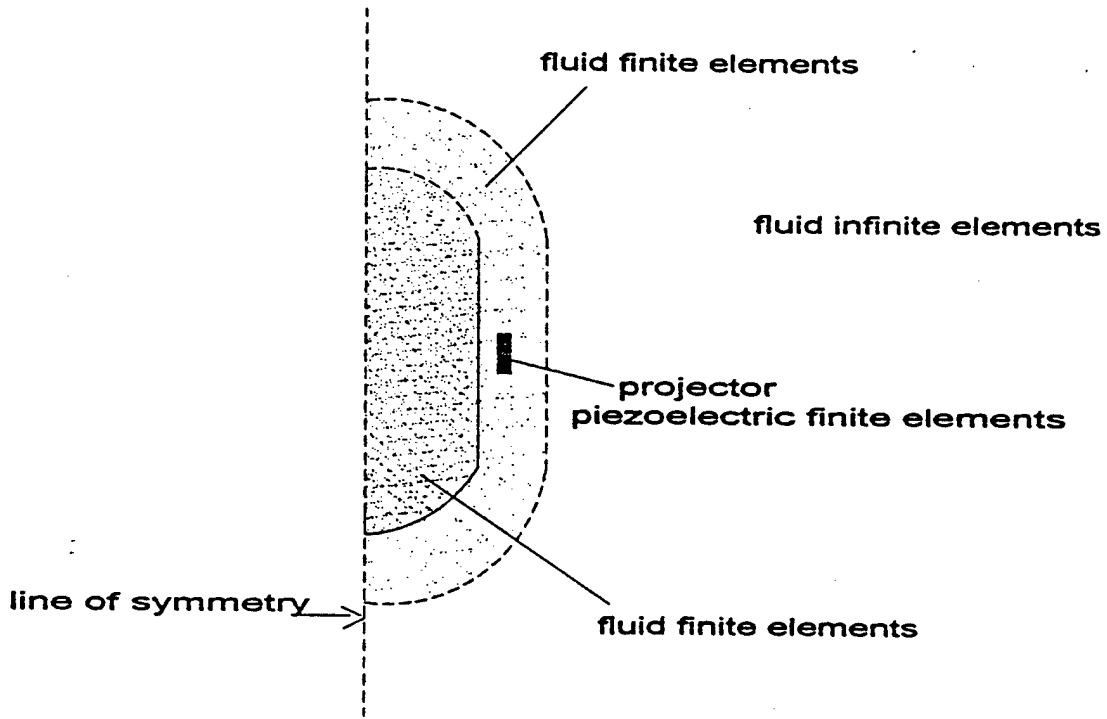
PLANE STRAIN CASE
PROJECTOR UNDER FREE FIELD CONDITIONS



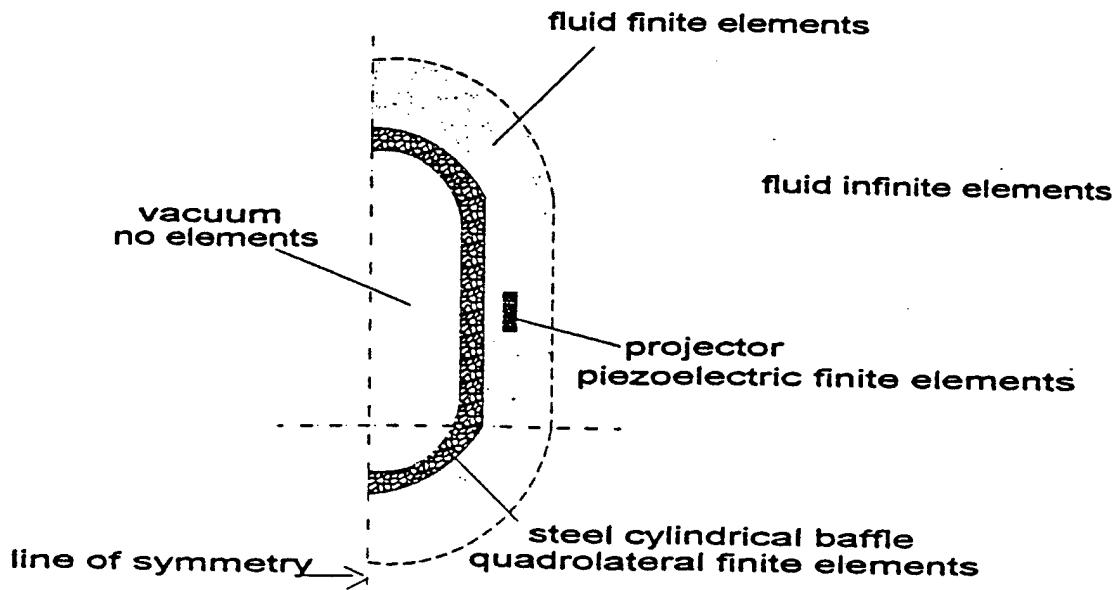
PLANE STRAIN CASE
PROJECTOR IN THE VICINITY OF THE BAFFLE



AXISYMMETRIC CASE
PROJECTOR UNDER FREE FIELD CONDITIONS



AXISYMMETRIC CASE
PROJECTOR UNDER FREE FIELD CONDITIONS



APPENDIX II

```

$ sara 2-D cylinder plane strain model for ka=2
$ thin hollow cylindrical shell in water driven by a piezoelectric
$ 9 deg cylindrical segment source acting perpendicular to the shell.
$ the piezoelectric source is driven with 853. volts.

```

```
plane, strain
```

```

ngrid=161., nelem=80.
e2m=0.0254, r=12.5*e2m
r2=r+1.0*e2m
r3=r2+1.0*e2m
r4=r3+0.5*e2m
r5=r4+.3
fstart=1376.0, fend=1376.0, finc=1.0

```

```

volt=853.
young=19.5e10, nu=0.28, rhos=7700.
rhof=1000., cf=1482.

```

```

e11=730.0., e33=635.0
s11=12.3, s12=-4.05, s13=-5.31
s33=15.5, s44=39.0
d31=-123.0, d33=289.0, d15=496.0
rhop=7500.0

```

```
setup
```

```

iso, qq, 1, young, nu, , rhos, ,
extflu, water, 2, cf, rhof, 0, 0, 0
fluid, water, 3, cf, rhof
iso, couple, 4, cf, , , rhof
iso, couple, 5, cf, , , rhof
iso, couple, 6, cf, , , rhof

```

```

piezo, pzt4, 7, s11, s33, s44, s12, s13, d31, d33, d15/
e11, e33, , , rhop, , , , , ,

```

```
end, materials $ -----
```

```

1, 1, 3, ngrid, , , , polar, 0.0, 0.0          $cylinder grids
r, r2, r2, r
0, 0, 360, 360

```

```

4, 1, 6, ngrid, , , , polar, 0.0, 0.0        $first fluid layer
r2, r3, r3, r2
0, 0, 360, 360

```

```

6, 1, 8, ngrid, , , , polar, 0.0, 0.0        $second fluid layer
r3, r4, r4, r3
0, 0, 360, 360

```

```

8, 1, 14, ngrid, , , , polar, 0.0, 0.0       $infinite fluid layer
r4, r5, r5, r4
0, 0, 360, 360

```

```
$*****pzt4 points*****
```

```

p, 38, 1, r3, 0, polar, 0, 0
p, 38, 2, r3, 2.25, polar, 0, 0
p, 38, 3, r3, 4.5, polar, 0, 0
p, 39, 1, r4, 0, polar, 0, 0
p, 39, 2, r4, 2.25, polar, 0, 0
p, 39, 3, r4, 4.5, polar, 0, 0
p, 40, 1, r4, 0, polar, 0, 0
p, 40, 2, r4, 2.25, polar, 0, 0
p, 40, 3, r4, 4.5, polar, 0, 0

```

p,38,159,r3,355.5,polar,0,0
 p,38,160,r3,357.75,polar,0,0
 p,39,159,rm,355.5,polar,0,0
 p,40,159,r4,355.5,polar,0,0
 p,40,160,r4,357.75,polar,0,0

end,grids \$ -----

jloop,expr(nelem-1)
 qq,quad,1,1,1 \$cylinder elements
 fqq,water,3,4,1 \$first fluid layer
 couple,,4,1,1,2,4,1,4 \$coupling elements for cylinder & first fluid
 jend

jloop,expr(nelem-2)
 fqq,water,3,6,3 \$second fluid layer
 iff,extflu,2,8,3 \$infinite fluid elements
 jend

qq,,1,1,159,3,159,3,1,1,1,2,159,3,160,2,1,1,160 \$last element in cylinder

pqq,piezo,7,38,159,40,159,40,1,38,1,39,159,40,160,39,1,38,160 \$source
 pqq,piezo,7,38,1,40,1,40,3,38,3,39,1,40,2,39,3,38,2 \$source

fqq,water,3,4,159,6,159,6,1,4,1,5,159,6,160,5,1,4,160 \$last fluid ele.
 couple,,4,1,159,2,4,159,4 \$last couple on struct.

iff,extflu,2,8,159,10,159,10,1,8,1,9,159,10,160,9,1,8,160 \$last inf. fluid elemen
 iff,extflu,2,8,1,10,1,10,3,8,3,9,1,10,2,9,3,8,2

couple,,5,38,1,38,2,38,3,6,1,6,2,6,3
 couple,,5,38,159,38,160,38,1,6,159,6,160,6,1
 couple,,6,40,159,39,159,38,159,8,159,7,159,6,159

couple,,5,40,1,40,160,40,159,8,1,8,160,8,159
 couple,,5,40,3,40,2,40,1,8,3,8,2,8,1
 couple,,6,38,3,39,3,40,3,6,3,7,3,8,3

bc,v,38,159,,volt \$nodal boundary conditions for sorce
 bc,v,38,160,,volt
 bc,v,38,1,,volt
 bc,v,38,2,,volt
 bc,v,38,3,,volt

bc,v,40,159,,0.0
 bc,v,40,160,,0.0
 bc,v,40,1,,0.0
 bc,v,40,2,,0.0
 bc,v,40,3,,0.0

end,elements \$ -----

fsweep,,fstart,fend,finc,2

post,,38,1,40,3,,,4,,
 post,,38,159,40,160,,,4,,


```
$post,,1,1,3,ngids,,,4,
```

```
$post,wet_nodes,4,4
```

```
$wet_vp,4,4,,1
```

```
$contours,pressure,r2,1.0,,360.0,1:0,,1,,,,,1
```

```
stop  
end
```

\$ sara 2-D cylinder with hemispherical end caps model - axisymmetric
\$ thin hollow cylindrical shell with hemispherical end caps submerged in water
\$ has a ring source boundary condition where grid in fluid is a source

axisym

begcyl=81., endcyl=131.
ngrid=211., nelem=105.
e2m=0.0254, r=12.5*e2m
r2=r+1.0*e2m
r3=r2+1.*e2m
r4=r3+0.5*e2m
r5=r4+.3

l=50.*e2m, a=1/2
b=-a
fstart=1376.0, fend=1376.0, finc=1.0

young=19.5e10, nu=0.28, rhos=7700.
rhof=1000., cf=1482.

setup

iso,qq,1,young,nu,, rhos,,
extflu,water,2,cf,rhof,0,0,0
fluid,water,3,cf,rhof
iso,couple,4,cf,,,rhof

end,materials \$ -----

1,1,3,begcyl,,,,polar,0.0,b \$bottom end cap
r,r2,r2,r
270,270,360,360

1,begcyl,3, endcyl \$cylinder
r,r2,r2,r
b,b,a,a

1, endcyl,3, ngrid,,,,polar,0,a \$top end cap
r,r2,r2,r
0,0,90,90

\$-----end of structure

4,1,6,begcyl,,,,polar,0.0,b \$bottom end cap
r2,r3,r3,r2
270,270,360,360

4,begcyl,6, endcyl \$cylinder
r2,r3,r3,r2
b,b,a,a

4, endcyl,6, ngrid,,,,polar,0,a \$top end cap
r2,r3,r3,r2
0,0,90,90

\$-----end of first fluid layer

6,1,8,begcyl,,,,polar,0.0,b \$bottom end cap
r3,r4,r4,r3
270,270,360,360

6,begcyl,8, endcyl \$cylinder
r3,r4,r4,r3

```

b,b,a,a
6,endcyl,8,ngrids,,,,polar,0,a      $stop end cap
r3,r4,r4,r3
0,0,90,90
$-----end of second fluid layer

8,1,10,begcyl,,,,polar,0.0,b      $bottom end cap
r4,r5,r5,r4
270,270,360,360

8,begcyl,10,endcyl                  $cylinder
r4,r5,r5,r4
b,b,a,a

8,endcyl,10,ngrids,,,,polar,0,a      $stop end cap
r4,r5,r5,r4
0,0,90,90
$-----end of infinite fluid layer

end,grids $ -----

jloop,nelem                          $cylinder elements
qq,quad,1,1,1                        $first fluid layer
fqq,water,3,4,1                      $second fluid layer
fqq,water,3,6,1                      $coupling elements
couple,,4,1,1,2,4,1,4               $infinite fluid elements
iff,extflu,2,8,1
jend

bc,source,6,106,,.00003173          $source boundary condition

end,elements $ -----

fsweep,,fstart,fend,finc,1

$post,,1,1,3,ngrids,,,4,
$post,wet_nodes,4,4

wet_vp,,4,,
contours,pressure,r2,1.0,,180.0,1.0,,1,,1,,,,

stop
end

```

BIBLIOGRAPHY

1. SARA 2D User's manual 1992. BBN Systems and Technologies
2. Mason, "Physical Acoustics" vol.I, part A. Academic press, (1964)
3. P. W. Smith, Jr. , "Phase Velocities and Displacement Characteristics of Free waves in a Thin Cylindrical Shell, " J. Acoust. Soc. Am. 27, 1065-1072 (1955)
4. James J. Faran, Jr. , "Sound Scattering by Solid Cylinders and Spheres," J. Acoust. Soc. Am. 23, 405-418 (1951).
5. R. D. Doolittle and H. Uberall, "Sound Scattering by Elastic Cylindrical Shells," J. Acoust. Soc. Am. 39, 272-275 (1966).
6. P. Uginčius and H. Uberall, "Creeping-Wave Analysis of Acoustic Scattering by Elastic Cylindrical Shells," J. Acoust. Soc. Am. 43, 1025-1035 (1968).
7. Y.H. Berthelot, Acoustics III unpublished class notes (used with permission of d. Blackstock).
8. G. N. Watson, Proc. Roy. Soc. (London) A95, 83-99, 546-563 (1919).
9. V. A. Borovikov and N. D. Veksler, "Scattering of Sound Waves by Smooth Convex Elastic Cylindrical Shells," Elsevier Science Publishers V. V. (north Holland), 143-152 (1984).
10. J. B. Keller, "Proceedings of SYmposia in Applied Mathematics," vol. 8.
11. Joshua E. Greenspon and Charles H. Sherman, "Mutual-Radiation Impedance and Near field Pressure for Pistons on a Cylinder," J. Acoust. Soc. Am. 36, 149-153 (1964).
12. M. C. Junger, "Surface Pressures Generated by Pistons on Large Spherical and Cylindrical Baffles," J. Acoust. Soc. Am. 41, 1336-1346 (1967).
13. Clay and Medwin, "Acoustical Oceanography", Wiley-Interscience Publication (1977).

14. Yuan-Ning Liu and M.L. Rummernan, "The effects of adjacent elastic structures on radiation by acoustic volume sources, "Ship Acoustics Dept. Departmental report, (1981).
15. Julius S. Bendat and Allan G. Piersol, "Engineering Applications of correlation and Spectral Analysis," Wiley-Interscience Publication (1980).
16. John L. Butler and David T. Porter, "A Fourier transform solution for the acoustic radiation from a source near an elastic cylinder," J. Acoust. Soc. Am. 89, 2774-2785 (1991).
17. Russel D. Miller, X.L. Bao, and H. Uberall "Acoustic Scattering from Elastic Cylinders and Cylindrical Shells of Finite Length"
18. Douglas D. Reynolds, "Engineering Principles of Acoustics", Allyn and Bacon Inc. (1981).
19. Varadan and V.V. Varadan, "Acoustic, Electromagnetic and Elastic Wave Scattering", Pergamon Press (1980).
20. Allan D. Pierce, "Acoustics", Published by the Acoustical Society of America, (1991).
21. A.L. Stanford and J.M. Tanner, "Physics for Students of Science and Engineering", Harcourt Brace Jovanovich, Inc. (1985).
22. A. E. Love, "A Treatise on the Mathematical Theory of Elasticity 4th ed," Dover publications, New York (1944).
23. Gordon S. Kino, "Acoustic Waves", Prentice-Hall Inc. (1987).
24. Larson and Hostetler, "Intermediate Algebra," Heath and Company (1992).
25. Neubaur, "Acoustic Reflection From Surfaces and Shapes," NRL publication.
26. Charles Cullen, "Matrices and Linear Transformations", Addison-Wesley Publishing Company (1966).
27. Oscar Brian Wilson, "An introduction to the theory and design of sonar transducers", U.S. Government Printing (1985).
28. Lawrence E. Kinsler and Austin R. Frey, "Fundamentals of Acoustics third edition", New York and Sons (1950).

29. Georgia Institute of Technology, Mechanical Engineering Department Doctorial Disortation by Kil.